Marie Marlen Augustin, BSc

Influence of gravel columns on development of pore pressures beneath water storage basin

MASTER'S THESIS

to achieve the university degree of

Diplom-Ingenieurin

Master's degree programme: Geotechnical and Hydraulic Engineering

submitted to

Graz University of Technology

Supervisor

Ao.Univ.-Prof. Dipl.-Ing. Dr.techn. M.Sc. tit.Univ.-Prof. Helmut Schweiger

Dipl.-Ing. Georg Michael Ausweger, BSc

Institute of Soil Mechanics and Foundation Engineering

Graz, September 2017

Eidesstattliche Erklärung

Ich erkläre an Eides statt, dass ich die vorliegende Arbeit selbstständig verfasst, andere als die angegebenen Quellen/Hilfsmittel nicht benutzt, und die den benutzten Quellen wörtlich und inhaltlich entnommenen Stellen als solche kenntlich gemacht habe.

Graz, am ……………………… …………………………………………………

(Unterschrift)

Statutory declaration

I declare that I have authored this thesis independently, that I have not used other than the declared sources / resources, and that I have explicitly marked all material which has been quoted either literally or by content from the used sources.

Graz, ……………………… …………………………………………………

(signature)

Preface of the author

I want to thank all those people who supported me during my time at university and especially during the last semester while I was working on my thesis.

A big thank you goes to the entire Computational Geotechnics Group of the Institute of Soil Mechanics and Foundation engineering at the TU Graz for all the helpful advice while I was writing my thesis. I want to thank my supervisors Prof. Dr.techn. Schweiger, and especially DI Ausweger for his extraordinary guidance and all his constructive input for my thesis, as well as his seemingly infinite patience with me constantly interrupting him during his working hours.

I also thank all my colleagues from the Stahlbauzeichensaal for the unforgettable time during the last 5 years - for all the creative group projects, the adventurous excursions, but also the instructive time studying together for exams. Special thank goes to my friend Bettina, who was always there for me, whenever a problem occurred at university or any other tricky situation in my life. Without you, life at university would have been much harder.

Furthermore, I would like to thank my family, especially my parents Johanna and Michael, for supporting me and my decisions whenever and however they could. A big thankful hug goes to my big brother Fabian for all the relaxing beers during the last years Thanks to you all for giving me motivation and advice in every situation of my life.

And finally, I would like to thank my boyfriend Patrick for always being supportive and inspiring since the day I have met you. Without you, my start at university would have been more challenging. Also, a special thanks to you for proofreading my thesis and constantly reminding me to improve my language skills.

THANK YOU!

Kurzfassung

Die Wasserspiegelschwankungen in einem Speicherteich, der sich nahe einer langsamen Massenbewegung befindet, führen zu Porenwasserüberdrücken im Untergrund. Ziel dieser Masterarbeit ist es, den Einfluss von Kiessäulen auf die Porenwasserdrücke unter dem Speicherteich zu untersuchen.

Zu Beginn wird ein geeignetes Kiessäulenmaterial mit Hilfe einer Literaturstudie über geometrische und hydraulische Filterkriterien gegen Kontakterosion gesucht. Anschließend wird eine numerische Untersuchung über den Einfluss der Kiessäulen im axisymmetrischen und im ebenen Verzerrungszustand mit der Finite Elemente Methode durchgeführt.

Auf Basis der Ergebnisse dieser Masterarbeit, wird empfohlen Hird et al. (1992)'s Ansatz mit verschmierter Störzone für die Umrechnung der Durchlässigkeiten vom axisymmetrischen zum ebenen Verzerrungszustand zu verwenden, weil die Ausdehnung der Störzone zufolge des Einbaus der Kiessäulen nicht bekannt ist. Außerdem zeigt die Studie, dass die Störzone rund um die Kiessäulen einen untergeordneten Einfluss auf die Porenwasserdrücke hat, aber einen bedeutenden Einfluss auf den hydraulischen Gradienten direkt neben der Säule. Der wichtigste Faktor für die Untersuchung der Porenwasserdrücke und des hydraulischen Gradienten neben den Säulen ist die horizontale Durchlässigkeit k_x des vorhandenen Bodens.

Die Erkenntnisse aus der Vorstudie werden auf ein reales Projekt im ebenen Verzerrungszustand angewandt. Dabei ist der Einfluss der Kiessäulen auf die Porenwasserdrücke in beiden Durchlässigkeitszuständen (isotrop und anisotrop) deutlich erkennbar, jedoch ist dieser nur begrenzt auf die unmittelbare Umgebung der Säulen. Wieder zeigt sich die Wichtigkeit der horizontalen Durchlässigkeit k_x für das untersuchte Projekt. Der Sicherheitsfaktor der angrenzenden langsamen Massenbewegung ist unbeeinflusst vom Einsatz der Kiessäulen.

Abstract

The fluctuating water level in a water storage basin of a pump storage power plant, which is located adjacent to a slow-moving slope, generates excess pore water pressures in the subsoil. The goal of this thesis is to investigate the influence of gravel columns on the pore water pressure beneath this water storage basin.

First, a suitable material for the gravel columns is defined on the basis of a literature review about geometrical and hydraulic filter criteria concerning contact erosion. Subsequently, a numerical study about the influence of the gravel columns under axisymmetric and 2D plane strain condition is conducted, applying the finite element method.

Based on the results of this thesis, it can be concluded that Hird et al.(1992)'s approach, which makes use of the averaged smear effect, should be used for the conversion from axisymmetric to plane strain conditions because of the unknown extent of the smear zone due to the installation of the columns. Furthermore, the study shows that the smear zone around the gravel columns has a minor effect on the pore water pressures, but a major effect on the hydraulic gradient next to the column. However, the most important factor for investigating the influence of such gravel columns on the pore water pressures and the hydraulic gradient next to the columns, is the horizontal permeability k_x of the subsoil.

The findings of the preliminary study are applied on a real project in plane strain conditions. The influence of the gravel columns on the pore water pressures is shown under both permeability conditions (isotropic and anisotropic), but the influence is limited to the area next to the columns. Again, the importance of the horizontal permeability k_x is proven for this project. The factor of safety (FOS) of the adjacent slope does not change due to the installed gravel columns.

Table of contents

List of figures

List of tables

List of symbols and abbreviations

Capital letters

$A_{50,vorh}$	[-]	existing distance ratio
$A_{50,zul}$	[-]	admissible distance ratio
A_{50}	[-]	distance ratio
A_{ax}	[m²]	Column area in axisymmetric condition
A_{pl}	[m²]	Column area in plane strain condition
B	[m]	half distance of drains in plane strain condition
$C_{U,B}$	[-]	coefficient of uniformity of the base material
$C_{U,F}$	[-]	coefficient of uniformity of the filter material
C_U	[-]	coefficient of uniformity
D	[mm]	diameter of the soil particle of a filter, which can hold back a soil aggregate in a cohesive dam with tensile strength of c_0 and a degree of safety of η
D_{squ}	[m]	Drainage zone around the column for square pattern
D_{tri}	[m]	Drainage zone around the column for square pattern
E'	[kN/m²]	(Effective) Young's modulus
E_{50}^{ref}	[kN/m²]	(Reference) Secant stiffness in standard drained triaxial test
E_{Oed}	[kN/m²]	Oedometric stiffness
E_{Oed}^{ref}	[kN/m²]	(Reference) Tangent stiffness for primary oedometer loading
E_{ax}	[kN/m²]	Young's modulus in axisymmetric condition
E_{pl}	[kN/m²]	Young's modulus in plane strain condition
E_{ur}^{ref}	[kN/m²]	(Reference) Unloading/reloading stiffness
$F_{0.074}$	[%]	mass% of soil $d_B < 0.074\ mm$ without grains $d_B > 4.75\ mm$
G_0^{ref}	[kN/m²]	(Reference) shear modulus at very small strains ($\varepsilon < 10^{-6}$)
K_0^{nc}	[-]	K0-value for normal consolidation
Q_w	[m³/s]	discharge capacity of drain in plane strain unit cell
R	[m]	radius of the axisymmetric FE-model
R_{ax}	[m]	radius of the axisymmetric unit cell (drain influence zone $D_{tri} = 2R$)
S	[m]	spacing between the column axis in plan view
U	[-]	degree of consolidation
X_i	[m]	distance from gravel column, i=1,2,3

Small letters

b_s	[m]	half width of smear zone in plane strain condition
b_w	[m]	width of column in plane strain condition
c_0	[kN/m²]	tensile strength
const.	[-]	constant factor
c'_{ref}	[kN/m²]	effective cohesion (at reference level)
d	[mm]	grain diameter
d_{10}, d_{20} ...	[mm]	specific grain diameter
$d_{100,B}$	[mm]	diameter base material at 100 mass %
$d_{15,F}$	[mm]	particle diameter at the filter material at 15 mass %
$d_{40,B}$	[mm]	Particle diameter of the base material at 40 mass %
$d_{50,B}$	[mm]	particle diameter of the base material at 50 mass %
$d_{50,F}$	[mm]	particle diameter of the filter material at 50 mass %
$d_{85,B}$	[mm]	particle diameter at the base material at 85 mass %
d_B	[mm]	diameter base material
d_F	[mm]	diameter filter material
d_i	[mm]	grain diameter
d_p	[cm]	decisive pore diameter by Pavcic
gw_1	[m]	groundwater head 1
gw_2	[m]	groundwater head 2
i	[-]	hydraulic gradient
$i_{I,vorh}$	[-]	present hydraulic gradient in base material
$i_{KE,krit}$	[-]	critical hydraulic gradient in base material
$i_{crit,transport}$	[-]	critical hydraulic gradient for particle transport
i_{crit}	[-]	critical hydraulic gradient
$i_{crit.fracture}$·	[-]	critical hydraulic gradient for crack propagation
k	[m/s]	permeability
k'_{hp}	[m/s]	horizontal permeability of smear zone in plane strain condition
k_h	[m/s]	horizontal permeability of subsoil in axisymmetric unit cell
k_{hp}	[m/s]	horizontal permeability of subsoil in plane strain condition
k_D	[mm]	Permeability of coarse bulk skeleton of the filter material
$k_{ax,s}$	[m/s]	horizontal permeability of smear zone in axisymmetric unit cell
k_{ax}	[m/s]	horizontal permeability of subsoil in axisymmetric unit cell

k_{pl}	[m/s]	horizontal permeability of subsoil in plane strain condition
k_x	[m/s]	horizontal permeability
k_y	[m/s]	vertical permeability
l	[m]	assumed flow length
m	[-]	Power for stress-level dependency of stiffness
n, s	[-]	geometry factors
p_{ref}	[kN/m²]	reference pressure
q_w	[m³/s]	discharge capacity of drain in plane strain unit cell
r	[m]	radius of the column
r_s	[m]	radius of the smear zone in the axisymmetric unit cell (measured from column axis)
r_w	[m]	radius of the column in the axisymmetric unit cell

Greek letters

α	[-]	factor for influence of time
α, β	[-]	geometry factors
$\bar{\alpha}$	[°]	angle between filter and base material
β_1	[°]	inclination of border between base and filter material
γ	[kN/m³]	unit weight of a material
γ'	[kN/m³]	unit weight of the soil under buoyancy
$\gamma_{0.7}$	[-]	threshold shear strain at which $G_S = 0.722 \cdot G_0$
γ_{sat}	[kN/m³]	saturated unit weight of soil
γ_{unsat}	[kN/m³]	unsaturated unit weight of soil
γ_w	[kN/m³]	unit weight of water
Δgw	[m]	difference of groundwater head
η	[-]	degree of safety
$\eta_{KE,H}$	[-]	hydraulic safety against contact erosion
v'	[-]	Poisson's ratio
v'_{ur}	[-]	unloading/reloading Poisson's ratio
φ'	[°]	effective friction angle
ψ	[°]	dilatancy angle

Abbreviations

acc.	according to
cf.	confer
e.g.	exepli gratia, for example
EPWP/EPP	excess pore water pressures
Equ.	equation
et al.	et alia, and others
FE	Finite element
Fig.	figure
FOS	factor of safety
GSD	grain size distribution
PVD	prefabricated vertical drain
Tab.	table

1 Introduction

Vertical drains are a well-known tool to increase the rate of pore water dissipation in soft soils. (Redana 1999) (Indraratna & Redana 1997, 2000) There are two types of vertical drains - prefabricated vertical drains (PVDs), which are very popular nowadays, and gravel columns. In comparison to the PVDs, the gravel columns' big advantage is that they also act as reinforcement for soft soil to provide an increased bearing capacity. (Redana 1999)

Due to the installation of vertical drains the drainage path in the subsoil is reduced significantly. With installed drains, the water flows radial to the column, instead of vertical drainage to the ground surface (which in general is a longer flow path). (Redana 1999)

1.1 Problem definition

Due to water level fluctuation in the storage basin, which is located next to a slow moving slope, excess pore water pressures are generated in the fine grained subsoil (which consists mainly of silty fine sand). These excess pore water pressures influence the factor of safety (FOS) of the adjacent slope. The mentioned slope, which is very near to an ultimate limit state, is slowly moving into the basin.

The idea of decreasing the slope movements and increasing the FOS of the slope is to install vertical drains in the subsoil next to the slope, to increase the dissipation rate of the excess pore water pressures in the subsoil. These gravel columns (=vertical drains) will be installed in a triangular pattern to provide a more uniform consolidation between the drains. Also the space for installing the columns is limited in the studied project.

1.2 Goals of this thesis

The goal of the thesis is to understand and analyse the behaviour of the gravel columns, which are interacting with the adjacent slow-moving slope and the fluctuating water level in the storage basin.

1.3   Methodology and structure of the thesis

At first, a comprehensive study about finding the suitable gravel column material is performed. The main problem during the material examination is the risk of contact erosion between a fine and a coarse-grained material. Well known, mostly empirical filter criteria for this specific problem are discussed and later on used to find the upper and lower suitable limit of a grain size distribution for the column material (see chapter 2 and 3).

After definition of the appropriate material, a numerical study about the behaviour of such gravel columns surrounded by fine-grained soil with low permeability, is carried out using Plaxis 2D (Brinkgreve 2016). This numerical study is subdivided into three parts:

- Preliminary study of an axisymmetric unit cell (see chapter 5),

- Conversion and verification from axisymmetric to plane strain conditions (see chapter 6), and

- Plane strain calculations, analysing the comprehensive system behaviour of gravel columns beneath a storage basin next to a slow-moving slope (see chapter 7).

After this numerical study, a conclusion and evaluation of the influence of the gravel columns on the pore water pressure and the FOS of the adjacent slope are presented (see chapter 8).

2 Problem of contact erosion for gravel columns in fine grained subsoil

In this chapter, the phenomena of contact erosion are investigated for subsequent filter designs, at first generally and later project related.

2.1 Definition of suffusion

In case of suffusion, the finer particles of a non-uniform non-cohesive soil, which fill up the pore space between the coarser grain skeleton, are relocated and transported. The coarse skeleton of the soil does not change throughout the process. Suffusion increases porosity n and permeability k and decreases the unit weight γ of the soil. Soil with a high coefficient of uniformity and especially gap-graded soils are endangered to be suffusive. In Fig. 1 the sub-types of suffusion (a) inner, (b) outer and (c) contact suffusion type 1/1 (same types as for contact erosion, see Fig. 2 and Tab. 1) are shown. (Busch et al. 1993)
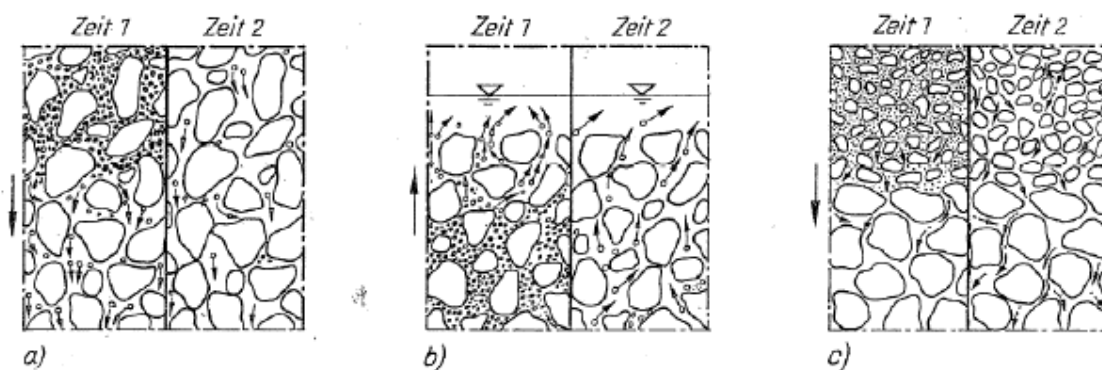
Fig. 1   Sub-types of suffusion (Busch et al. 1993) cf. (Ziems 1969)

In the special case of the contact zone between the stone column and the cohesive material there is more an erosion than a suffusion problem. Therefore, there are no further explanations about the verification of suffusion. (A summary of common criteria for suffusion is available by BAW (2013b).)

2.2 Definition of contact erosion

Erosion is the transport and/or rearrangement of all soil particles. There are different sub-types of erosion (shown in Fig. 2), like outer (a), inner (b), joint (c) or contact (d) erosion.
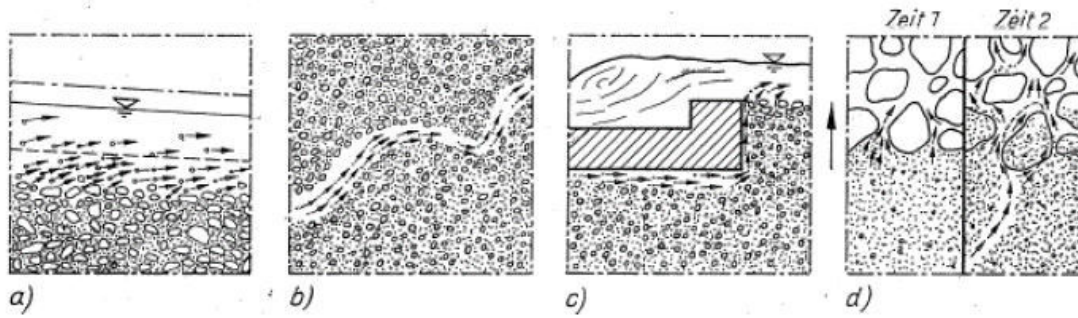
Fig. 2   Sub-types of erosion (Busch et al. 1993) cf. (Ziems 1969)

Contact erosion (shown in Fig. 2 d) and Fig. 3), also called clogging, internal erosion or sometimes even piping (in German this phenomenon is called "Kontakterosion"), starts at the border of two soil layers, e.g. a coarse- and a fine-grained soil. The soil particles of the finer soil are transported into the pore space of the coarse layer; that could lead to changes in the grain structure and may result in settlements. (Busch et al. 1993)
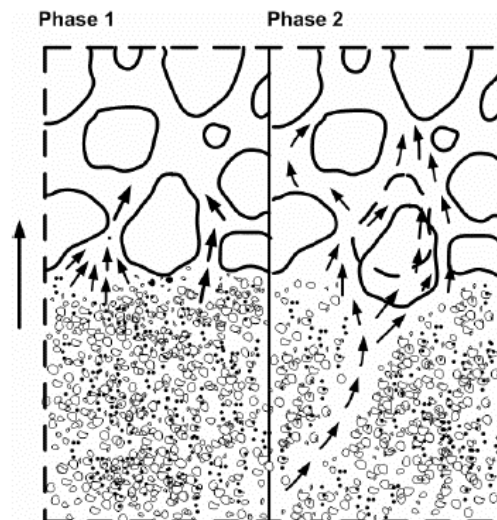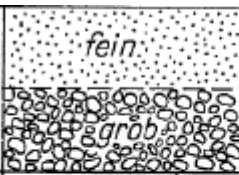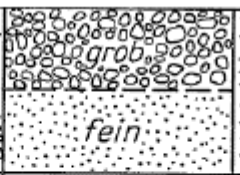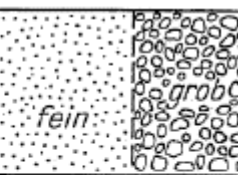
Fig. 3   Contact erosion due to hydraulic seepage (Schmitz 2007)

Additionally, Busch et al. (1993) defined the main types of contact erosion due to seepage direction, which are shown in Tab. 1. The green marked types are the most important cases in Geotechnical Engineering, the red marked describes the special case of this thesis. For verification of safety against contact erosion filter criteria are used.

Tab. 1   Main types of contact erosion due to seepage direction (Busch et al. 1993)

2.3 General information about filter design to prevent contact erosion

A filter must provide a high permeability, but also has to build up a stable well-distributed grain-pore-structure to prevent base material transport through the filter, e.g. clogging or instability of the filter material structure itself. There are two categories of filter criteria, which ensure these properties: (a) geometric and (b) hydraulic criteria. These criteria should prevent or reduce material transport in the soil to an acceptable level. Most geometric criteria are defined by a specific grain diameter or a certain pore diameter. In literature, many of geometric criteria depending only on the geometry of filter and base material can be found. Unfortunately, most criteria are only suitable for non-cohesive soils. For cohesive soils, criteria from research papers have to be considered. These criteria provide verification formulas for the critical hydraulic gradient, which are based on the acting forces. (Schmitz 2007). If particle transport is geometrically possible and a seepage force with a certain value is available, material transport will occur. The hydraulic criteria are generally defined by a critical hydraulic gradient (Busch et al. 1993) & (BAW 2013b).

In non-cohesive soils, the potential risk of material transport is higher because there are no "bonding-forces" - such as physical and/or chemical forces - between the particles. If the structure of the pores of the filter material has certain properties, free movement of grain particles from the base material to the filter material is possible. In cohesive soils, however, the particles are bound due this already mentioned forces, but along weak zones, e.g. at borders between different layers of soils, soil aggregates could form and start to move. In general, the risk of material transport in cohesive soils is much lower than in non-cohesive soils. (BAW 2013b)

Since in most cases the grain size distribution can be examined easily, the geometrical criteria are often used and therefore well-known. (Heibaum 2001) In practical

engineering, geometrical criteria which were developed for non-cohesive soils, were also used for cohesive soils. (Biswas 2005) & (Locke 2001) This led to a conservative filter design because cohesive soils have a higher resistance against erosion, as discussed before. With decreasing grain diameter, the result of these geometrical criteria is becoming more and more conservative. At lower grain sizes, the filtration process is influenced by hydrodynamic effects (Witt & Brauns 1988). Also, Sherard et. al (1984a), Sherard et. al (1984b), Biswas (2005), Locke (2001) and Dar (2006) agree that the conventional geometrical filter criteria (originally developed for non-cohesive soils) are relative conservative for intact fine grained cohesive soils. Unfortunately, (Biswas 2005) cf. Vaughan (2000) and also Dar (2006) mention that design criteria for non-cohesive soils used for cohesive soils may become non-conservative, if cracks occur in cohesive soils – that could change the entire filtration design process.

2.4 Geometrical criteria for contact erosion

Geometrical criteria depend only on the grain size distributions (GSD) of the base and the filter material. Many of these geometrical criteria were developed empirically using laboratory tests. (Dar 2006), (Locke 2001)

At naturally-grown layer-borders no verification against contact erosion is necessary, but at man-made filtration-borders the criteria for contact erosion have to be fulfilled. In Tab. 2 an overview of geometrical filter criteria for contact erosion (recommended by (BAW 2013b)) is given.

Tab. 2   Overview of geometrical criteria for contact erosion

Criteria	Assumption	Application limits
Terzaghi	Based on distance ratio	Non-cohesive materials (uniform sands), $C_U<2$, $i≤8$
Cistin & Ziems	Based on distance ratio	Recommended for non-cohesive materials, $C_{U,B}≤20$, $C_{U,F}≤18$, $i≤9$, $d_F≤100$ mm
Lafleur	A few fine particles are always washed out at the border between two soils	Non-cohesive materials, also for suffusive soils, $i≤8$, grain size diameter restrictions
Myogahara	Considers that in pore space of very coarse particles turbulent stream is possible at low hydraulic gradients	Non-cohesive materials, for scour protection between very coarse particles

Sherard	Based on stream channel of 1 to 10 mm diameter and water pressure of approximately 4 bar	Cohesive materials, especially in case of potential cracks in the less permeable material

2.4.1 Terzaghi/Peck (1961)

This criterion (Equ. (1)) is one of the first popular filter criteria and is therefore well-known and often used. Sherard et a. (1984a) showed that in laboratory tests using sand and gravel the filter fails approximately at $d_{15,F}/d_{85,B} = 9$, which proves that the criterion is conservative.

$$\frac{d_{15,F}}{d_{85,B}} \leq 5$$

(1)

$d_{15,F}$ [-]   particle diameter at the filter material at 15 mass %

$d_{85,B}$ [-]   particle diameter at the base material at 85 mass %

Application limits of Terzaghi/Peck method: The method is only valid for uniform non-cohesive soils (base and filter) with $C_U < 2$ and a hydraulic gradient $i \leq 8$.

Terzaghi/Peck's method cannot be used for the contact erosion problem between the gravel column and the base material because one material is cohesive and the other is non-cohesive. Additionally, the coefficient of uniformity of the base material is too high ($C_{U,B} = 8$, see Chapter 3).

2.4.2 Cistin & Ziem's method (BAW 2013b)

This method is recommended for suffusion and contact erosion between two non-cohesive soils. As literature ((Sherard et al. 1984a), (Sherard et al. 1984b), (Locke 2001), (Biswas 2005), (Dar 2006)) shows geometric criteria are often used for non-cohesive soils and therefore this criterion is also used in the course of the presented project for the border between a cohesive and a non-cohesive soil layer.

Contact erosion is geometrically not possible if $A_{50,vorh} \leq A_{50,zul}$ is valid. The existing distance ratio $A_{50,vorh}$ is calculated using Equ. (2). The admissible distance ratio $A_{50,zul}$ is read off the diagram in Fig. 4.

$$A_{50,vorh} = \frac{d_{50,F}}{d_{50,B}}$$

(2)

$d_{50,F}$ [-] particle diameter of the filter material at 50 mass %

$d_{50,B}$ [-] particle diameter of the base material at 50 mass %
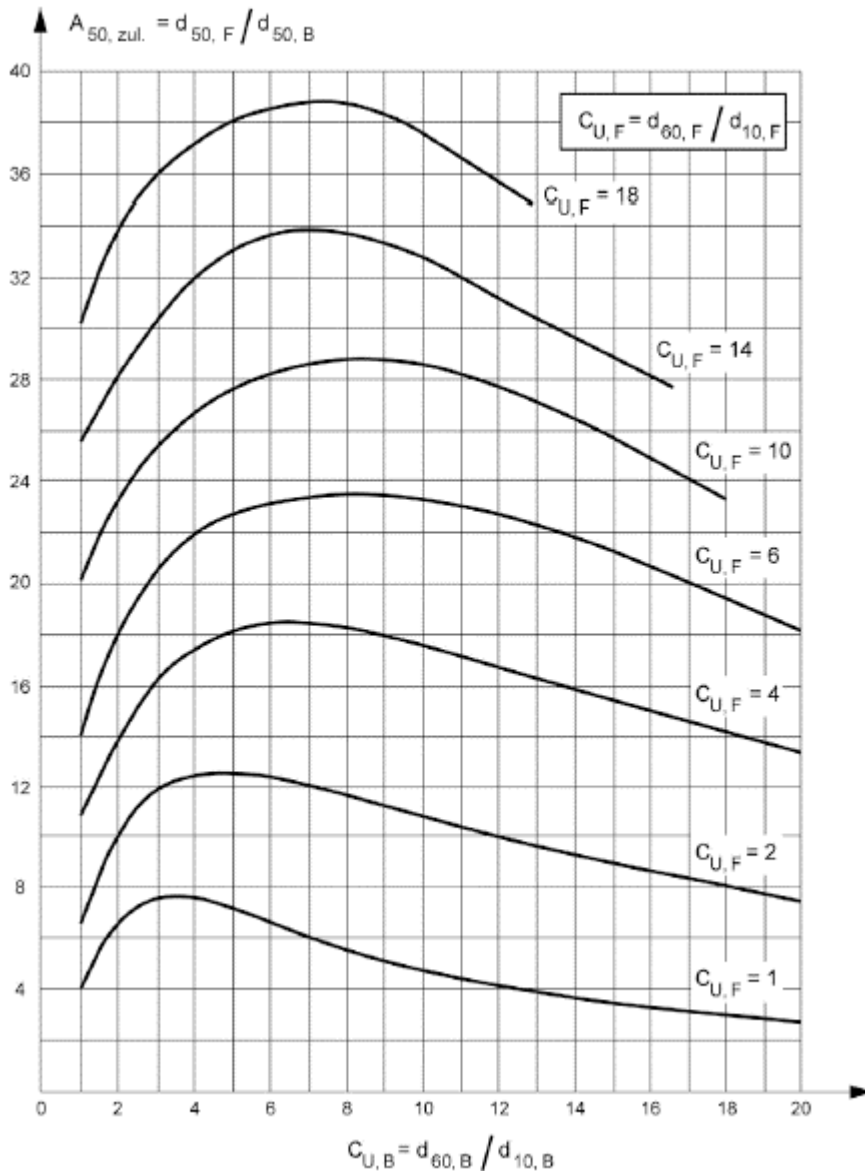
Fig. 4 Admissible distance ratio $A_{50,zul}$ after Cistin & Ziems (BAW 2013b)

Application limits for Cistin & Ziem's method: The method shall be used for non-cohesive base materials with $C_{U,B} \leq 20$ and for filters with $C_{U,F} \leq 18$. The filter material grain size has to fulfil grain size of $d_i \leq 100\ mm$. The hydraulic gradient has to be lower than nine and both soils have to be non-suffusive (explanation see chapter 2.1). The verification is valid for all flow directions.

Cistin & Ziem's method is only recommend for non-cohesive soils which fulfil $C_{U,B} \leq 20, C_{U,F} \leq 18,\ i \leq 9, and\ d_F \leq 100\ mm$. Generally, the method is not suitable for the contact erosion problem between the stone column and the cohesive base material, but the criterion is used to get an idea about the problem. As literature shows, criteria for

non-cohesive soils were also used for cohesive ones – this leads to a conservative solution ((Sherard et al. 1984a), (Sherard et al. 1984b), (Biswas 2005), (Locke 2001), (Dar 2006)).

2.4.3   Lafleur

BAW (2013b) cf. Lafleur et al. (1993) describes that at the contact between base and filter material always some fine particles get washed out. It depends on the specific combination of the GSD of the two soils, if the pore-particle-structure is stable, although some particles get washed out.

Application limits for Lafleur's method: The method is based on experiments with non-cohesive soils with a maximum 40 mass % of fines and a hydraulic gradient i ≤ 8. Additionally, there are grain size restrictions (filter: $0.06 < d_F < 50\ mm,\ d_{15,F} > 0.2\ mm$, base: $d_B < 50\ mm$).

Lafleur's method cannot be used for the contact erosion problem between the gravel column and the base material, because one material is cohesive and the other is non-cohesive.

2.4.4   Myogahara

BAW (2013b) cf. Myogahara (1993) is a contact erosion criterion between very coarse layers. It is considered that in the pore space of very coarse particles turbulent stream is possible, even at low hydraulic gradients.

Application limits for Myogahara's method: The method is only for very coarse non-cohesive soils, e.g. for scour protection.

Myogahara's method cannot be used for the contact erosion problem between the gravel column and the base material, because both soils are not coarse and the base is cohesive.

2.4.5   Sherard (Sherard & Dunnigan 1989)

The considered soil has to be cohesive, otherwise this method must not be used. All particles with sizes $d_B > 4.75$ mm have to be excluded from calculation. For the rest of the verification only the finer part ($d_{100,B}$ = 4.75 mm) is used. In the next step, the appropriate soil category has to be selected from Tab. 3 and the corresponding criteria have to be fulfilled.

Tab. 3   Soil categories and criteria acc. to Sherard (1989)

Soil category	Description	Criteria
Soil category 1	$d_{85,B}$ < 0.074 mm	$d_{15,F} \leq 9 \cdot d_{85,B} \; und \; d_{15,F} > 0.2 \; mm$
Soil category 2	$d_{40,B}$ < 0.074 mm $d_{85,B}$ ≥ 0.074 mm	$d_{15,F} = 0.07 \; mm$
Soil category 3	$d_{15,B}$ < 0.074 mm $d_{40,B}$ ≥ 0.074 mm	$d_{15,F} \leq \dfrac{40 - F_{0.074}}{40 - 15} \cdot (4 \cdot d_{85} - 0.7) + 0.7$ $F_{0.074}$ is the mass % of soil with d_B < 0.074 mm without grains d_B > 4.75 mm

Index F…filter (coarse grained soil)

Index B…base material (finer material)

<u>Application limits for Sherard's method</u>: The method can be used only for cohesive soils, especially if they have a risk of crack growing. (BAW 2013b)

Sherad's method is used for the geometric verification of the contact erosion problem between the stone column and the cohesive material, because the problem is within the recommend application limits.

2.5 Hydraulic criteria

Generally valid hydraulic criteria for contact erosion do not exist. Many of scientific hydraulic criteria from research papers are not well known in practical engineering and therefore not used on a daily basis. For using the appropriate criterion, the water flow direction relative to the layer orientation has to be considered. Many hydraulic criteria were developed and presented in papers over time, but all of them have very special limits of application, e.g. just valid for upwards or horizontal flow or only for specific soil types.

The factor of safety against contact erosion is defined in Equ. (3) by Busch et al. (1993).

$$\eta_{KE,H} = \frac{i_{KE,krit}}{i_{I,vorh}} \tag{3}$$

$\eta_{KE,H}$ [-]   hydraulic safety against contact erosion

$i_{KE,krit}$ [-]   critical hydraulic gradient in base material

$i_{I,vorh}$ [-]   present hydraulic gradient in base material

In Tab. 4 a summary of hydraulic criteria for contact erosion for type 3/3 (acc. to Tab. 1) is shown.

Tab. 4   Overview of hydraulic criteria for contact erosion for perpendicular flow direction (type 3/3)

Criteria	Assumption	Application limits
Zweck/Davidenkoff[1,2]	Based on mean grain diameter of base and filter material	For Type 3/3, non-cohesive uniform soils ($C_{U-B,F}<2$), no vibrations, no water pulsation, stationary flow
Davidenkoff[6,7]	Based on assumption that cohesive soil aggregate gets teared out of the rest of the soil mass by the hydraulic force	For toe filter in cohesive dams[7], for flow direction perpendicular to the layer direction, border between non-cohesive and cohesive soils[6]
Muckenthaler[3]	Based on critical flow velocity for sediment transport at river soles by Shields and Bonnefille (1936), high influence of geometric effects	Type 3/3
Istomina[2,6]	Based on laboratory tests with constant and step-wise increased hydraulic gradient	For cohesive soils, for parallel[2] and perpendicular[3] flow direction, only approximation[2]
Rehfeld[6]	Based on Davidenkoff, tensile strength of cohesive material is important	High variation of pore diameter $\rightarrow$ high variation of result
Jung[6]	Based on Rehfeld, undrained shear strength of cohesive material is important	Only clay with $\gamma=12$ kN/m³
Zou[5,6]	Stress-dependent critical gradient	Only for highly plastic clay from Hambach and vertical (perpendicular to layer direction) flow through layers
Schmitz[6]	Based on Zou	Generally valid for clay & silt, only for vertical (perpendicular to layer direction) flow through layers, interpretation of parameters for calculation is difficult

[1]   (Busch et al. 1993) cf. (Davidenkoff 1967)

[2]   (Henzinger 2009) cf. (Busch et al. 1993)

[3]   (Henzinger 2009) cf. (Muckenthaler 1989)

[5]   (Zou 2000)

6   (Schmitz 2007) cf. (Davidenkoff 1964)

7   (Davidenkoff 1964)

In the next chapters, the assumptions and application limits of the different hydraulic criteria from Tab. 4 are described.

2.5.1   Zweck/Davidenkoff

Zweck (1958) used different sands as base materials and different types of gravel as filter materials in the laboratory tests.

Davidenkoff (1967) defined the difference between the critical hydraulic gradient for the start of particle transport ($i_{crit,transport}$) and for the initiation of crack propagation ($i_{crit,fracture}$) (shown in Fig. 5). In fact, there are only recommendations available for base material with d > 0.06 mm. Davidenkoff (1967) defined the distance ratio in Equ. (4).

$$A_{50} = \frac{d_{50,F}}{d_{50,B}}$$

(4)

A_{50} [-]   distance ratio

$d_{50,F}$ [-]   filter diameter at 50%

$A_{50,B}$ [-]   base material diameter at 50%

In Fig. 5 it is shown that the critical hydraulic gradient for particle transport $i_{crit.transport}$ is always lower than the critical gradient for crack propagation $i_{crit.fracture}$.
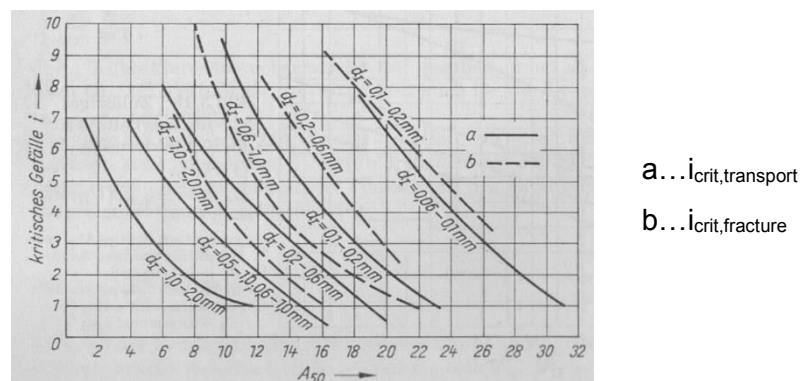
Fig. 5   Critical hydraulic gradient in base material (I) for contact erosion type 3/3 (Busch et al. 1993)

<u>Application limits for Zweck/Davidenkoff's method:</u> Busch et al. (1993) recommend this method for type 3/3 (acc. to Tab. 1) in uniform non-cohesive soils with $C_{U,B}$<2 and $C_{U,F}$<2

with no vibrations or water pulsation. The criterion should only be used at stationary flow conditions.

Zweck/Davidenkoff's method is not suitable for the contact erosion problem between stone columns in cohesive material, because it's use is only recommended for type 3/3 (acc. to Tab. 1) in non-cohesive uniform materials ($C_{U-B,F}$<2).

2.5.2 Davidenkoff

Davidenkoff (1964) introduced a method for design of filters around a toe drainage at the airside of a dam in cohesive material (shown in Fig. 6). The idea is based on the assumption that cohesive soil particles are sticked together and if a seepage force is big enough not one particle gets washed out, but a larger soil aggregate. Equ. (5) is based on a limit equilibrium of a soil particle at the side MP (Fig. 6) of the toe drainage under gravity and seepage force through the dam.

Fig. 6   Toe drainage with filter at the air side of a dam (Davidenkoff 1964)

$$D = \frac{15 \cdot c_0}{\eta \cdot (\gamma' \cdot \cos(\bar{\alpha}) + \gamma_w \cdot i)}$$

(5)

D [-]   diameter of the soil particle of a filter, which can hold back a soil aggregate in a cohesive dam with tensile strength of c_0 and a degree of safety of η

c_0 [kN/m²]   tensile strength

η [-]   degree of safety

γ' [kN/m³]   unit weight of the soil under buoyancy

$\bar{\alpha}$.   [°]   angle between filter and base material (see Fig. 6)

γ_w [kN/m³]   unit weight of water

i   [-]   hydraulic gradient of the seepage flow at the dam toe

<u>Application limits for Davidenkoff's method:</u> Davidenkoff (1964) developed the method for filters around a toe drainage in dams out of cohesive soil and therefore it should be used only in similar conditions.

Davidenkoff's method is only valid for toe drainage filters (Davidenkoff 1964) and is therefore not used to quantify the contact erosion problem between stone columns and cohesive base material. Although Schmitz (2007) mentions a possible usage of the method for layer-normal flow through cohesive soil.

2.5.3 Muckenthaler

Henzinger (2009) cf. Muckenthaler (1989) recommends another criterion, which is based on the critical flow velocity for particle transport at river beds. With the nonlinear resistance formula of Kovacs, the critical hydraulic gradient in relation to the particle diameter and permeability can be calculated. This relationship is shown in Fig. 7 for permeability values of the coarser (involved) material from 10^{-4} to 10^{0} m/s. (For lower permeability no data is available.)
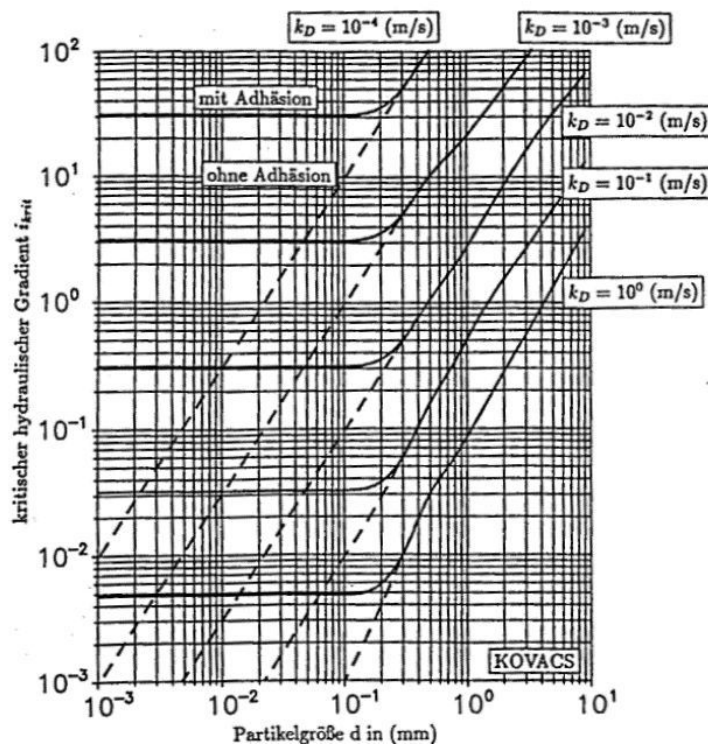
Fig. 7   Critical hydraulic gradient in base material for horizontal flow direction depending on particle size d and permeability k_D of the coarse bulk skeleton of the filter material (for n=0.35 and T=2/π) (Henzinger 2009)

A disadvantage of this criterion is the large influence of geometric effects, e.g. if particles of the base material are larger than the minimal pore diameters of the filter. In addition, the permeability of the preferred water flow paths in the base material has a large

influence on the critical gradient – this permeability can vary by a factor of 10 in comparison to other flow directions in the base soil. Therefore, the criterion should be used on the smallest and the largest particle diameter of the base material, in correlation with the permeability of the filter material to find the rage of the critical hydraulic gradient. (Henzinger 2009)

Application limits for Muckenthaler's method: This method is recommended for type 2/3 and 3/3 (acc. to Tab. 1). Due to lack of additional diagrams about other permeabilities and/or particle sizes the method is limited to the case, which is shown in Fig. 7.

Muckenthaler's method can be used to get a rough estimation for the contact erosion problem between the stone column and the cohesive base material, but due to uncertainties it has to be verified and compared to other methods.

2.5.4 Istomina

Schmitz (2007) describes the use of Istomina for perpendicular flow directions in general, but Henzinger (2009) recommends to use this criterion only for type 3/2 according to Tab. 1. The lab test procedure (shown in Fig. 8) models vertical flow perpendicular to the layers – so a further description of the criterion is not necessary, as the task of this thesis is the verification of contact erosion for gravel columns in fine grained soils. In such cases the flow direction is mainly horizontal.
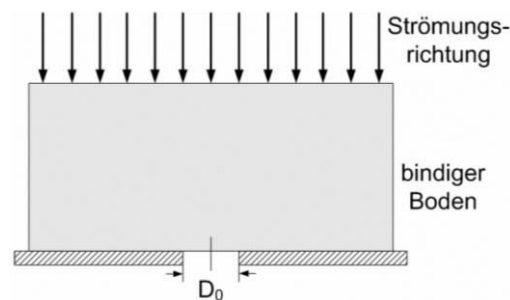
Fig. 8   Lab test procedure by Istomina (Schmitz 2007)

2.5.5 Rehfeld

Rehfeld (1967) based his criterion on Davidenkoff (1967). In his formulation, the critical hydraulic gradient mainly depends on the tensile strength c_0 of the cohesive material, the mean pore diameter (by Pavcic) and the inclination β_1 of the border between base and filter material. Rehfeld (1967) introduced partial safety factors in his calculations and noted that the usage of Pavcic' formula for the pore diameter may lead to a diameter variation of ± 100 %. Nevertheless, Pavcic' diameter provides a quantitative value for the contact erosion verification. In Fig. 9 the idea of Davidenkoff (1967) is shown. Using

Equ. (6), Rehfeld's critical gradient is calculated. Rehfeld (1967) outlines that the tensile strength (=suction) c_0 has the biggest influence on the deformation-resistance of the cohesive material. Especially for soil, it is very important to distinguish between shear and tension. In case of seepage, tension (=suction) is the main influence on the soil – aggregates of soil could be washed out by the seepage force. The tensile strength (=suction) of soil is highly dependent on the saturation level of the soil. Rehfeld (1967) mentions that laboratory tests on soils with very high saturation level often result in inexact tensile strength values. It is very important to gain proper values of the tensile strength (=suction) c_0 before using Rehfeld's criterion. Nevertheless, as a first approach $c_0 = c_s$ can be used (with caution).
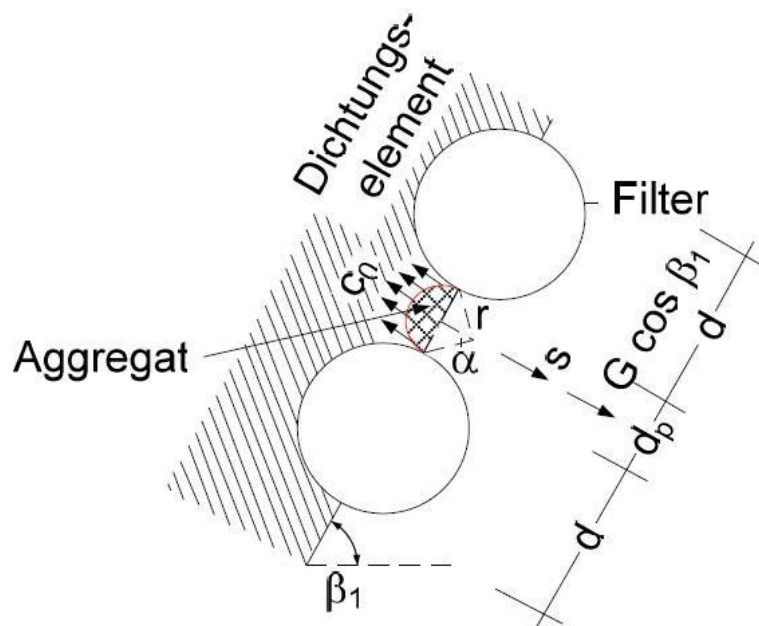
Fig. 9   Model of forces and geometry (Schmitz 2007) cf. Davidenkoff (1967)

$$i_{crit} = \frac{c_0}{4 \cdot d_p \cdot 1.1 \cdot \gamma_w} - \frac{\gamma \cdot \cos(\beta_1)}{1.1 \cdot \gamma_w} \qquad (6)$$

c_0	[kN/m²]	tensile strength
d_p	[cm]	decisive pore diameter by Pavcic
γ	[kN/m²]	unit weight of base material
γ_w	[kN/m³]	unit weight of water
β_1	[°]	inclination of border between base and filter material

Application limits for Rehfeld's method: The method is valid for contact erosion problems which include cohesive material. (Rehfeld 1967)

Rehfeld's method is used in this thesis to estimate the critical hydraulic gradient in the cohesive base material next to the stone columns, but the verification has to be examined carefully due to the uncertainties in the decisive pore diameter by Pavcic and the tensile strength c_0 of the cohesive material.

2.5.6 Jung

Schmitz (2007) cf. Jung (2000) defines an estimation of the critical hydraulic gradient only for clays with $\gamma' = 12\ kN/m^3$ under hydrostatic loading. The gradient depends on the pore diameter by Pavcic and the undrained shear strength c_u.

For the specific problem of this thesis this method is not used due to lack of data about the undrained shear strength c_u and its variation with depth.
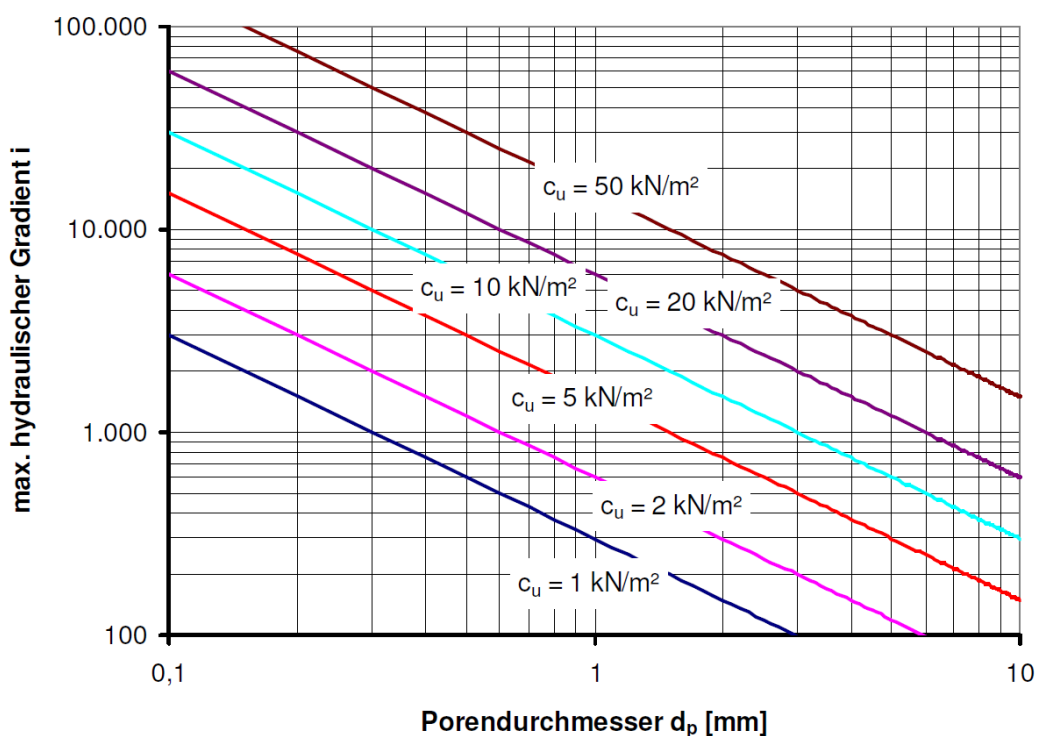
Fig. 10   Calculated hydraulic gradient for contact erosion due to hydrostatic loading (Schmitz 2007)

2.5.7 Zou

Zou (2000) defined a new stress-dependent approach to calculate the critical hydraulic gradient for perpendicular flows. He used clay from surface mining pit "Hambach" as base material and gravel, sand and punched filtration plates as filter material for his laboratory tests. In his model a circular load on top of a coarse-grained layer which lays above the fine-grained base material is defined.

The special case of this thesis does not fulfil the boundary conditions (vertical flow through a coarse grained non-cohesive and a fine grained cohesive soil) and the base material is not this special clay from "Hambach" – so Zou's method cannot be used.

2.5.8 Schmitz

Schmitz' idea (2007) is based on Zou (2000). Schmitz tried to develop a general criterion to calculate the stress-dependent critical hydraulic gradient at soil layer boundaries. He did many lab tests and numerical calculations to define his different factors, which are necessary for the calculation of i_{crit}.

This criterion does not fulfil the boundary conditions for the gravel column beneath a storage basin and is therefore not used.

2.6 Overview of filter criteria for contact erosion and suitability for gravel column beneath a storage basin

In Tab. 5 all mentioned criteria are summarized and their suitability for the specific problem (contact erosion between gravel columns and fine-grained soil) is evaluated.

Tab. 5   Overview of filter criteria for contact erosion of a gravel column beneath a storage basin

Type	Criteria	Suitability	Reason
Geometric	**Terzaghi/Peck**	-	Only for non-cohesive materials (uniform sands, $C_U < 2$, $i \leq 8$)
Geometric	**Cistin & Ziems**	+/-	Recommended for non-cohesive materials, ($C_{U,B} \leq 20$, $C_{U,F} \leq 18$, $i \leq 9$, $d_F \leq 100$ mm) → generally not suitable, but chosen geometric criterion to get an idea about the problem (earlier criteria for non-cohesive soils were also used for cohesive ones – this leads to an conservative solution) ((Sherard et al. 1984a), (Sherard et al. 1984b), (Biswas 2005), (Locke 2001), (Dar 2006))
Geometric	**Lafleur**	-	Only for non-cohesive materials ($i \leq 8$)

Geometric	**Myogahara**	–	Only for non-cohesive materials (scour protection - between very coarse particles)
Geometric	**Sherard**	+	For cohesive materials, for borders between coarse and fine grained material → suitable because of cohesive base material
Hydraulic	**Zweck/Davidenkoff**	–	For Type 3/3 in non-cohesive materials, uniform soils ($C_{U-B,F}<2$)
Hydraulic	**Davidenkoff**	–	Developed for toe drainage filters in dams out of cohesive material
Hydraulic	**Muckenthaler**	+/-	For Type 3/3, only for special cases diagram available, high influence of geometric effects → suitable because the problem is defined as type 3/3, but only one diagram for evaluation available
Hydraulic	**Istomina**	–	Only for vertical perpendicular flow direction (only approximation)
Hydraulic	**Rehfeld**	+	For cohesive material → suitable because of cohesive base material
Hydraulic	**Jung**	–	Only for clay with $\gamma=12$ kN/m³
Hydraulic	**Zou**	–	Only for highly plastic clay from Hambach & specific boundary condition (stress dependent shear and normal stress over depth)
Hydraulic	**Schmitz**	–	Only for clay & silt base material in specific boundary conditions (stress dependent shear and normal stress over depth)

+   criterion is suitable

-    criterion is not suitable

+/-   criterion is not suitable, but used to get an idea for the problem. If criteria for non-cohesive soils are used for cohesive soils, the result is generally conservative. ((Sherard et al. 1984a), (Sherard et al. 1984b), (Biswas 2005), (Locke 2001), (Dar 2006))

2.7 Empirical permeability formulation from the particle size distribution

For the further analyses of the problem of this thesis (pore water distribution around a stone column beneath a water storage basin) the permeability of the chosen column material, which is suitable for this case (see chapter 3), had to be examined. To get an idea about the range of the permeability a literature review was done.

Most of the permeability formulations have the same structure. They consist of an empirical established factor and a specific grain diameter of the grain size distribution, e.g. d_{10} or d_{20}.

Two well-known formulations (summarized in Tab. 6) to estimate the permeability, using the grain size distribution which are recommended by BAW (2013a) and Fuchs (2010) are used in this thesis. These formulations are within their specific application limits for the expected grain size distributions.

Tab. 6 Summary of two appropriate useful permeability formulation (Fuchs 2010), (BAW 2013a) (d in [mm], k in [m/s])

Method	Formulation	Suitable Soil	Application limits
Hazen (1893)	$k = c \cdot (d_{10})^2 \cdot (0.7 + 0.03 \cdot T_{GW})$ (7)	sand	$C_U < 5;$ $0.1\,mm < d_{10} < 3\,mm;$
Beyer (1964)	$k = c(C_U) \cdot (d_{10})^2$ (8)	sand and gravel	$C_U < 20;$ $0.06\,mm < d_{10} < 0.6\,mm;$ $2 \cdot 10^{-5}\,m/s < k < 4 \cdot 10^{-3}\,m/s$

Tab. 7 c-factor for Hazen (Fuchs 2010)

C_U	c
1.0 to 3.0	0.0139
3.0 to 5.0	0.0116

Tab. 8 c-factor for Beyer (BAW 2013a)

C_U	1.0-1.9	2.0-2.9	3.0-4.9	5.0-9.9	10.0-19.9	>20.0
$c(C_U)$	0.011	0.010	0.009	0.008	0.007	(0.006)

3 Suitable material for gravel column beneath a storage basin

In this chapter a suitable material for the use as a stone column beneath a storage basin is defined. The material has to be stable against contact erosion in combination with the existing base material at the construction site and the permeability of the chosen column material should be as high as possible. Therefore, the permeability of the examined material has to be calculated, using the formulas mentioned in Tab. 6.

3.1 Base material

In Fig. 11 a typical grain size distribution of the material beneath the water basin is shown. The material consists mainly of silt with small amounts of sand and clay.

part smaller than 0.002	clay	silt	sand	gravel
13.0%	13.0%	82.50%	4.50%	0.0%
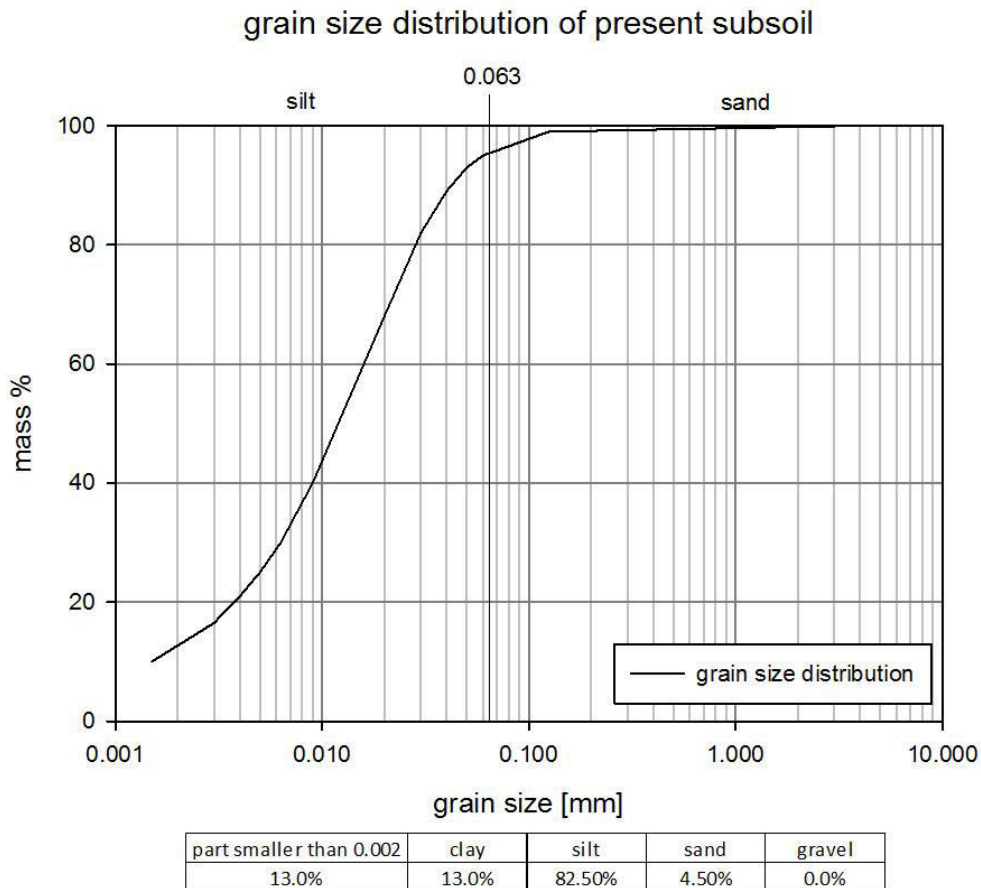
Fig. 11   Typical grain size distribution of the base material beneath the storage basin

Some additional information about the subsoil beneath the storage basin:

- Permeability: $k = 5 \cdot 10^{-5}\ to\ 5 \cdot 10^{-9}\ m/s$ depending on the layer, maybe anisotropic permeability conditions $(k_x > k_y)$

- Unit weight: unsaturated $\gamma_{unsat} \approx 19.0 \ kN/m^3$, saturated $\gamma_{sat} \approx 20.0 \ kN/m^3$

- Strength parameters: cohesion $c'_{ref} = 2 \ to \ 3 \ kN/m^2$, friction angle $\varphi' = 27.5 \ to \ 35°$ dilatancy angle $\psi = 0°$

- Stiffness parameters: $E_{Oed,up} \approx 35 \cdot 10^3 \ kN/m^2$. (This high stiffness is only valid in the upper sandy material (approximately upper 10 m below ground level)), $E_{Oed,low} \approx 12 \ to \ 15 \cdot 10^3 \ kN/m^2$ (In deeper layers the amount of silt is increasing and the stiffness is decreasing.)

3.2 Suitable gravel column material

In the chapters 3.2.1 and 3.2.2 different grain size distribution were examined to find a suitable material for the stone column in this specific base soil. The goal was to find a suitable area between the upper and lower grain size distribution (= upper and lower boundary), which is suitable for this case and then to determine the different permeability values of the boundaries.

3.2.1 Suitability of the uniform middle sand (lower boundary)
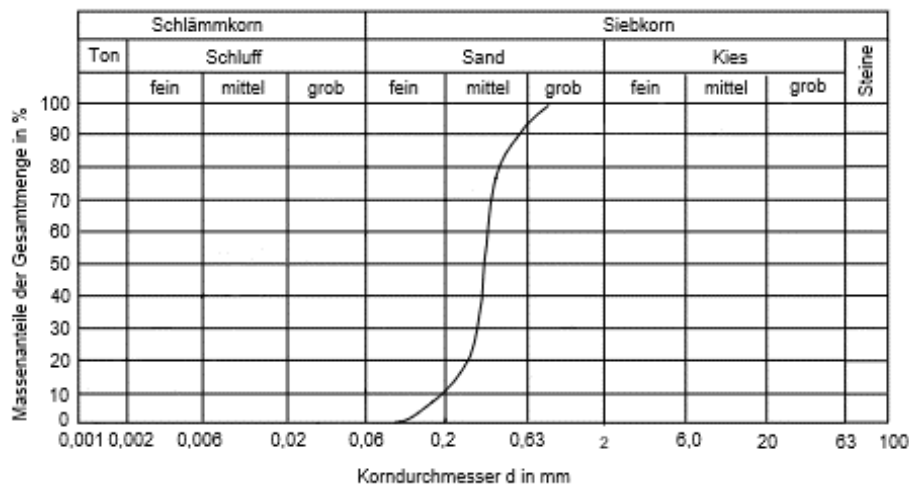
Fig. 12   Lower border of suitable material – uniform middle sand

- **Cistin & Ziem's method:**

Base material: $C_{U.B} = \frac{d_{60}}{d_{10}} = \frac{0.012}{0.0015} = 8 \leq 20$ ✓   (9)

Filter material – uniform middle sand: $C_{U.F} = \frac{d_{60}}{d_{10}} = \frac{0.40}{0.20} = 2 \leq 18$ ✓   (10)

$$d_{i,F} = 0.01 \ to \ 0.8 \ mm < 100 \ mm \ ✓$$ (11)

$$A_{50,vorh} = \frac{d_{50,F}}{d_{50,B}} = \frac{0.38}{0.15} = 2.53 < A_{50,zul} \cong 11.9 \ (see\ \text{Fig. 13}) \ \checkmark \tag{12}$$

Remark: Method is developed for non-cohesive granular soils.
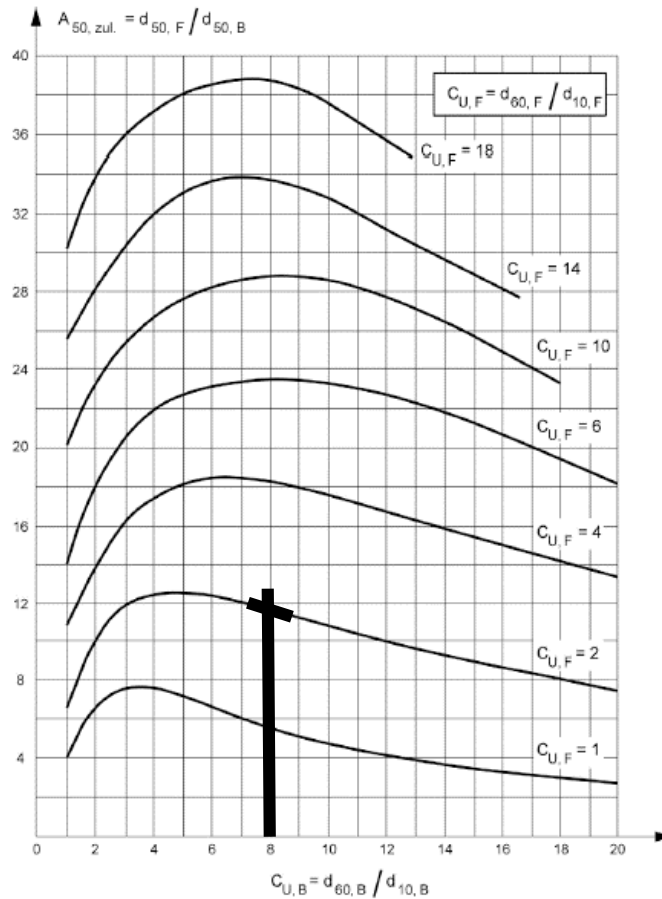
Fig. 13   Specific admissible distance ratio $A_{50,zul}$ after Cistin & Ziems for uniform middle sand (BAW 2013b)

- **Sherard's method:**

$$d_B < 4{,}75 \ mm \ \checkmark \tag{13}$$

$$d_{85,B} = 0.035 \ mm < 0.074 \ mm \rightarrow Category \ 1 \tag{14}$$

$$Category\ 1{:}\ d_{15,F} = 0.25 \ mm \ \leq 9 \cdot d_{85,B} = 9 \cdot 0.035 = 0.32 \ mm \ \checkmark \tag{15}$$

$$d_{15,F} = 0.25 \ mm > 0.2 \ mm \ \checkmark \tag{16}$$

- **Muckenthaler's method:**

$assumption: k_{D,Filter} = 10^{-4}\, m/s \;(probably\; even\; smaller, but\; no\; diagram\; available)$

$$d_{0\%} < 1.5 * 10^{-3} mm \rightarrow 10^{-3} mm \Longrightarrow i_{crit,with\; ad} = 30\; [-] \qquad (\,17\,)$$

$$\Longrightarrow i_{crit,without\; ad} = 10^{-2}\; [-] \qquad (\,18\,)$$

$$d_{100\%} = 1.25 * 10^{-1} mm \rightarrow 10^{-1} mm \Longrightarrow i_{krit,with\; ad} = 30\; [-] \qquad (\,19\,)$$

$$\Longrightarrow i_{krit,without\; ad} = 10\; [-] \qquad (\,20\,)$$
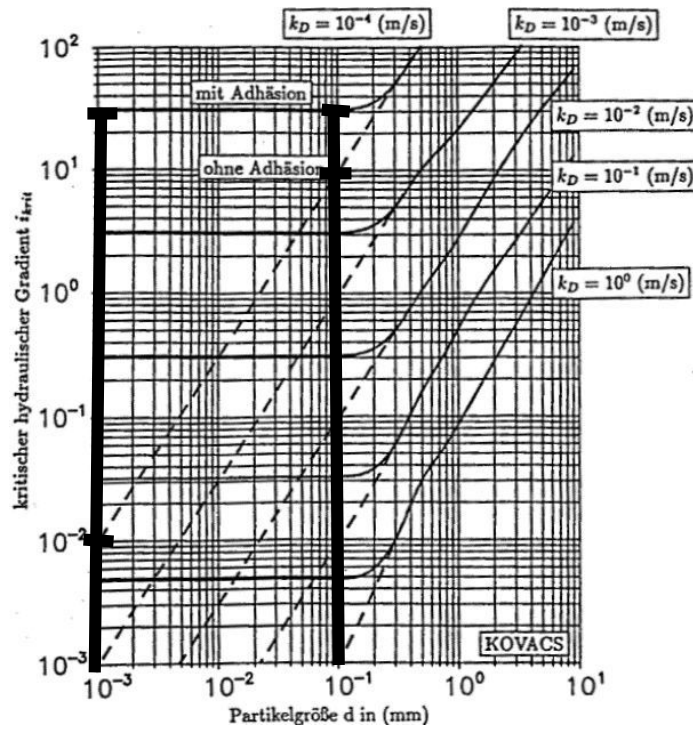
Fig. 14　Evaluation of critical hydraulic gradient in base material for horizontal flow direction depending on particle size d and permeability k_D of the coarse bulk skeleton of the filter material (for n=0.35 and T=2/π) (Henzinger 2009)

The significance of this method must be checked due to the assumptions for the permeability of the base material.

- **Rehfeld's method:**

$$i_{crit} = \frac{c_0}{4 \cdot d_p \cdot 1.1 \cdot \gamma_w} - \frac{\gamma \cdot \cos(\beta_1)}{1.1 \cdot \gamma_w} \qquad (\,21\,)$$

$$Pavcic: d_p = 0.535 \cdot \sqrt[6]{C_U} \cdot e \cdot d_{17} = 0.535 \cdot \sqrt[6]{2} \cdot 0.6 \cdot 0.27 = 0.097 \cong 0.1\; mm \qquad (\,22\,)$$

$$\beta_1 = 90° \rightarrow \cos(\beta_1) = 0 \qquad (\,23\,)$$

$$c' = 3 - 5 \frac{kN}{m^2} \rightarrow assume: c' = c_0 \tag{24}$$

$$i_{crit} = \frac{3}{4 \cdot 0.1 \cdot 1.1 \cdot 10} \cong 0.68 \tag{25}$$

$$i_{crit} = \frac{5}{4 \cdot 0.1 \cdot 1.1 \cdot 10} \cong 1.14 \tag{26}$$

- **Filter permeability estimation:**

Hazen: $k = c \cdot \left(d_{10\,[mm]}\right)^2 \cdot \left(0.7 + 0.03 \cdot T_{GW\,[°]}\right)\ [m/s] \tag{27}$

$$0.1\,mm < d_{10} < 3\,mm \rightarrow d_{10} = 0.2\,mm\ \checkmark \tag{28}$$

$$C_U < 5 \rightarrow C_{U,F} = 2 < 5\ \checkmark \tag{29}$$

$$choose\ from\ (\text{Tab.}\,7)\!: 1.0 < C_U < 3.0 \rightarrow c = 0.0139 \tag{30}$$

$$k_{sand,10°} = 0.0139 \cdot (0.2)^2 \cdot (0.7 + 0.03 \cdot 10) = 5.56 \cdot 10^{-4}\,m/s \tag{31}$$

$$k_{sand,15°} = 0.0139 \cdot (0.2)^2 \cdot (0.7 + 0.03 \cdot 15) = 6.39 \cdot 10^{-4}\,m/s \tag{32}$$

$$k_{sand,20°} = 0.0139 \cdot (0.2)^2 \cdot (0.7 + 0.03 \cdot 15) = 7.23 \cdot 10^{-4}\,m/s \tag{33}$$

$$\boldsymbol{k_{Hazen,mean} \cong 6.4 \cdot 10^{-4}\,m/s} \tag{34}$$

Beyer: $k = c(C_U) \cdot (d_{10\,[mm]})^2\ [m/s] \tag{35}$

$$0.06\,mm < d_{10} < 0.6\,mm \rightarrow d_{10} = 0.2\,mm\ \checkmark \tag{36}$$

$$C_U < 20 \rightarrow C_{U,F} = 2 < 20\ \checkmark \tag{37}$$

$$choose\ from\ (\text{Tab.}\,8)\!: C_U = 2 \rightarrow c = 0.010 \tag{38}$$

$$k_{sand} = 0.010 \cdot 0.2^2 = 4 \cdot 10^{-4}\,m/s \tag{39}$$

$$2 \cdot 10^{-5}\,m/s < k < 4 \cdot 10^{-3}\,m/s\ \checkmark \tag{40}$$

$$\boldsymbol{k_{Beyer} = 4 \cdot 10^{-4}\,m/s} \tag{41}$$

3.2.2 Suitability of the sandy gravel (upper boundary)
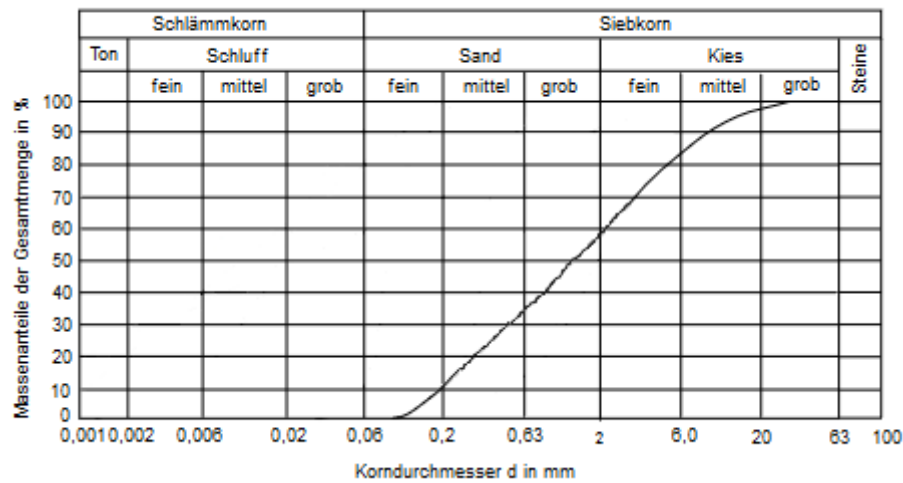
Fig. 15　　Upper border of suitable material – sandy gravel

- **Cistin & Ziem's method:**

Base material: $C_{U.B} = \frac{d_{60}}{d_{10}} = \frac{0.012}{0.0015} = 8 \leq 20 ✔$ (42)

Filter material – sandy gravel: $C_{U.F} = \frac{d_{60}}{d_{10}} = \frac{2.00}{0.20} = 10 \leq 18 ✔$ (43)

$$d_{i,F} = 0.01 \; to \; 30 \; mm < 100 \; mm ✔$$ (44)

$$A_{50,vorh} = \frac{d_{50,F}}{d_{50,B}} = \frac{1.00}{0.15} = 6.67 < A_{50,zul} \cong 26.5 ✔$$ (45)

Remark: Method is developed for non-cohesive granular soils
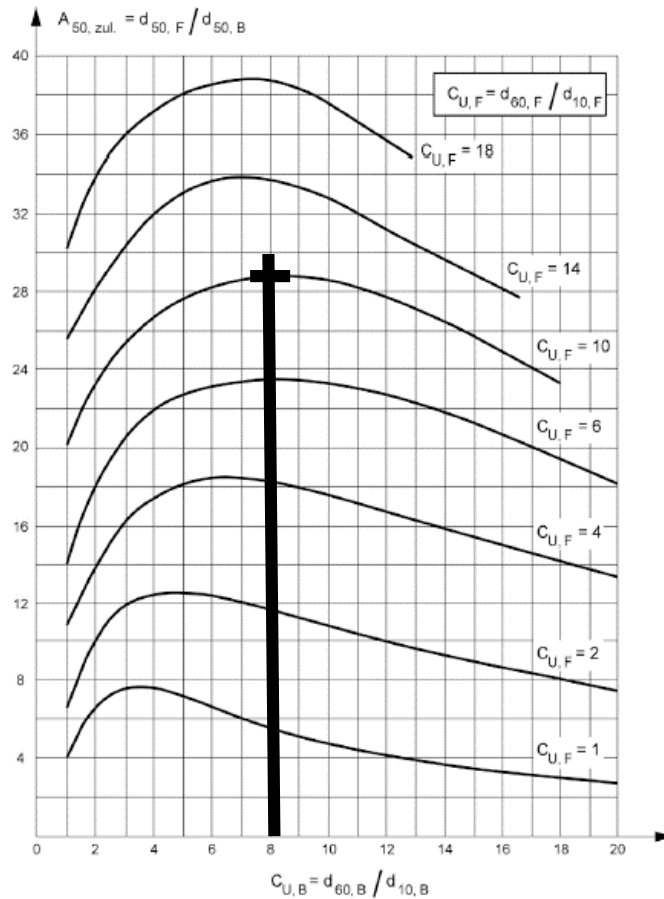
Fig. 16   Specific admissible distance ratio $A_{50,zul}$ after Cistin & Ziems for sandy gravel (BAW 2013b)

- **Sheard's method:**

$$d_B < 4{,}75 \; mm \; \checkmark \tag{46}$$

$$d_{85,B} = 0.035 \; mm < 0.074 \; mm \rightarrow Category \; 1 \tag{47}$$

$$Category \; 1: d_{15,F} = 0.30 \; mm \; \leq 9 \cdot d_{85,B} = 9 \cdot 0.035 = 0.32 \; mm \; \checkmark \tag{48}$$

$$d_{15,F} = 0.30 \; mm > 0.2 \; mm \; \checkmark \tag{49}$$

- **Muckenthaler's method:**

$$assumption: k_{D,Filter} = 10^{-4} \; m/s \; (probably \; even \; smaller, but \; no \; diagram \; available)$$

$$d_{0\%} < 1.5 * 10^{-3} mm \rightarrow 10^{-3} mm \Longrightarrow i_{krit,with \; ad} = 30 \; [-] \tag{50}$$

$$\Rightarrow i_{krit,without\ ad} = 10^{-2}\ [-] \tag{51}$$

$$d_{100\%} = 1.25 * 10^{-1} mm \rightarrow 10^{-1} mm \Rightarrow i_{krit,with\ ad} = 30\ [-] \tag{52}$$

$$\Rightarrow i_{krit,without\ ad} = 10\ [-] \tag{53}$$
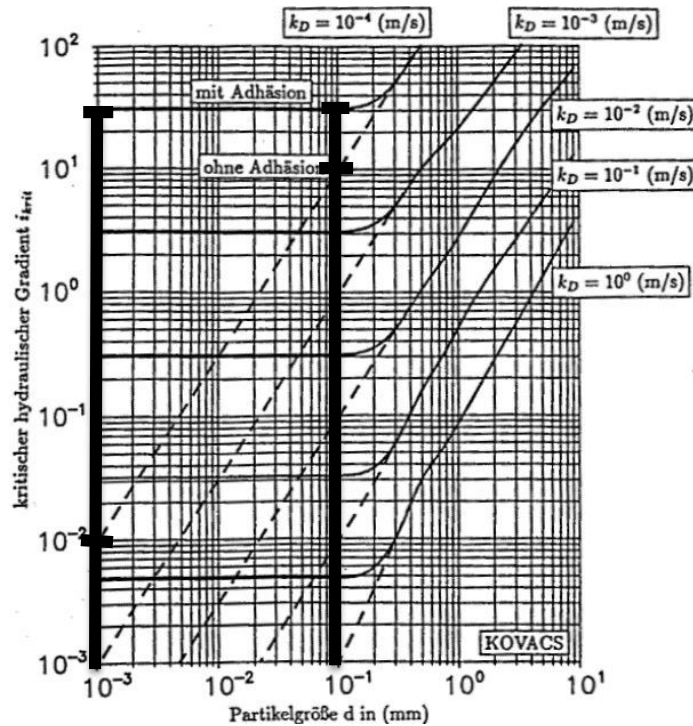
Fig. 17 Evaluation of critical hydraulic gradient in base material for horizontal flow direction depending on particle size d and permeability k_D of the coarse bulk skeleton of the filter material (for n=0.35 and T=2/π) (Henzinger 2009)

The significance of this method has to be checked due to assumptions for the permeability.

- **Rehfeld's method:**

$$i_{crit} = \frac{c_0}{4 \cdot d_p \cdot 1.1 \cdot \gamma_w} - \frac{\gamma \cdot cos(\beta_1)}{1.1 \cdot \gamma_w} \tag{54}$$

$$Pavcic: d_p = 0.535 \cdot \sqrt[6]{C_U} \cdot e \cdot d_{17} = 0.535 \cdot \sqrt[6]{10} \cdot 0.63 \cdot 0.27 = 0.131\ mm \tag{55}$$

$$d_p \cong 0.13\ mm \tag{56}$$

$$\beta_1 = 90° \rightarrow cos(\beta_1) = 0 \tag{57}$$

$$c' = 3 - 5 \ kN/m^2 \rightarrow \ assume: c' = c_0 \tag{58}$$

$$i_{crit} = \frac{3}{4 \cdot 0.13 \cdot 1.1 \cdot 10} \cong 0.52 \tag{59}$$

$$i_{crit} = \frac{5}{4 \cdot 0.13 \cdot 1.1 \cdot 10} \cong 0.87 \tag{60}$$

- **Filter permeability estimation:**

Hazen: $k = c \cdot \left(d_{10 \ [mm]}\right)^2 \cdot \left(0.7 + 0.03 \cdot T_{GW \ [°]}\right) \ [m/s]$ $\tag{61}$

$$0.1 \ mm < d_{10} < 3 \ mm \rightarrow \ d_{10} = 0.2 \ mm \ ✓ \tag{62}$$

$$C_{U,F} < 5 \rightarrow C_{U,F} = 10 \not< 5 \ ✗ \tag{63}$$

$$choose \ from \ (Tab. 7): 3.0 < C_U < 5.0 \rightarrow c = 0.0116 \tag{64}$$

$$k_{sandy \ gravel,10°} = 0.0116 \cdot (0.2)^2 \cdot (0.7 + 0.03 \cdot 10) = 4.64 \cdot 10^{-4} \ m/s \tag{65}$$

$$k_{sandy \ gravel,15°} = 0.0116 \cdot (0.2)^2 \cdot (0.7 + 0.03 \cdot 15) = 5.34 \cdot 10^{-4} \ m/s \tag{66}$$

$$k_{sandy \ gravel,20°} = 0.0116 \cdot (0.2)^2 \cdot (0.7 + 0.03 \cdot 20) = 6.03 \cdot 10^{-4} \ m/s \tag{67}$$

$$\boldsymbol{k_{Hazen,mean} \cong 5.3 \cdot 10^{-4} \ m/s} \tag{68}$$

Beyer: $k = c(C_U) \cdot (d_{10 \ [mm]})^2 \ [m/s]$ $\tag{69}$

$$0.06 \ mm < d_{10} < 0.6 \ mm \rightarrow \ d_{10} = 0.2 \ mm \ ✓ \tag{70}$$

$$C_U < 20 \rightarrow C_{U,F} = 10 < 20 \ ✓ \tag{71}$$

$$choose \ from \ (Tab. 8): C_U = 10.5 \rightarrow c = 0.007 \tag{72}$$

$$k_{sandy \ gravel} = 0.007 \cdot 0.2^2 = 2.8 \cdot 10^{-4} \ m/s \tag{73}$$

$$2 \cdot 10^{-5} \ m/s < k < 4 \cdot 10^{-3} \ m/s \ ✓ \tag{74}$$

$$\boldsymbol{k_{Beyer} = 2.8 \cdot 10^{-4} \ m/s} \tag{75}$$

4 Factors influencing the model of a gravel column in subsoil

Before the simulation of the system behaviour of gravel columns in the present subsoil, a literature review was done to determine the relevant factors for the modelling.

The purpose of installing gravel columns in fine grained soils is to increase the bearing capacity of the subsoil and to accelerate the consolidation process in the subsoil. For the specific problem of this thesis the main goal of the installed columns is to provide quick pore pressure dissipation by reducing the drainage path in radial direction. (Redana 1999), (Weber et al. 2010)

The behaviour of gravel columns, acting as vertical drains, is generally analysed using axisymmetric unit cells with radial drainage. (Weber et al. 2010) cf. (Barron 1984; Hansbo 1979) For more complex projects and multidrain analyses equivalent plane strain solutions must be used. (Hird et al. 1992) (Indraratna & Redana 1997, 2000) (Redana 1999)

4.1 Permeability conditions in present subsoil

Before installing any columns, the in situ permeability of the subsoil has to be analysed carefully. The drainage path in the subsoil without any columns is dependent on the permeability conditions in the subsoil and the system boundaries. Due to anisotropy, an increased horizontal permeability could influence the preferred drainage path, or if isotropic permeability conditions are present in the subsoil a vertical drainage direction will prevail. (Weber et al. 2010) cf. (Jamiolkowski et al. 1983) & (DeGoot &Lutenegger 1994)

4.2 Smear zone

The smear effect is one of the main influencing factors for the behaviour of gravel columns. Due to the installation process of vertical drains in fine grained soils a "disturbed zone", the so-called "smear zone", in the vicinity near the column is produced. Within this zone the permeability of the soil decreases, especially the horizontal permeability. (Redana 1999) & (Weber et al. 2010) cf. (Onoue et al. 1991) This smear effect is acting instantaneously after installing the columns and will not be reduced with time or during service of the columns. (Weber et al. 2010)

Redana (1999) cf. Barron (1948) claims the installation procedure of a cased hole and afterwards refilling the hole at the same time as the casing is withdrawn, causes reorientation of the soil particles in the fine grained subsoil and therefore permeability reduction.

Concerning the extent of the smear zone, many of laboratory tests and field tests with subsequent back calculations can be found in literature, but there is no real consensus about this topic.

"*The extent of the smear zone and the disturbance effects depend on the construction method and on the installation tool.* "(Weber et al. 2010) cf. (Singh & Hattab 1979)

"*The size of the disturbed zone depends also on the stiffness of the subsoil: the stiffer the soil, the lager the zone of influence.*" (Weber et al. 2010) cf. (Hansbo 2004)

The ratio r_w/r_s (r_w drain radius, r_s disturbed zone, both measured from column axis) ranges from approximately 1.2 to 6 according to the literature. (Weber et al. 2010) In the same paper, the authors define the maximum extent of the smear zone surrounding the gravel column from their lab tests by approximately $r_w/r_s = 2.5$, which lies within the range of previous recommendations in literature (Weber et al. 2010).

The determination of the permeability of the disturbed zone is also very difficult and there are again various recommendations in literature. (Weber et al. 2010) As a first assumption, it is recommended to use 50 % of the subsoil's permeability for the smear zone. (Weber 2008)

The smear effect is considered in the following simulations. Indraratna & Redana (2000) mentioned that the predictions of pore water pressure will be much more realistic, if smear effect is considered.

4.3 Well resistance

Another influencing factor is the so-called "well resistance". In case of deep installation of vertical drains, the discharge capacity of such a drain may be reduced. This effect is called "well resistance". (Redana 1999)

Indraranta & Redana (2000) describe reasons for well resistance, as following:

"*For long vertical drains that are vulnerable to well resistance, Hansbo (1981) and Holtz et al. (1988, 1991) pointed out that in the field the actual reduction of the discharge capacity can be attributed to*

(1) reduced flow in the drain core due to increased lateral earth pressure,

(2) folding and crimping of the drain due to excessive settlements, and

(3) infiltration of fine silt or clay particles through the filter (siltation)."

Due to the fact, that all three issues are not relevant for the specific project of this thesis, the effect of well resistance is not further considered during the following simulation. Concerning the increased earth pressure, no clear statement can be made, gravel columns will not fold or crimp (could be a problem for prefabricated drains) and the column material suitability was checked in chapter 3.2 and therefore infiltration of clay or in the case of this thesis is prevented.

Additionally, Indraratna & Redana (2000) emphasize that the effect of well resistance has a minor effect on the pore pressure in comparison with the smear effect. Also Redana (1999) writes that well resistance has less influence on the system behaviour than the smear effect and the drain spacing.

4.4 Drain Influence Zone

Vertical drains, prefabricated ones or gravel columns, are usually installed in a square or triangular pattern (see Fig. 18). The spatial extent of the radial drainage zone can be calculated using Equ. (76) or (77). In general, the square pattern is easier to install, but the triangular pattern provides a more uniform consolidation between the drainage columns than the triangular pattern. (Redana 1999)

$$square\ pattern: D_{squ} = 1.13 \cdot S \qquad\qquad (76)$$

$$triangular\ pattern: D_{tri} = 1.05 \cdot S \qquad\qquad (77)$$

D_{squ} [m]   Drainage zone around the column for square pattern

D_{tri} [m]   Drainage zone around the column for square pattern

S [m]   spacing between the column axis in plan view
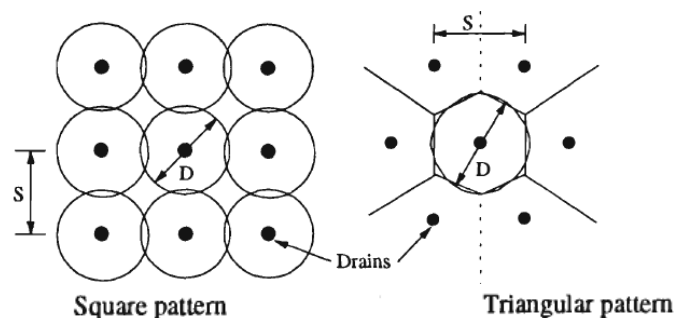
Fig. 18   Plan view of drain pattern with its corresponding radial drainage zone (Redana 1999)

5 Preliminary study – axisymmetric model of gravel column

In this chapter, the preliminary study about the behaviour of the stone column in cohesive material under water level fluctuation is summarized. All the simulations were carried out with PLAXIS 2D Version 2016.01. (Brinkgreve 2016)

5.1 Numerical model

The preliminary study is based on an axisymmetric model with 6-noded elements. 6-noded triangular elements are sufficiently accurate for the preliminary study and the calculation with this element type is less time consuming than with 15-noded ones. The model dimensions are 2 m x 40 m. The brown area in the lower part of the model (see Fig. 19) represents the subsoil, the light blue block at the top of the model represents a highly permeable block, which helps to generate excess pore water pressures in the subsoil and the blue area surrounded by (brown) subsoil is the gravel column (with additional clusters for different column diameters and the smear zone). The highly permeable block is defined with an unsaturated γ_{unsat} and a saturated unit weight γ_{sat}. If the water level is fluctuating, the block's total weight is always changing and therefore the acting load on the ground surface is also changing. This changing load produces excess pore water pressures in the subsoil.

The columns are installed in a triangular pattern for uniform consolidation (Redana 1999) with a spacing of 2.31 m. As a result, the drainage zone has a diameter of 2.43 m (acc. to Equ. (77)). At the beginning of the preliminary study the spacing of the columns on-site was not fixed yet, so a radius of 2 m was chosen for the current preliminary study. For the analyses of the real project, the real spacing was considered (see chapter 7).
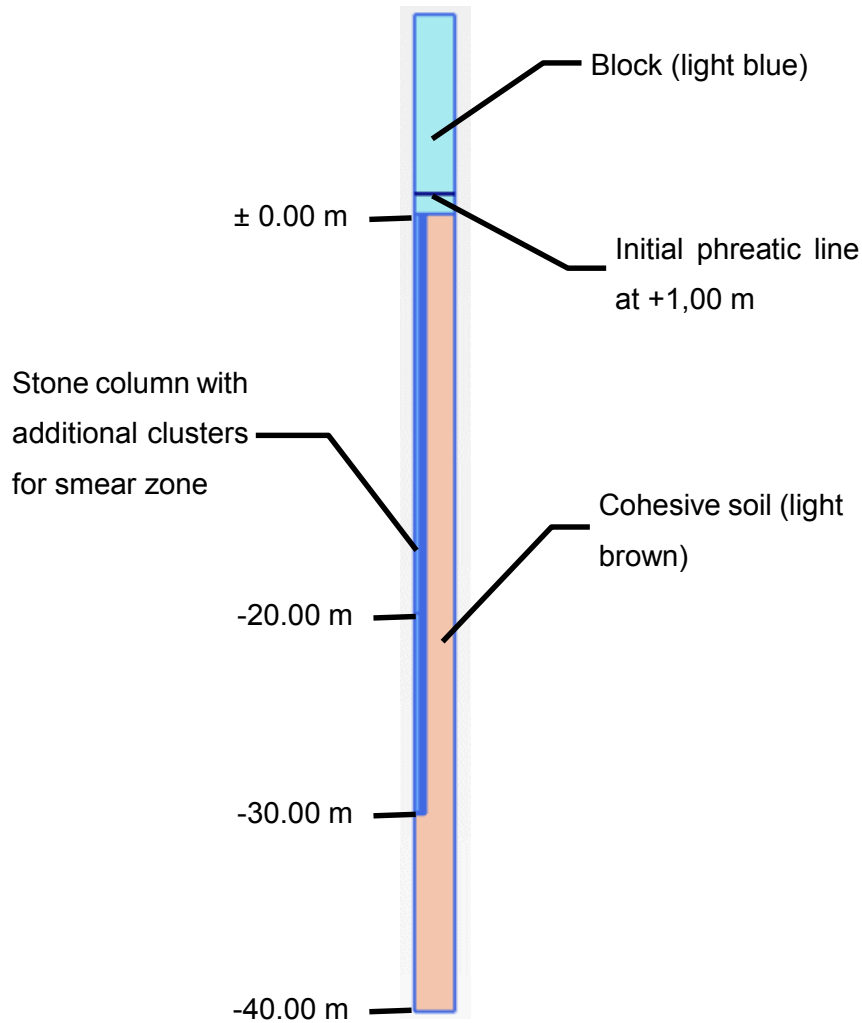
Fig. 19   Screenshot of model in Plaxis 2D

5.2   Input parameters for the preliminary study with anisotropic and isotropic permeability conditions

The input parameters for the preliminary study with anisotropic permeability conditions in the subsoil are summarized in Tab. 9, Tab. 10, Tab. 11 and Tab. 12.

Tab. 9   Input parameters for block material

block – linear elastic		
Drainage type	Drained	[-]
γ_{unsat}	20.00	[kN/m³]
γ_{sat}	22.00	[kN/m³]
E'	300.00 E3	[kN/m²]
ν'	0.3	[-]

k_x	0.1	[m/s]
k_y	0.1	[m/s]

Tab. 10   Input parameters for soil material

soil body – HS small – anisotropic case		
Drainage type	Undrained (A)	[-]
γ_{unsat}	18.00	[kN/m³]
γ_{sat}	21.00	[kN/m³]
E_{50}^{ref}	18.00 E3	[kN/m²]
E_{Oed}^{ref}	15.00 E3	[kN/m²]
E_{ur}^{ref}	37.50 E3	[kN/m²]
m	0.7	[-]
c'_{ref}	2.00	[kN/m²]
φ'	32.50	[°]
ψ	0.00	[°]
$\gamma_{0.7}$	0.10 E-3	[-]
G_0^{ref}	62.50 E3	[kN/m²]
v'_{ur}	0.20	[-]
p_{ref}	100.00	[kN/m²]
K_0^{nc}	0.4627	[-]
k_x	1 E-7	[m/s]
k_y	1 E-8	[m/s]

Due to the installation process of the stone columns, a smear zone around the column has to be considered. This zone has reduced permeability conditions, as explained in chapter 4.2.

In a first simple approach, for this smear zone all parameters were taken the same as for the soil body, but the horizontal and the vertical permeability were reduced by a factor of 50 % (see Tab. 11). (Weber 2008)

Tab. 11   Input parameters for smear zone material

Smear zone – HS small – anisotropic case		
k_x	5 E-8	[m/s]
k_y	5 E-8	[m/s]

Tab. 12   Input parameters for column material

column – Mohr-Coulomb		
Drainage type	Drained	[-]
γ_{unsat}	17.00	[kN/m³]
γ_{sat}	20.00	[kN/m³]
E_{Oed}	20.00 E3	[kN/m²]
v'	0.3	[-]
c'_{ref}	1.00	[kN/m²]
φ'	30.00	[°]
ψ'	0.00	[°]
k_x	5 E-4	[m/s]
k_y	5 E-4	[m/s]

The changed input parameters for the case with isotropic permeability are summarized in Tab. 13 and Tab. 14. For the soil body, all parameters were set to the same value as in the anisotropic case, only the permeability of the subsoil is adjusted. The permeability in this case is the same in horizontal and vertical direction. Also in this case, the permeability in the smear zone is reduced by a factor of 0.5. (Weber 2008) (The rest of the input parameters for the soil is shown in Tab. 10.)

Tab. 13   Input parameters for soil material

Soil body – HS small – isotropic case		
$k_x = k_y$	1 E-8	[m/s]

Tab. 14   Input parameters for smear zone material

Smear zone – HS small – istropic case		
$k_x = k_y$	1 E-8	[m/s]

5.3   Mesh

The mesh consists of 6-noded elements and is generated using a coarseness factor of medium. The most important areas of the model are shown in Fig. 20 and Fig. 21.
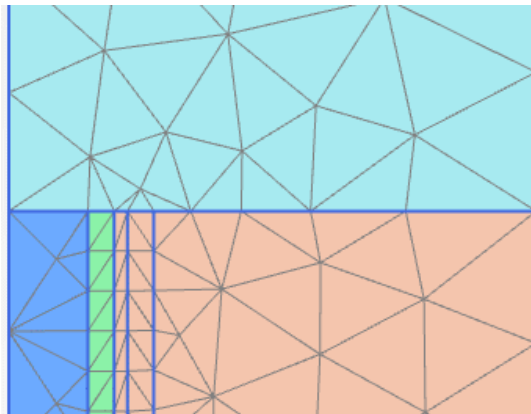
Fig. 20   Mesh in the upper part of the model - boundary between soil body and block (approximate depth: +1.0 to -1.0 m)
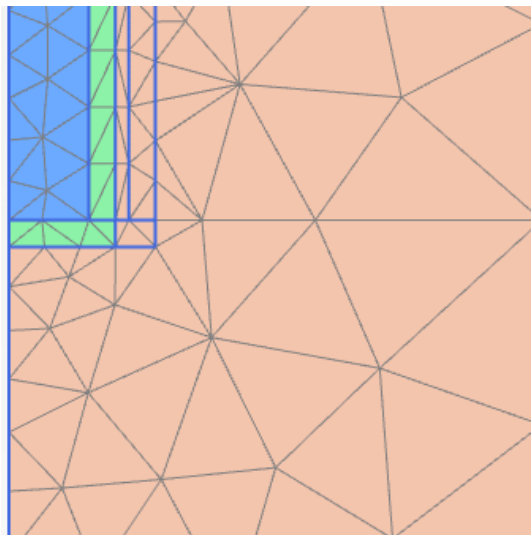
Fig. 21   Mesh at the lower end of the column (aproximate depth: -29.0 to 31.5 m)

The flow boundary conditions of the model should provide a similar behaviour as in the real project. Therefore, the flow boundaries are closed.

5.4 Flow function

In the Initial phase, the initial water level was set to +1.00 m above ground level. As a next step, the time-dependent head function was created, which simulates the impoundment and drawdown of the water level in the storage basin. The fluctuating water level is considered in a fully-coupled flow deformation calculation phase. During the simulation three types of flow function with different velocities were used:

- **Case 1 - 7m / 0.33 days:** A water height difference of 7 m within a period of 0.33 days is applied to the FE model. The water level fluctuation was simulated 20 times, which took a time of 13.33 days.

- **Case 2 - 7m / 0.5 days:** A water height difference of 7 m within a period of 0.5 days is applied to the FE model. The water level fluctuation was simulated 20 times, which took a time of 20 days.

- **Case 3 - 7m / 1 day:** A water height difference of 7 m within a period of 1 day is applied to the FE model. The water level fluctuation was simulated 20 times, which took a time of 40 days.

These different fluctuation velocities are important for the study of the hydraulic gradient (discussed in chapter 5.6.4). The system behaviour is analysed after drawdown and after impoundment. The results are always compared with each other.

5.5 Analysed nodes

For a comparable evaluation of the pore water pressure development, ten nodes were chosen within the model. The distances of these nodes from the column are selected according to Equ. (78). The definition of the parameters is shown in Fig. 22 and their coordinates are summarized in Tab. 15.

$$\frac{X_i}{R - r} = const. \tag{78}$$

X_i [m]   distance from gravel column, i=1,2,3

R [m]   radius of the axisymmetric FE-model, R = 2.0 m

r [m]   radius of the column (version 1: r = 0.3 m, version 2: r = 0.45 m)

$const.$ [-]   constant factor (section A: 1, section B: 0.5, section C: 0.25)
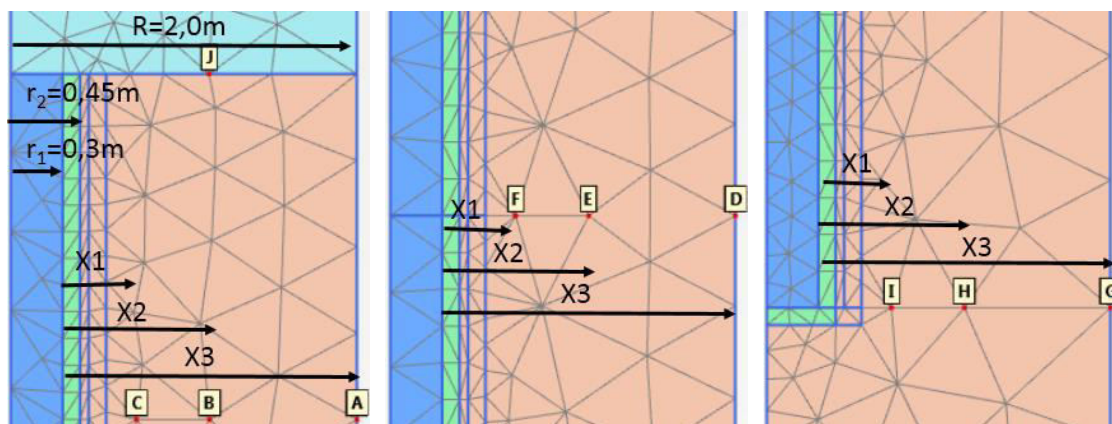
a) top of the layer	b) middle of column	c) bottom of column
(+0.5 to -2 m)	(-28 to -32 m)	(-38 to 41 m)

Fig. 22   Nodes for evaluation of the preliminary study (with approximate depth)

Tab. 15   Coordinates of the evaluated nodes

Point	X (r=0.3 m)	X (r=0.45 m)	Y
A	2.0 m	2.0 m	-2.0 m
B	1.15 m	1.225 m	-2.0 m
C	0.725 m	0.838 m	-2.0 m
D	2.0 m	2.0 m	-20.0 m
E	1.15 m	1.225 m	-20.0 m
F	0.725 m	0.838 m	-20.0 m
G	2.0 m	2.0 m	-30.0 m
H	1.15 m	1.225 m	-30.0 m
I	0.725 m	0.838 m	-30.0 m
J	1.14 m	1.14 m	± 0.0 m

5.6   Pore water pressure in the subsoil around the gravel column due to a fluctuating water level

5.6.1   Reference case

The so-called "reference case" represents the model without installed columns. This simulation is done with closed boundaries, using the flow function "Case 1" (acc. to

chapter 5.4). The results are evaluated at Point E (acc. to Tab. 15), which is located at a depth of -20 m below ground level. For the evaluation of the two different radii due to Equ. (78), the x-coordinate of the evaluated point differs by approximately 12 cm.

In Fig. 23 p_{water} over time (t=12.00 to 13.33 days) is presented. The hydrostatic water pressure (yellow) differs significantly from the p_{water}-curve – after drawdown excess pore water pressures (see Fig. 25) are generated in the subsoil, in contrast after impoundment negative excess pore water pressures (Fig. 24) occur. The difference of the generated pore water pressures at Point E for r=0.3 m and r=0.45 m is minor. (Therefore, only one reference case can be used for further evaluation.)
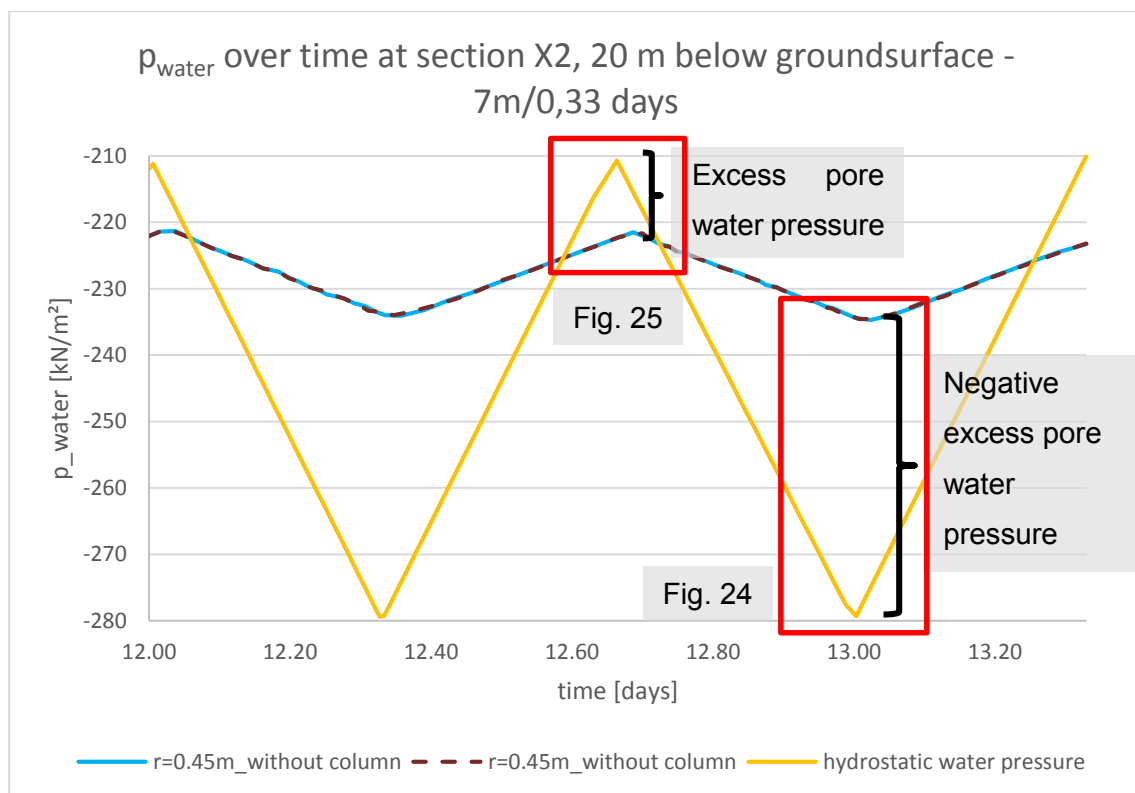
Fig. 23 p_{water} of the reference case (without column) over time at section X2, 20 m below ground surface (Point E)
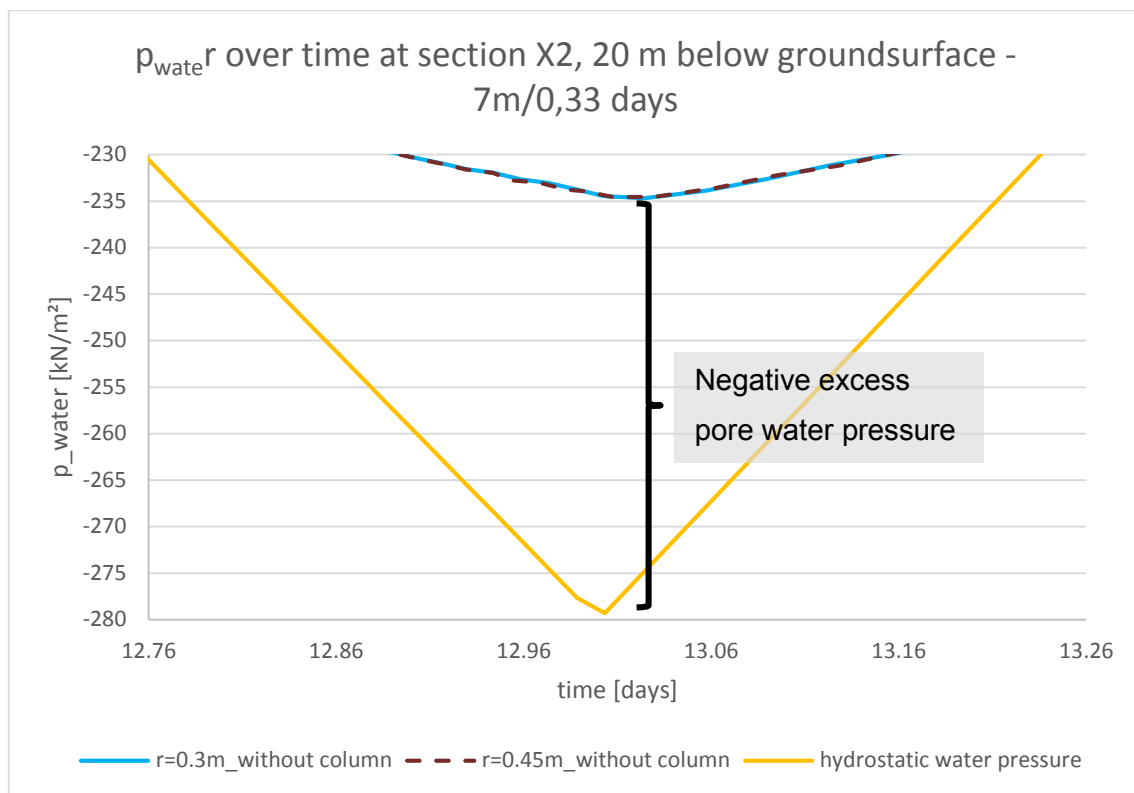
Fig. 24   Zoomed sector of p_water of the reference case (without column) of time (t=12.76 to 13.26 days) – after impoundment (Point E)
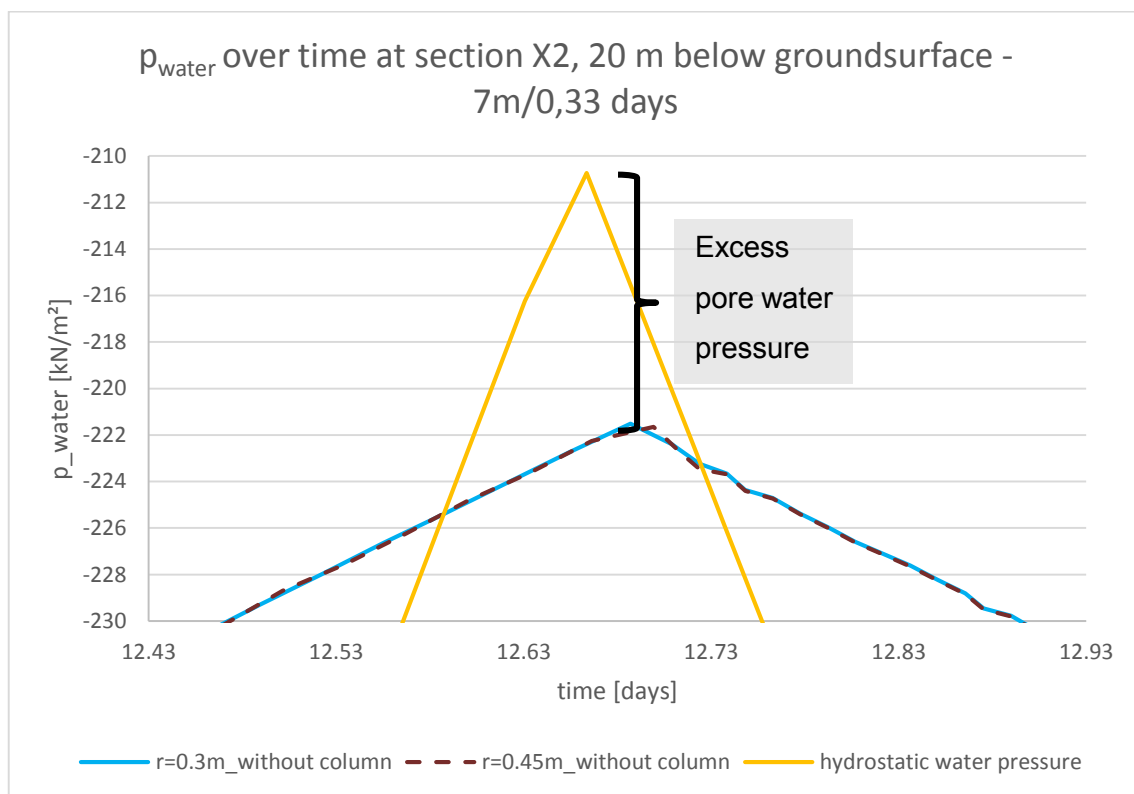
Fig. 25   Zoomed sector of p_water of the reference case (without column) of time (t=12.43 to 12.93 days) – after drawdown (Point E)

5.6.2 Pore water pressure over time

All the results, which are presented in this chapter are calculated with flow function "Case 1" (acc. to chapter 5.4) with the highest fluctuation velocity (7m/0.33 days) of the water level. In Fig. 26, Fig. 27 and Fig. 28 the development of p_{water} over time is shown for different depths at the section X2 (acc. to Fig. 22 and Tab. 15) with anisotropic permeability conditions. The yellow curve represents the hydrostatic water pressure in all figures. In Fig. 26 it is shown, that at a depth of -2 m approximately after two days of fluctuating water level a "steady state"-mean pore water pressure is reached, but at deeper levels (compare Fig. 27, Fig. 28) the continuous increase of the mean pore water pressure indicates that no steady state is reached within 13.33 days.

The effect of the columns on the pore water pressure in the subsoil can be recognized over the entire simulation time and also over the full column length. The generated excess pore water pressures after drawdown of the water level are decreasing with depth.
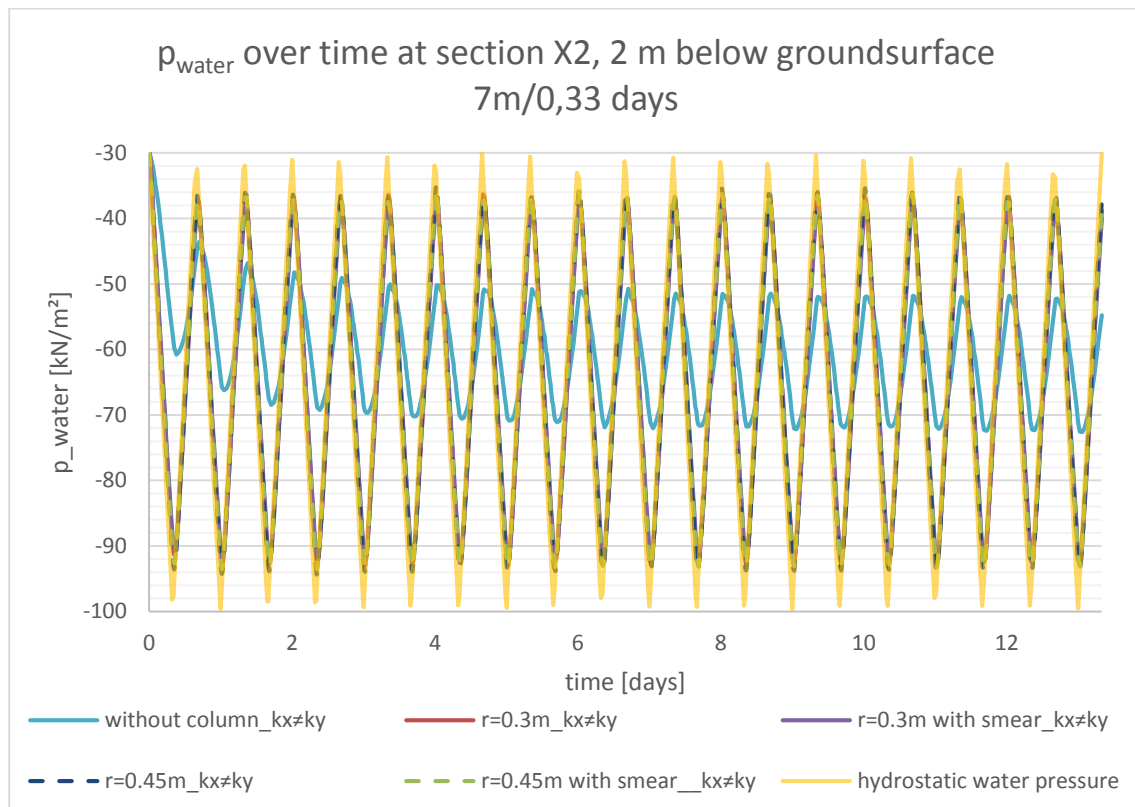
Fig. 26 p_{water} over time at section X2, 2 m below ground surface, closed boundaries (Point B)
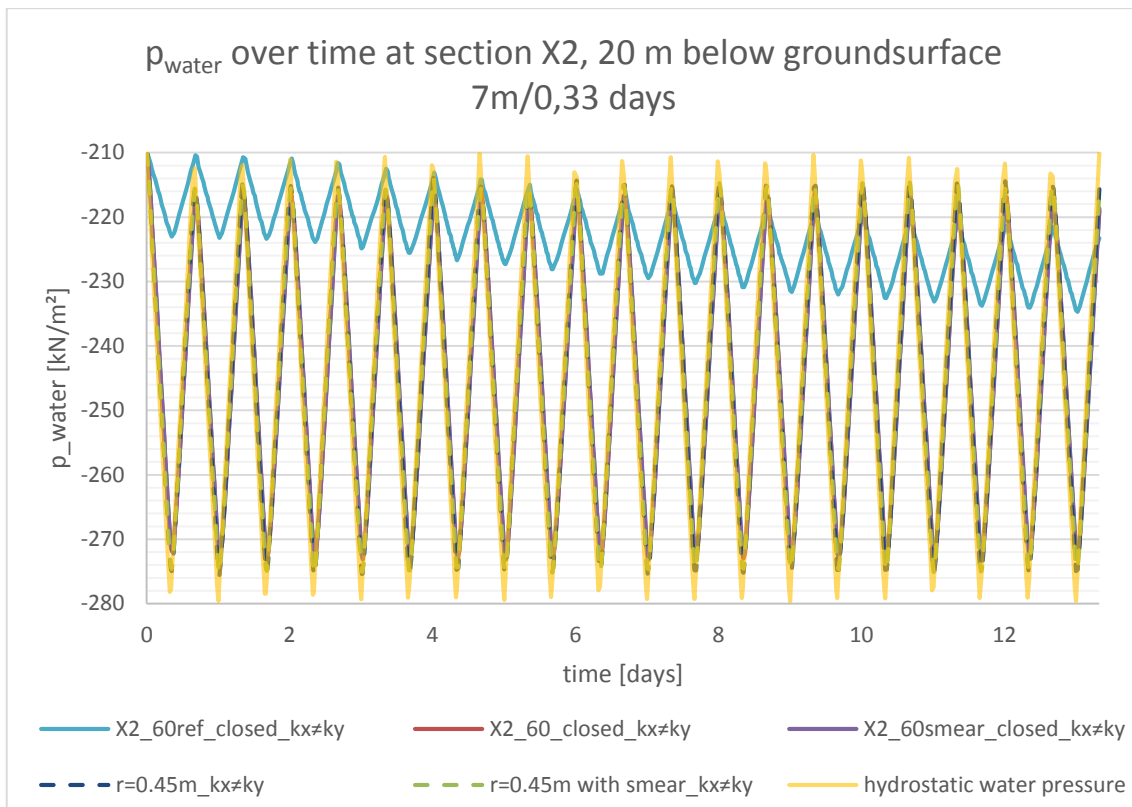
Fig. 27   p_water over time at section X2, 20 m below ground surface, closed boundaries (Point E)
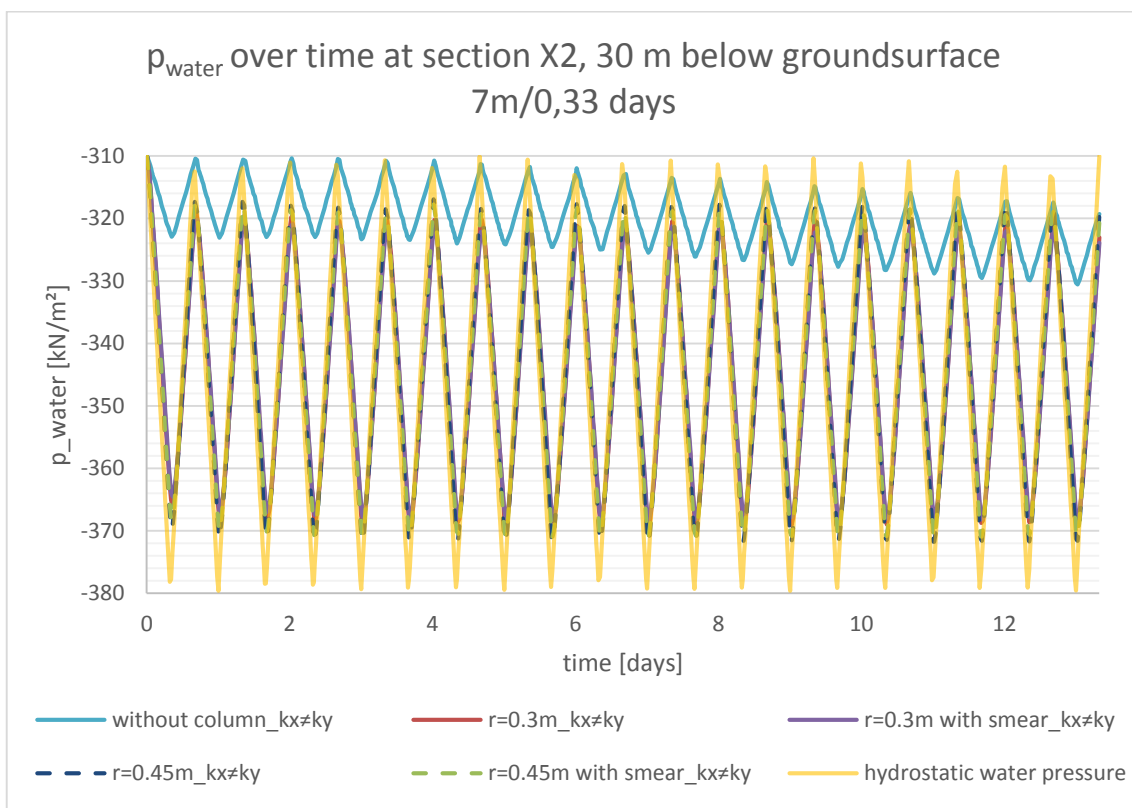
Fig. 28   p_water over time at section X2, 30 m below ground surface, closed boundaries (Point H)

In Fig. 29 and Fig. 30 zoomed sections of the p_{water}-curve over time are presented. The effect of the smear zone (compare red and purple curve for r=0.3 m) is very small (approximately 1 kN/m²). For a higher radius (r=0.45 m) the effect of the smear zone (compare blue and green dotted curve) is also very small.

In the same figures is presented that an increased column radius leads to less excess pore water pressures of approximately 2 kN/m²(compare purple and green dotted curve in Fig. 30).
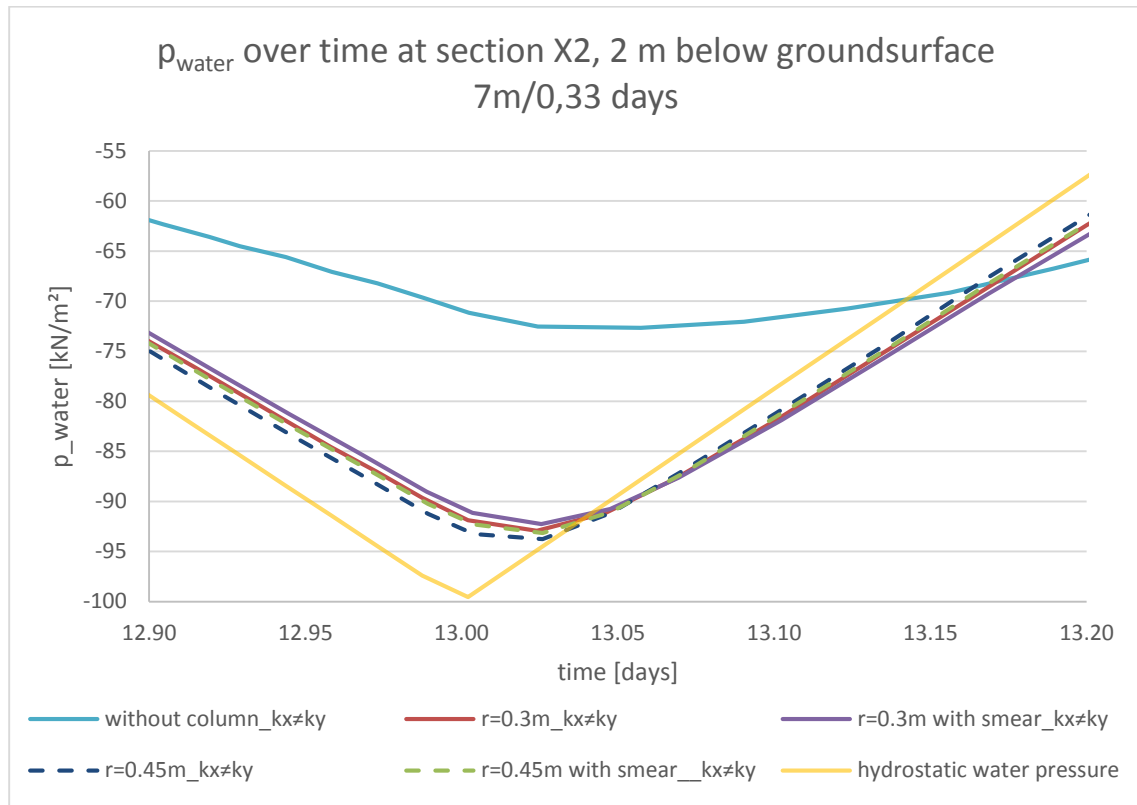
Fig. 29   Zoomed section of p_{water} over time at section X2, 2 m below ground surface, closed boundaries (Point B) – after impoundment

Computational Geotechnics Group
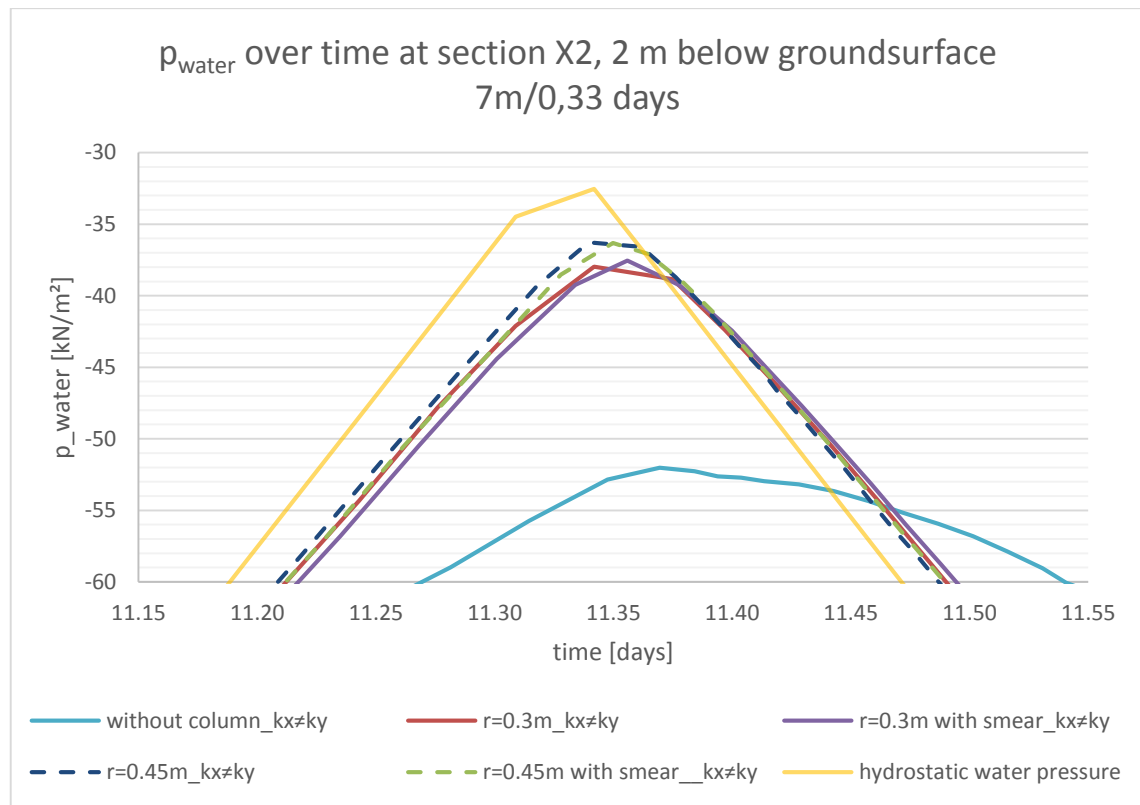
Fig. 30   Zoomed section of p_water over time at section X2, 2 m below ground surface, closed boundaries (Point B) – after drawdown

In Fig. 31, Fig. 32 and Fig. 33 the influence of the smear zone on the groundwater head is shown. In the upper (-2 m) and lower (-30 m) areas, a small influence of the smear zone can be recognized. For those two areas, in case of impoundment the thicker smear zone (45 cm) reduces the reached groundwater head by approximately 15 cm compared to the thin smear zone. In the middle of the column (-20 m), the smear zone has the smallest influence of less than 10 cm compared to the original curve, which does not consider smear. In general, one can notice that the effect of the smear zone on the pore water pressure is relatively small.
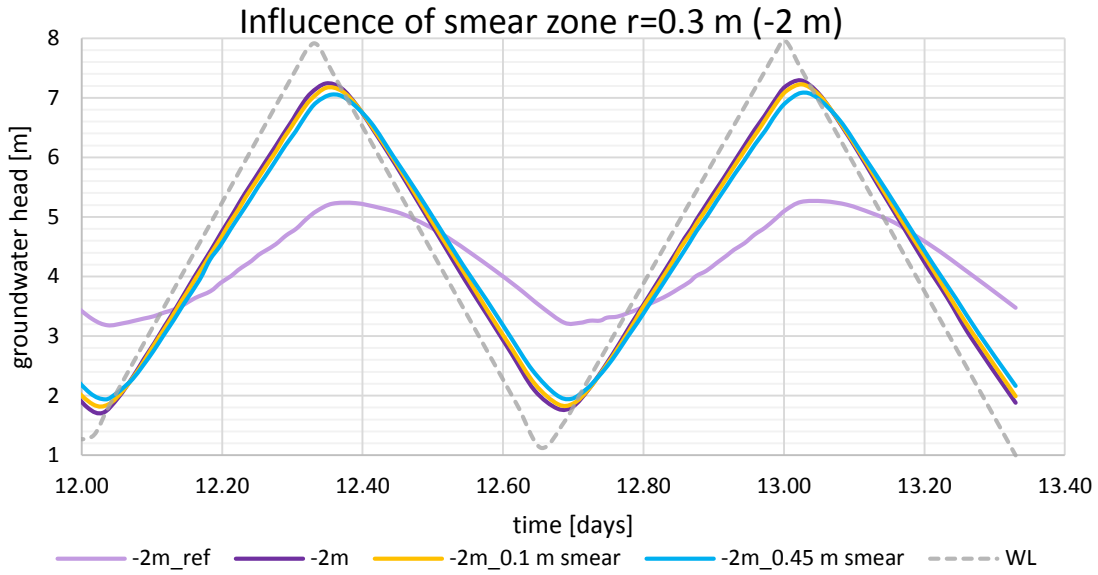
Fig. 31   Influence of the smear zone (groundwater head over time) in -2 m (section X2)
(Point B)
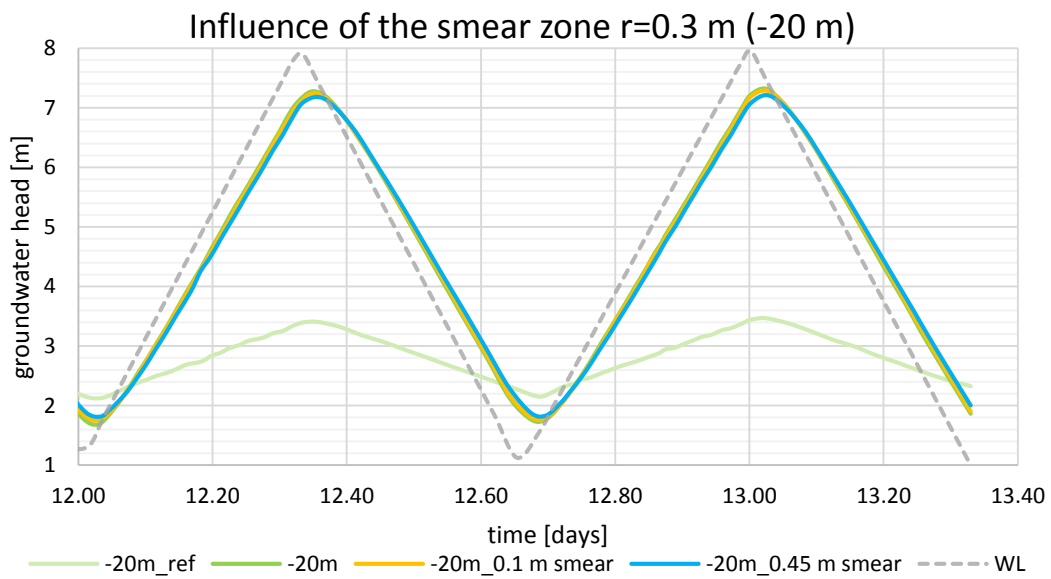
Fig. 32   Influence of the smear zone (groundwater head over time) in -20 m (section X2)
(Point E)
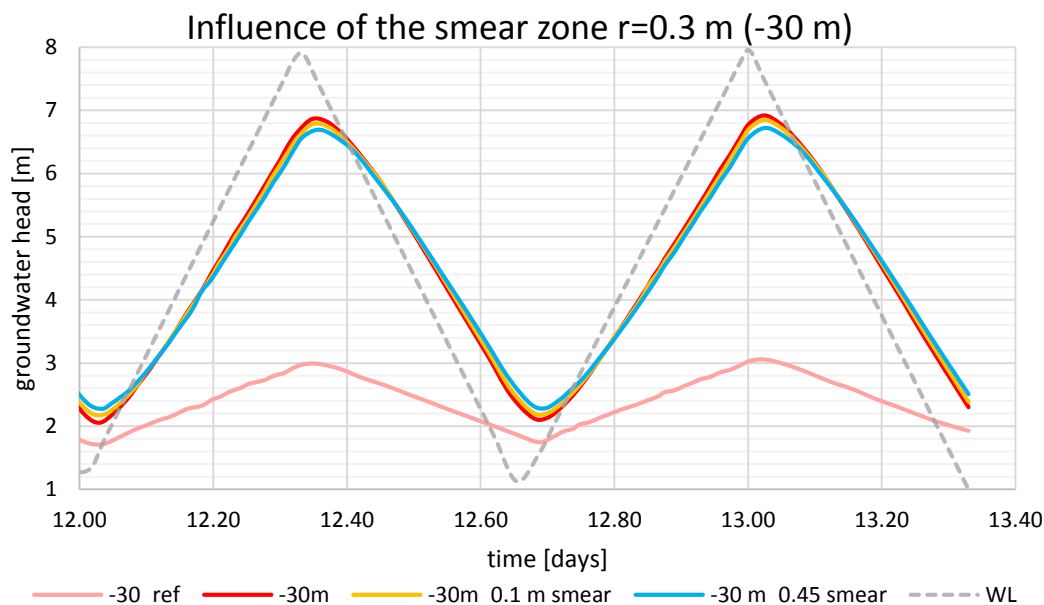
Fig. 33   Influence of the smear zone (groundwater head over time) in -30 m (section X2) (Point H)

5.6.3 Influence of the columns at -2 m below soil surface

The following diagrams show the groundwater head over time for the anisotropic case ($k_x \neq k_y$) (Fig. 34) and the isotropic case ($k_x = k_y$) (Fig. 35) without considering a smear zone (=perfect drainage conditions) around the column for a column radius r= 0.3 m.

For the anisotropic case in Fig. 34 the groundwater head has nearly the same value over the entire model width (compare blue, red and green curve). For the isotropic case, shown in Fig. 35, the groundwater head differs over the model width. At the farther edge (point C) (2 m from column axis) the groundwater head reaches the highest value, in the middle of the model (point B) and near to the column (point A) (compare blue and red curve) the groundwater head is similar.

The importance of the horizontal permeability can be seen in Fig. 35 for the isotropic case ($k_x = k_y$) and in Fig. 34 for the anisotropic case ($k_x \neq k_y$). In the isotropic case, k_x is reduced to $1 \cdot 10^{-8} \, m/s$. In both mentioned figures, the Δgroundwater head for point B (approximately in the middle of the model width at -2 m below ground level) is marked. For the anisotropic case with the higher horizontal permeability (Fig. 34) this Δgroundwater head (≈1.5 m) is larger than for the isotropic case (Fig. 35) (Δgroundwater head ≈0.5 m). Thus, the reduced horizontal permeability in the subsoil reduces the influence of the columns significantly.
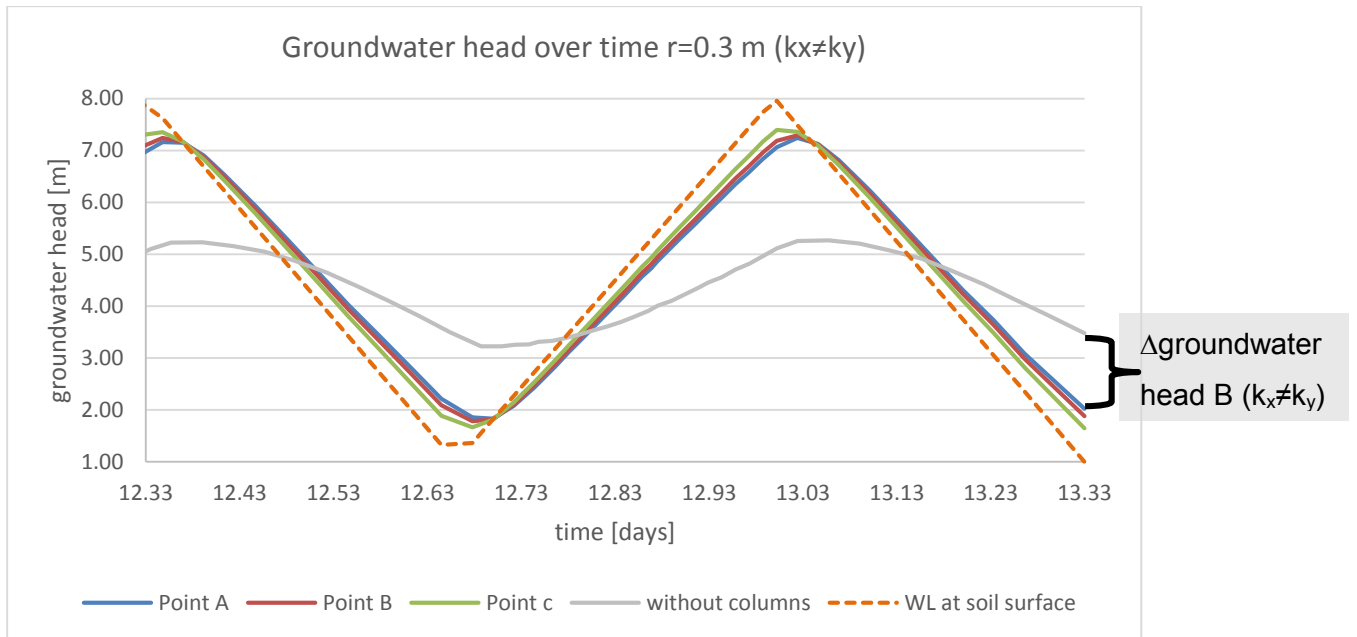
Fig. 34   Groundwater head at -2 m below ground surface (Point A, B, C) for the anisotropic case ($k_x \neq k_y$) without smear zone
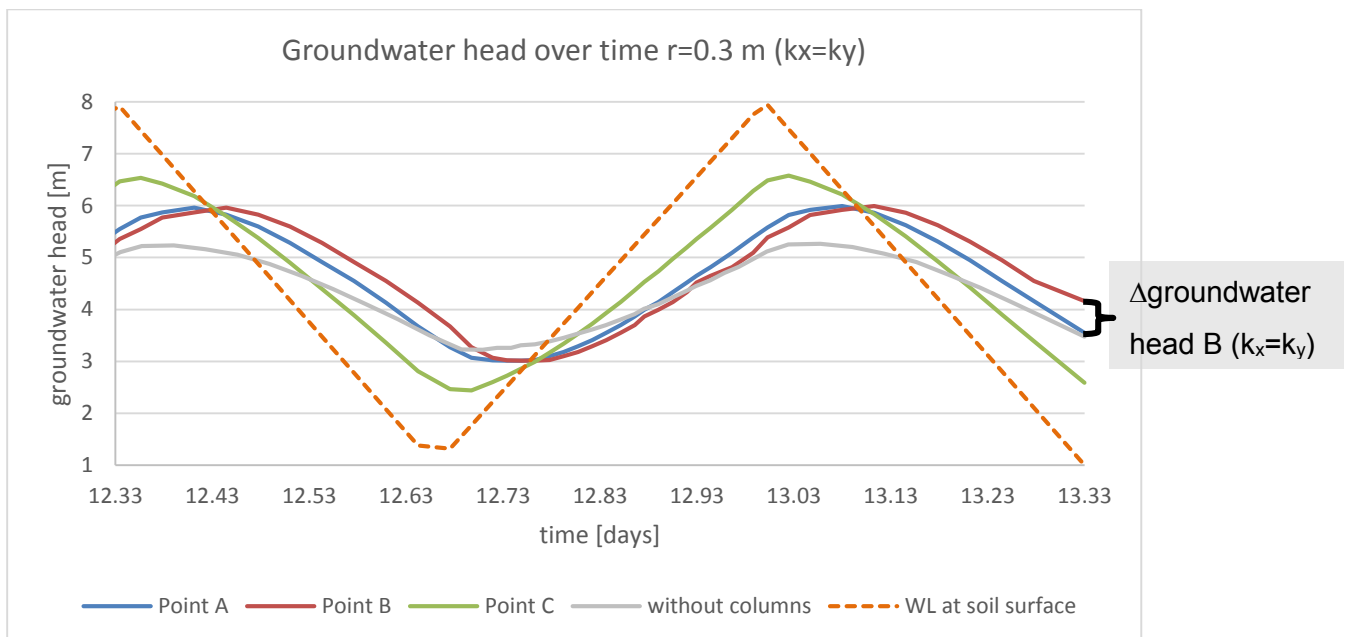
Fig. 35   Groundwater head at -2 m below ground surface (Point A, B, C) for the isotropic case ($k_x = k_y$) without smear zone

5.6.4   Hydraulic gradient over depth for different simulation cases

In addition to the pore water pressures, the hydraulic gradient next to the column was investigated. For the evaluation of the gradient, a horizontal flow was assumed 10 cm next to the column. In Fig. 36 the groundwater head next to the column after drawdown

in 10 m depth is shown. Using (79) the hydraulic gradient i is calculated over the column length.

$$\frac{\Delta gw}{l} = \frac{gw_1 - gw_2}{0.1\ m} \qquad (\ 79\ )$$

Δgw	[m]	difference of groundwater head
gw_1	[m]	groundwater head 1 (right side of column)
gw_2	[m]	groundwater head 2 (left side of column)
l	[m]	assumed flow length (= extent of smear zone = 0.1m)
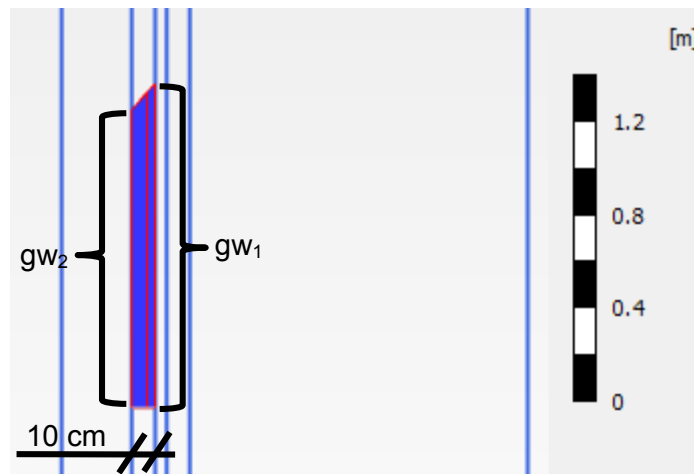
Fig. 36   Groundwater head for calculating the hydraulic gradient next to the column after drawdown (depth~10.0)

The case with anisotropic permeability conditions was studied very carefully, as shown in Fig. 37, Fig. 39 and Fig. 38.

The hydraulic gradient reduces from top to the bottom of the column, but at the bottom at -30 m a peak is recognized. This peak results from non-horizontal flow conditions next to the column in that area, as the groundwater head screenshots in Fig. 40 and Fig. 41 indicates. Therefore, the calculated hydraulic gradient is wrong due to the wrong assumption of a horizontal groundwater flow. Also, at the top, the flow direction is slightly inclined. Therefore, the assumption of horizontal flow is only valid between approximately -5 m and -28 m (between the red lines). (see Fig. 37, Fig. 39 and Fig. 38)

As shown in Fig. 37, the highest fluctuating velocity (7m / 0.33 days) results in the highest hydraulic gradient, the slowest fluctuation with 7m / 1 day results in the lowest gradient. Additionally, without the smear zone (blue dotted curves) the gradient next to the column is approximately 50% smaller than with a 10 cm wide smear zone (purple curves) (see Fig. 38). In Fig. 39, the influence of the higher radius of the column (orange curves) can be recognized easily. Observing the same velocity of fluctuating water level, the column

with a radius of 0.45 m (orange curves) produces an approximately 15 % smaller gradient next to the column than the columns with a radius of 0.30 m (purple curves).
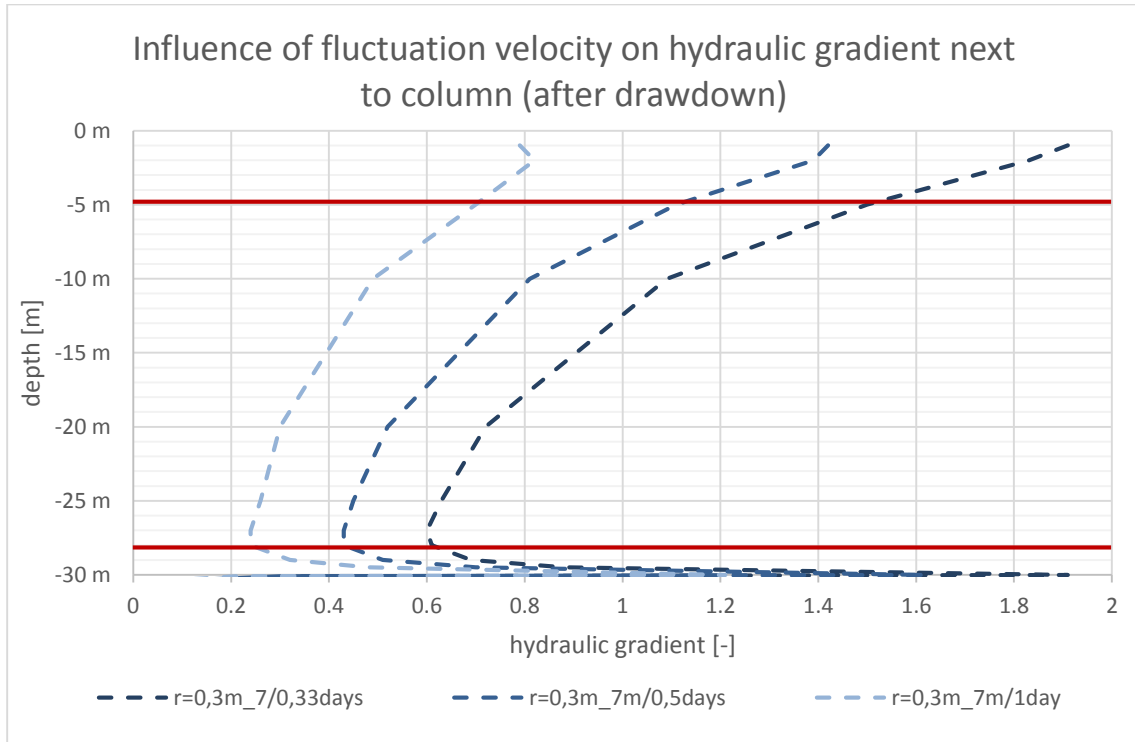
Fig. 37   Influence of the fluctuation velocity on the hydraulic gradient next to the column (after drawdown) ($k_x \neq k_y$)
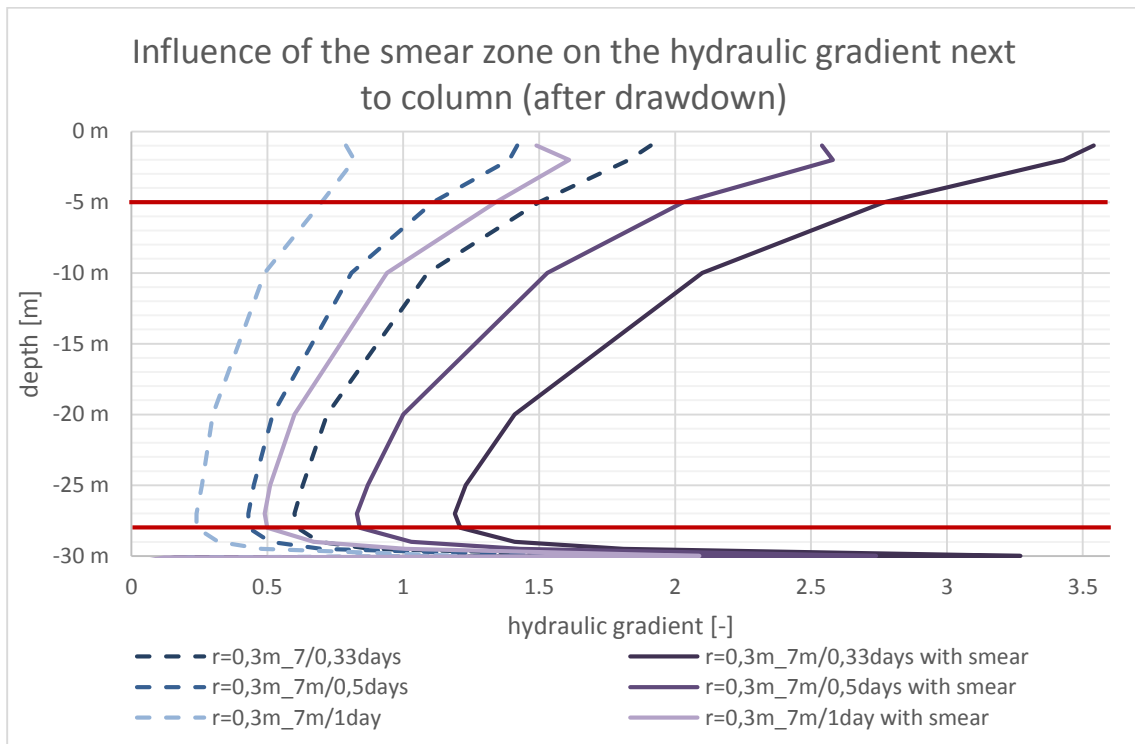
Fig. 38   Influence of the smear zone on the hydraulic gradient next to the column (after drawdown) ($k_x \neq k_y$)
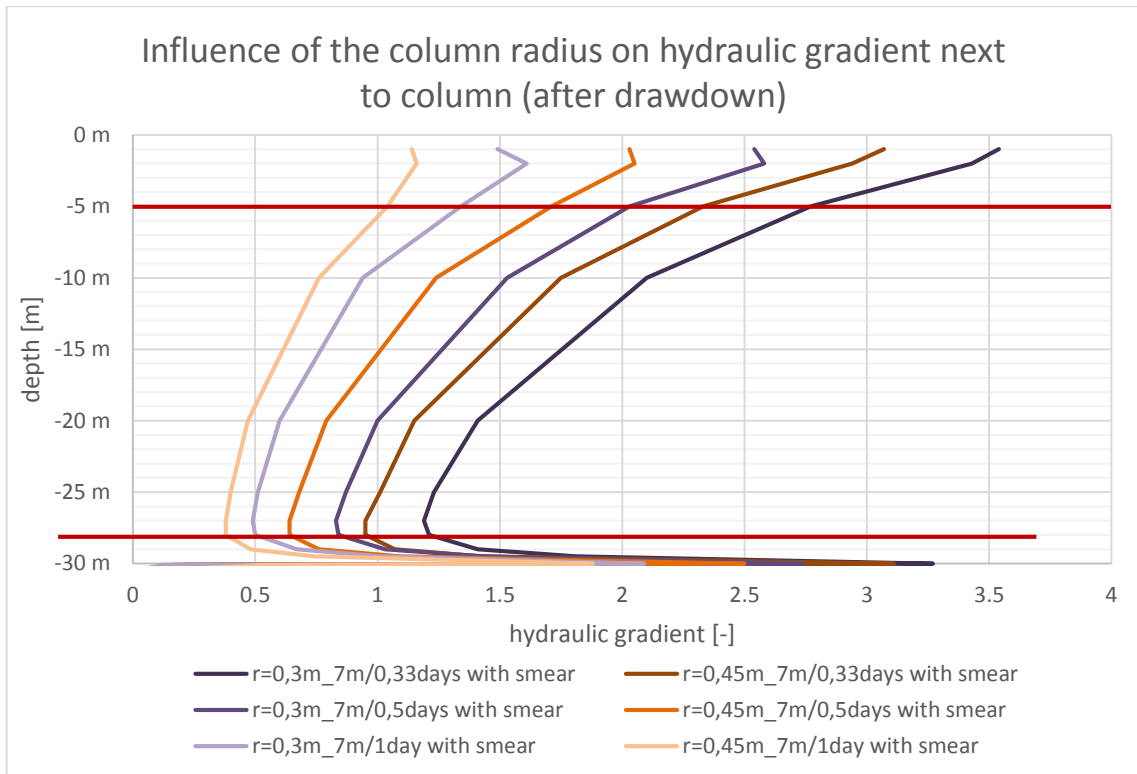
Fig. 39   Influcence of the column radius on hydraulic gradient next to the column (after drawdown) ($k_x \neq k_y$)
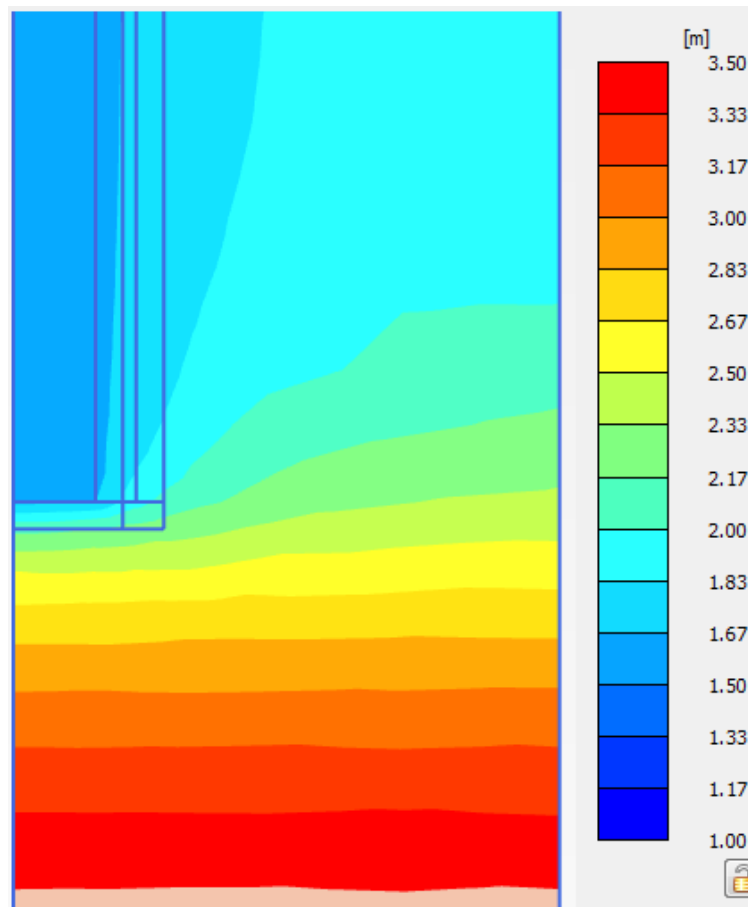
Fig. 40   Groundwater head at the bottom of the column (-30 m) with $k_x \neq k_y$, 7m/0.33 days, without smear zone
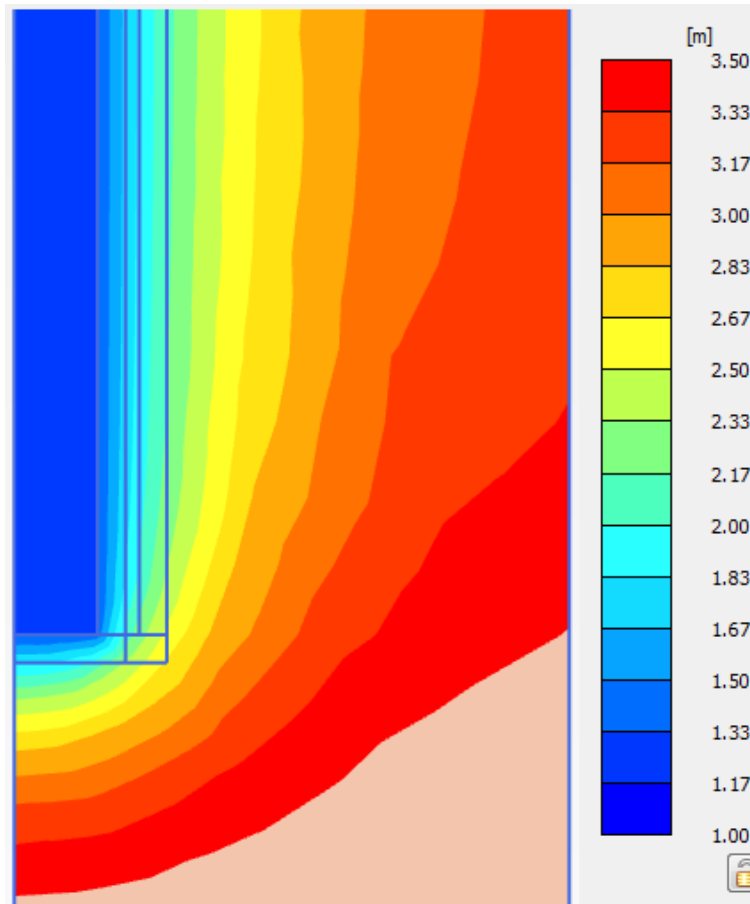
Fig. 41   Groundwater head at the bottom of the column (-30 m) with $k_x=k_y$, 7m/0.33 days, without smear zone

In Fig. 40 and Fig. 41 the groundwater head at the bottom of the column at -30 m below ground surface is plotted. The difference of the behaviour of the anisotropic case compared to the isotropic permeability case can be easily recognized. For the anisotropic case, the equipotential lines below the column are horizontally very near to the column. Additionally, at the far end of the model (2 m from the model axis) the groundwater head is higher in the isotropic case than in the anisotropic.

In Fig. 42 the hydraulic gradient next to the column after an impoundment is presented. The resulting hydraulic gradients differ slightly, but are similar to the one after drawdown. (compare Fig. 38). Again, only values between -5 m and -28 m are representative due to inclined flow directions at the top and at the bottom of the column.
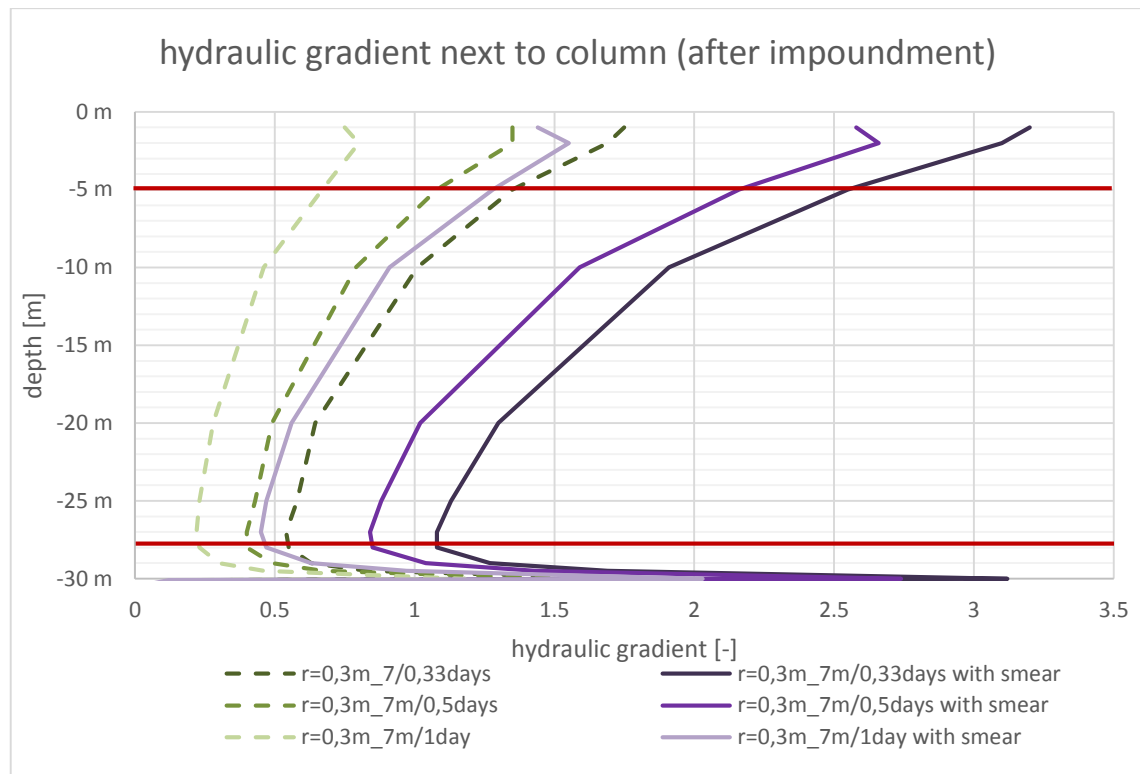
Fig. 42   Hydraulic gradient after impoundment over depth for different cases with and without smear zone ($k_x \neq k_y$)

In Fig. 43 the hydraulic gradients next to the column are compared for different column lengths with a radius of r=0.30 m. The hydraulic gradient in a certain depth is nearly the same for different column lengths and the curves look similar (compare dark red and dark blue dotted curve). In Fig. 44 the influence of the permeability conditions in the subsoil on the hydraulic gradient is illustrated. For the isotropic permeability case (dark and light green), the hydraulic gradient is much higher than for the increased horizontal permeability (k_x) (anisotropic permeability case, dark purple and dark blue).
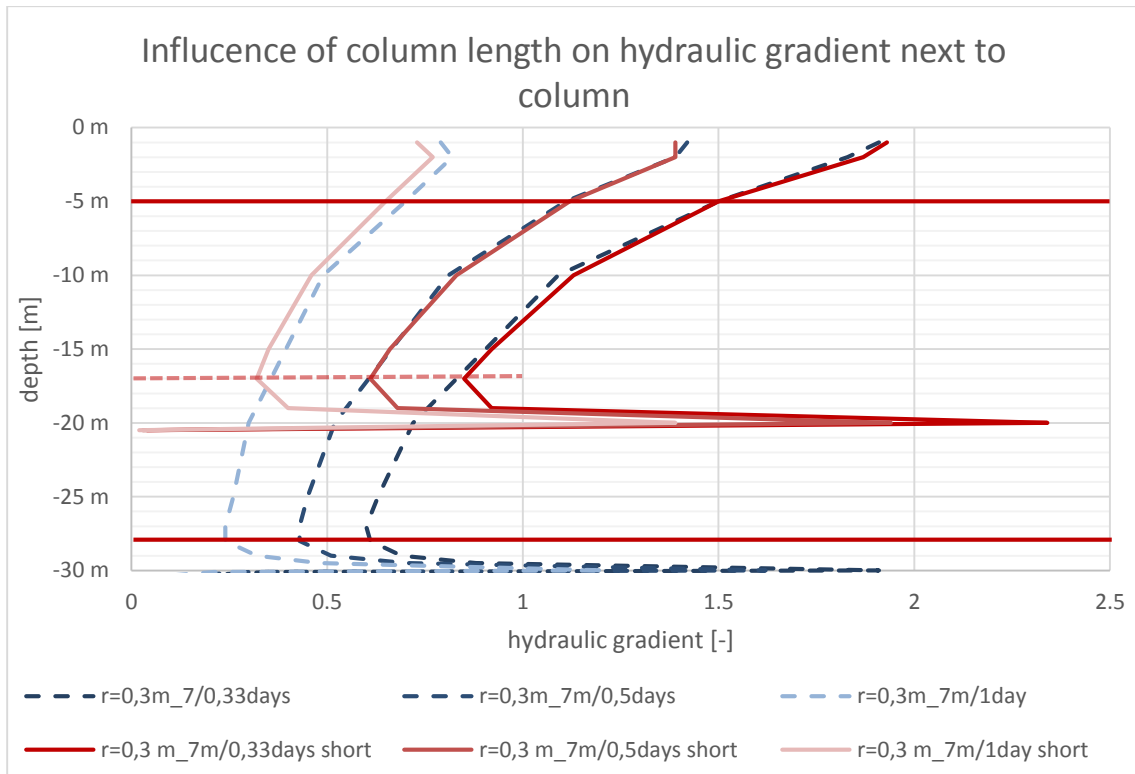
Fig. 43 Influence of the column length on the hydraulic gradient for r=0.30 m in anisotropic permeability conditions ($k_x \neq k_y$)
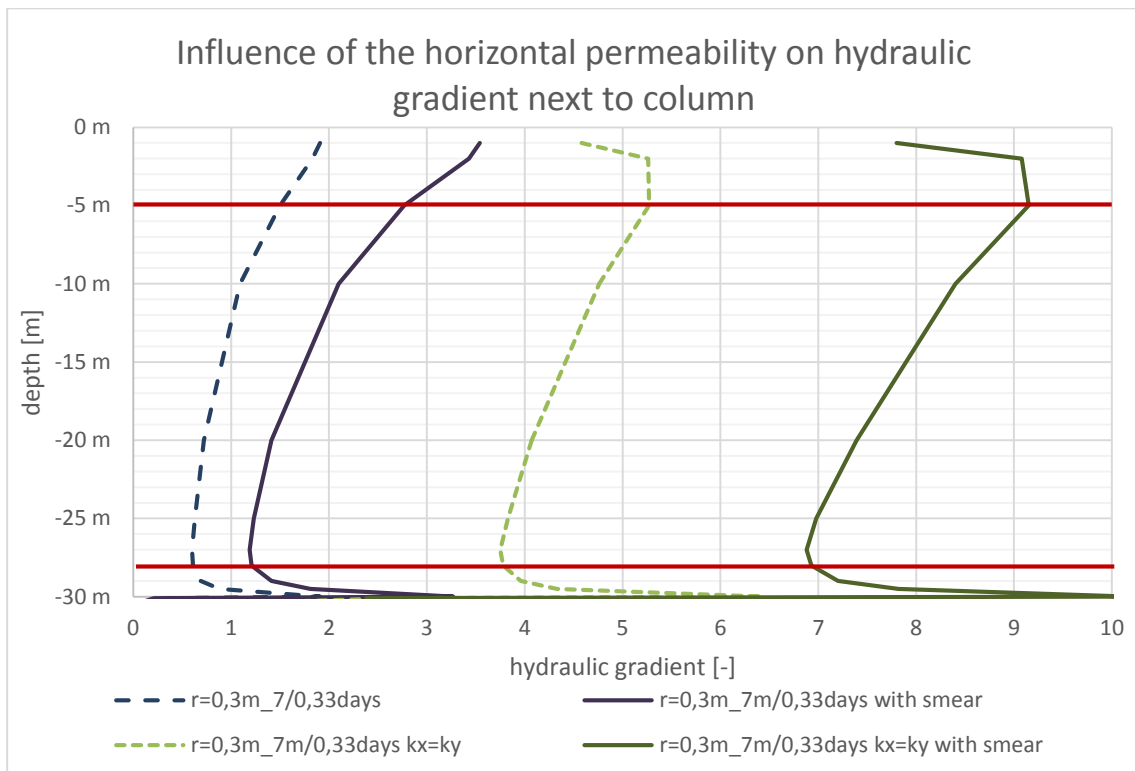
Fig. 44 Influence of the horizontal permeability of the subsoil on the hydraulic gradient for r=0.30 m ($k_x \neq k_y$ vs. $k_x = k_y$)

Computational Geotechnics Group

5.7 Consolidation process

A consolidation analysis was performed after the fully coupled flow-deformation analysis to see the long-time effect of the stone columns on the pore water pressures in the subsoil. For this simulation, only the water level case 1 (7m/0.33 days) was used. The curves shown in Fig. 45, Fig. 46, Fig. 47 are for point E in a depth of -20 m (acc. Tab. 15).

5.7.1 Consolidation for anisotropic permeability
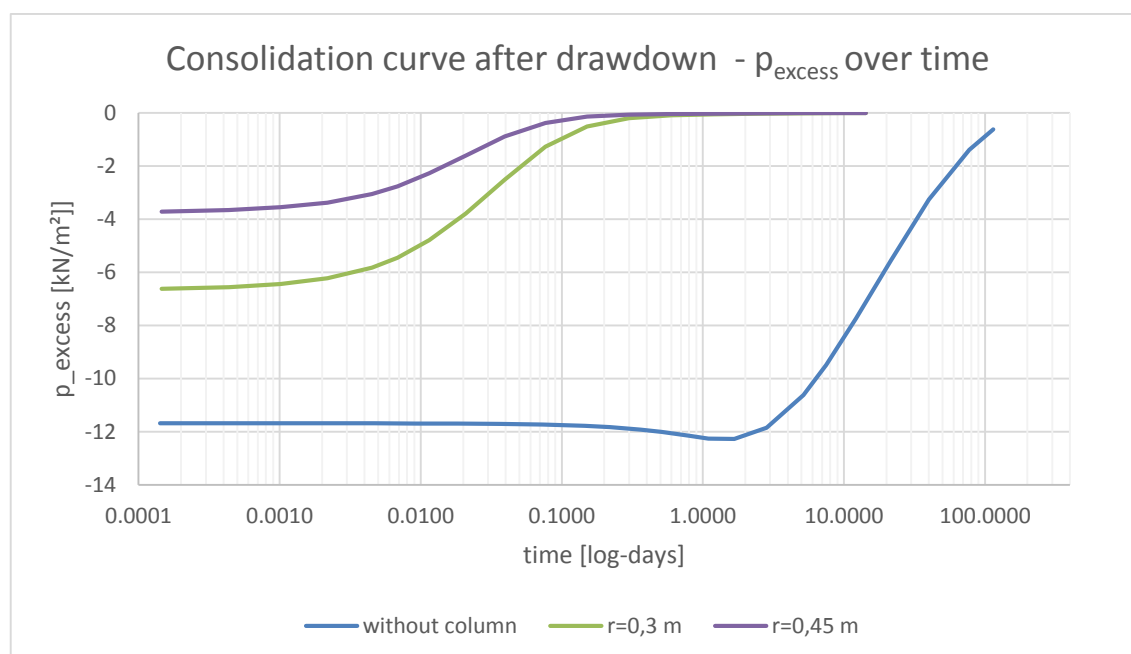
Fig. 45   Consolidation curve of the anisotropic permeability case after drawdown (with smear zone) ($k_x \neq k_y$) (point E)

As shown in Fig. 45 and Tab. 16, without any column, $|p_{excess}|$ at the beginning of the consolidation calculation after drawdown reaches a much higher value than with columns. Additionally, the time effect of the columns can be seen easily – with columns the time to reach 1 kN/m² excess pore water pressure reduces by approximately 100 days. Using a column radius of r=0.30 m consolidation takes as much time as using a column radius of r=0.45 m, even for r=0.45 m $|p_{excess}|$ at the start of the phase is already lower (see Tab. 16).

It seems that the slope of the consolidation curve without columns is steeper than with columns, but this effect is due to the logarithmic time scale.

Tab. 16   Summary of the consolidation analysis – anisotropic permeability conditions (with smear zone) after drawdown ($k_x \neq k_y$)

	p_{excess} at time = 0 days	Time until 1 kN/m² left
Without column	~ -11.7 kN/m²	~ 114.6 days
r = 0.30 m	~ -6.6 kN/m²	~ 14.3 days
r = 0.45 m	~ - 3.7 kN/m²	~ 14.3 days
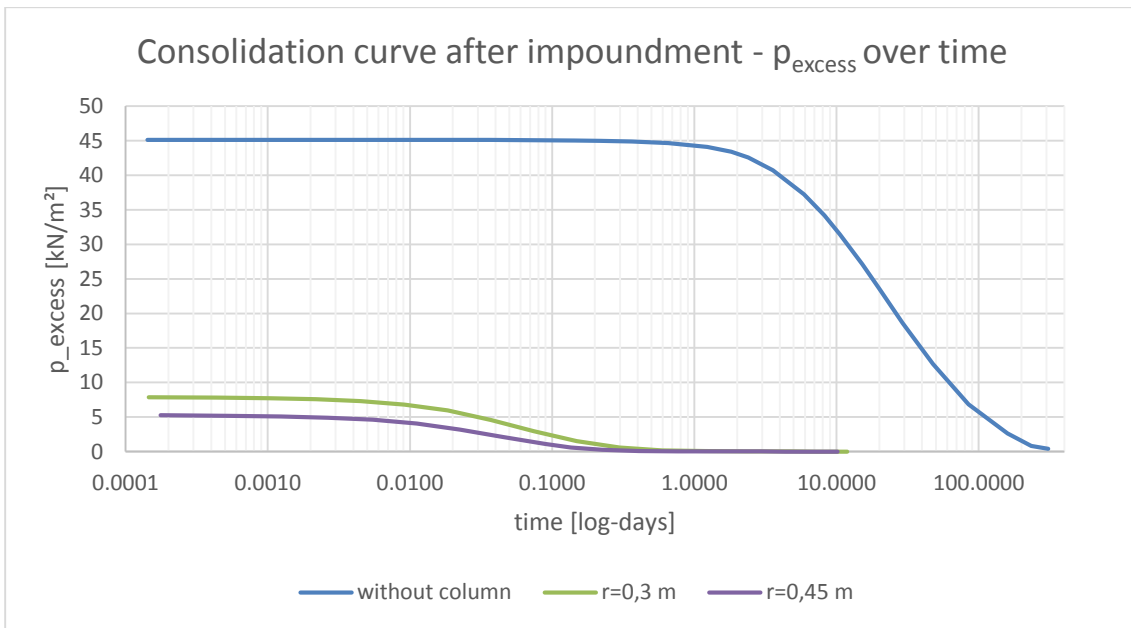
Fig. 46   Consolidation curve of the anisotropic permeability case after impoundment (with smear zone) ($k_x \neq k_y$) (point E)

Fig. 46 and Tab. 17 show, that without any column the $|p_{excess}|$ at the beginning of the consolidation calculation after impoundment reaches a much higher value than with installed columns. Also, the time effect of the columns can be seen easily – with installed columns the time to reach 1 kN/m² reduces by approximately 300 days. The effect of the columns can be seen in both cases - after impoundment and after drawdown (compare Fig. 46 and Fig. 45). Also after impoundment, the column radius has only a slight influence on the consolidation time. The higher radius of r=0.45 m reduces the consolidation time by approximately 1.5 days. (see Tab. 17)

Tab. 17 Summary of the consolidation analysis – anisotropic permeability conditions (with smear zone) after impoundment ($k_x \neq k_y$)

	p_{excess} **at time = 0 days**	**Time until 1 kN/m² left**
Without column	~ 45.1 kN/m²	~ 308.5 days
r = 0.30 m	~ 7.9 kN/m²	~ 11.9 days
r = 0.45 m	~ 5.3 kN/m²	~ 10.2 days

The consolidation curves of all points of interest (acc. to Tab. 15) after drawdown and after impoundment can be found in "Appendix A – Consolidation for anisotropic permeability".

5.7.2 Consolidation for the isotropic permeability conditions
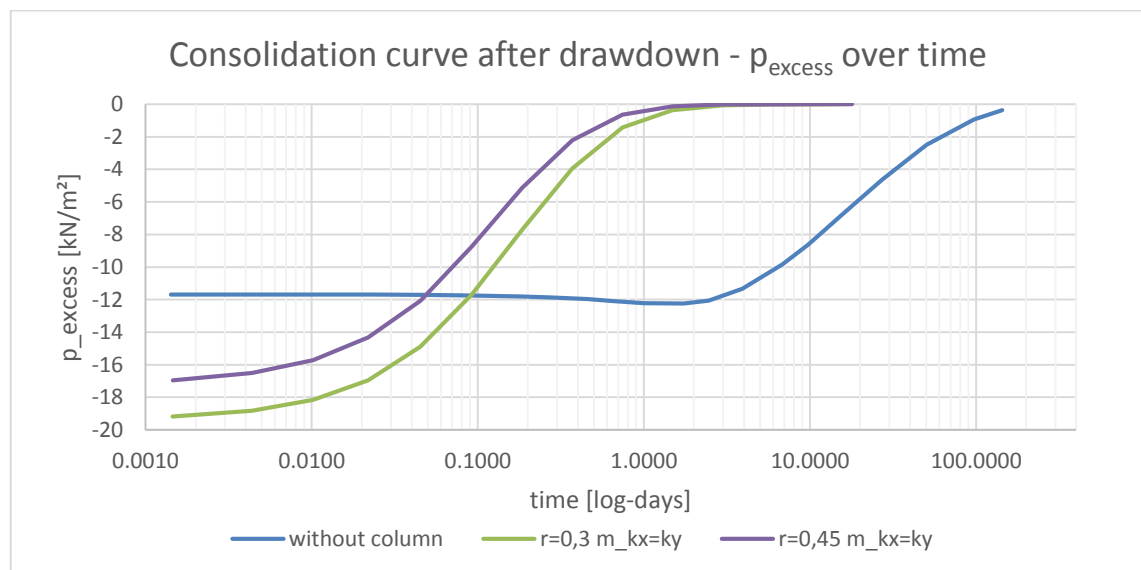
Fig. 47 Consolidation curve of the isotropic permeability case after drawdown (with smear zone) ($k_x \neq k_y$) (point E)

The results of the consolidation analysis after drawdown for the isotropic permeability case are summarized in Fig. 47 and Tab. 18. If the subsoil has an isotropic permeability of $k_x = k_y = 1 \cdot 10^{-8}\ m/s$, the value of excess pore water pressure $|p_{excess}|$ at the beginning of the consolidation analysis without columns is lower than with installed columns. The lower $|p_{excess}|$ without columns is due to the fact that without columns no "steady state"-mean pressure could be reached (during the simulation time). But even if the p_{excess} with columns is higher at the beginning of the calculation phase for the isotropic case, the consolidation is approximately 125 days faster than without column. However,

there is again no time reduction due to the different diameter of the column (see Tab. 18; compare to Tab. 16, Tab. 17).

Tab. 18   Summary of the consolidation analysis – isotropic permeability case (with smear zone)

	p_{excess} at time = 0 days	Time until 1 kN/m² left
Without column	~ -11.7 kN/m²	~ 143.6 days
r = 0.30 m	~ -19.2 kN/m²	~ 17.9 days
r = 0.45 m	~ - 17.0 kN/m²	~ 17.9 days

The consolidation curves of all points of interest (acc. to Tab. 15) after drawdown and after impoundment can be found in "Appendix B - Consolidation for isotropic permeability".

5.8   Conclusion of the preliminary axisymmetric study

The scope of this preliminary study was to understand the behaviour of the system and to see if the use of gravel columns could reduce the excess pore water pressures in the surrounding subsoil.

The model consists of a gravel column and the surrounding subsoil, therefore an axisymmetric model was chosen to analyse the behaviour.

The main conclusions of the preliminary study are:

- Steady state of the reference case without column is reached only in the upper part of the model (-2m), in deeper levels the p_{water} curve of the reference case is still inclined after 13.33 days (equivalent to 20 times up and down of water level). With column, the steady state is reached over the entire depth of the column.

- The smear zone has a minor influence on the system behaviour of the pore water pressures. Even the increased thickness of the smear zone of 45 cm had only a small influence on the generated pore water pressures.
  Looking at the hydraulic gradient next to column, the smear zone has a high influence. Assuming a smear zone of 10 cm the hydraulic gradient next to the column increases by approximately 50 %. According to the criteria, presented in

chapter 3.2 the gradients are a too high for the chosen material of the gravel columns. Even for the uniform middle sand (=lower limit) the critical hydraulic gradient is only 1.1 [-]. Therefore, the geometric criteria should be fulfilled for a stable material behaviour in case of the present project.

- The highest hydraulic gradient is reached with the highest fluctuation velocity. An increased column radius (r=0.45 cm) reduces the hydraulic gradient by approximately 15%.

- If the anisotropic permeability and the isotropic permeability case are compared, it can be seen easily that the horizontal permeability k_x has a high influence on the pore water pressures. If the horizontal permeability is set to the value of $1 \cdot 10^{-8}\ m/s$ the influence of the columns is reduced significantly (compare Fig. 34, Fig. 35 and Fig. 40, Fig. 41).Therefore, it is very important to know the appropriate input value for the horizontal permeability.

  Furthermore, the hydraulic gradient is 2-3 times higher, if isotropic permeability conditions are assumed in the subsoil.

6 Matching methods for plane strain analyses

For further investigations, concerning the influence of gravel columns on pore water pressures beneath a storage basin, the specific problem is studied under plane strain conditions. Therefore, a conversion of soil permeability from axisymmetric conditions to equivalent plane strain conditions is necessary.

6.1 Conversion of permeability

To model the influence of vertical drains or gravel columns on the hydraulic behaviour of the soil in a plane strain calculation, conversions concerning the permeability and / or the geometry are necessary. Aim of this conversion is to obtain the same drainage conditions in axisymmetric and plane strain conditions. For this, many of conversion methods are available in literature. In this section, a short summary of available conversion formulas is given.

6.1.1 Conversion of geometry and/or permeability of the subsoil around the column

Hird et al. (1992) developed a conversion formula from radial drainage to plane strain conditions. In his formulation, either the geometry, the permeability or even both can be adjusted to obtain similar drainage conditions. The smear zone around the columns and the well resistance can be taken into account. In Hird et al. (1992)'s approach, the smear effect is averaged over the entire drainage zone D. The drainage zone D depending on the installation pattern of the columns is calculated using Equ. (76) or (77) (see chapter 4.4). Half of the axisymmetric unit cell D is called R (for radius), therefore D=2R is valid. The equivalent plane strain unit cell is defined as B (compare Fig. 48). If B=R, the permeability and well resistance are calculated with Equ. (80) and (82).

$$k_{pl} = \frac{2 \cdot k_{ax}}{3 \cdot [ln\left(\frac{n}{s}\right) + \left(\frac{k_{ax}}{k_{ax,s}}\right) ln(s) - 0.75]} \qquad (80)$$

$$n = \frac{R_{ax}}{r_w}, \qquad s = \frac{r_w}{r_s} \qquad (81)$$

$$Q_w = \left(\frac{2}{\pi \cdot R}\right) \cdot q_w \qquad (82)$$

k_{pl} [m/s]   horizontal permeability of subsoil in plane strain condition

k_{ax} [m/s]   horizontal permeability of subsoil in axisymmetric unit cell

$k_{ax,s}$ [m/s]   horizontal permeability of smear zone in axisymmetric unit cell

n, s	[-]	geometry factors
R_{ax}	[m]	radius of the axisymmetric unit cell (drain influence zone $D_{tri} = 2R_{ax}$, calculated acc. to Equ.(76) or (77))
r_w	[m]	radius of the column in the axisymmetric unit cell
r_s	[m]	radius of the smear zone in the axisymmetric unit cell (measured from column axis)
Q_w	[m³/s]	discharge capacity of drain in plane strain unit cell
q_w	[m³/s]	discharge capacity of drain in axisymmetric unit cell

Hird et al. (1992)'s approach is recommended because the average degree of consolidation is matched to the soil in axisymmetric condition. However, Hird et al. (1992) point out that even if equal matching is reached by the conversion, the excess pore water pressures at comparable points in the unit cell will not be the same. The different pore water pressure distribution could influence the response of the subsoil, in particular for elasto-plastic soil models.

6.1.2 Matching procedure based on well resistance

Chai et al. (1995)'s matching procedure is based on Hird et al (1995). The new procedure provides good agreement of the horizontal consolidation between axisymmetric and plane strain conditions and a more realistic excess pore water distribution in plane strain conditions than Hird et al.'s (1995) formulation. But as discussed in chapter 4, the well resistance is not considered for the specific problem of this thesis and therefore the procedure is not described in detail.

6.1.3 Time-depending permeability matching

Weber (2008) describes the formulation of CUR 191 (1997) for a conversion within a spatial structure of gravel columns (=drains) for a 2D analysis in his dissertation. In this formulation the equivalent horizontal permeability depends on the time. The factor α (see Equ. (86)) is a function of the degree of consolidation U. The degree of consolidation U is changing with time and so is the factor α. The degree of consolidation U must be predicted before starting the calculations, which is a disadvantage of this method. Nevertheless, if the degree of consolidation U is higher than 50 %, the factor α is higher than 2 and with increasing degree of consolidation U converges to 3.2. In the formulation shown below (Equ. (83) et seq.) the smear zone and well resistance are not considered. (Weber 2008) cf. (CUR 191 1997)

$$k_{hp} = \alpha \cdot \frac{B^2}{\mu \cdot 4R^2} \cdot k_h \qquad (83)$$

$$\mu = \frac{n^2}{n^2 - 1} \cdot \left[\ln(n) - \frac{3}{4} + \frac{1}{n^2} \cdot \left(1 - \frac{1}{4 \cdot n^2} \right) \right] \qquad (84)$$

$$n = \frac{R_{ax}}{r_w} \qquad (85)$$

$$\alpha = 3.24 \cdot \frac{\ln(1 - U) + 0.1}{\ln(1 - U)} \qquad (86)$$

k_{hp}	[m/s]	horizontal permeability of subsoil in plane strain condition
k_h	[m/s]	horizontal permeability of subsoil in axisymmetric unit cell
α	[-]	factor for influence of time
B	[m]	half distance of drains in plane strain condition
R_{ax}	[m]	radius of the axisymmetric unit cell (drain influence zone $D = 2R_{ax}$, calculated acc. to Equ.(76) or (77))
r_w	[m]	radius of the column in the axisymmetric unit cell
U	[-]	degree of consolidation

6.1.4 Improved plane strain modelling of vertical drains including smear effects

Indraratna & Redana (1997, 2000) developed an improved conversion approach which is based on Hird et al. (1992). The main goal of this new conversion was to model the smear zone explicitly. With this approach, different extents of the smear zone can be examined easily. In Fig. 48 the geometry for the conversion is shown.

If the geometry is not changed (R=B) during conversion and smear effect and well resistance are ignored, Equ. (87) gives the ratio of plane strain k_{hp} to axisymmetric k_h horizontal permeability. (Indraratna & Redana 2000)

$$\frac{k_{hp}}{k_h} = \frac{0.67}{ln(n) - 0.75} \qquad (87)$$

$$n = \frac{R_{ax}}{r_w} \qquad (88)$$

k_{hp}	[m/s]	horizontal permeability of subsoil in plane strain condition
k_h	[m/s]	horizontal permeability of subsoil in axisymmetric unit cell

R_{ax} [m] radius of the axisymmetric unit cell (drain influence zone $D = 2R$, calculated acc. to Equ.(76) or (77))

r_w [m] radius of the column in the axisymmetric unit cell

Fig. 48 Geometry description for converison of an axisymmetric (a) unit cell to a plane strain (b) unit cell (Indraratna & Redana 1997) , (Indraratna & Redana 2000)

If the effect of smear is considered, but the well resistance is neglected, Equ. (89) gives the ratio between the horizontal permeability in the smear zone k'_{hp} and the horizontal permeability in the sub soil k_{hp} (both for plane strain conditions, as the Index p indicates).

$$\frac{k'_{hp}}{k_{hp}} = \frac{\beta}{\frac{k_{hp}}{k_h} \cdot \left[\ln\left(\frac{n}{s}\right) + \left(\frac{k_h}{k'_h}\right) \cdot \ln(s) - 0.75\right] - \alpha} \tag{89}$$

$$n = \frac{R_{ax}}{r_w}, \qquad s = \frac{r_w}{r_s} \tag{90}$$

$$\alpha = \frac{2}{3} - \frac{4b_s^3}{3B^3} + \frac{2b_s^2}{B^2} - \frac{2b_s}{B} \tag{91}$$

$$\beta = \frac{b_s^2}{B} - \frac{b_s^3}{3B^3} - \frac{2b_w^3}{3B^3} - \frac{2b_w b_s}{B^2} + \frac{b_w^2}{B^2} + \frac{b_w^2 b_s}{B^3} \tag{92}$$

k_{hp} [m/s] horizontal permeability of subsoil in plane strain condition

k_h [m/s] horizontal permeability of subsoil in axisymmetric unit cell

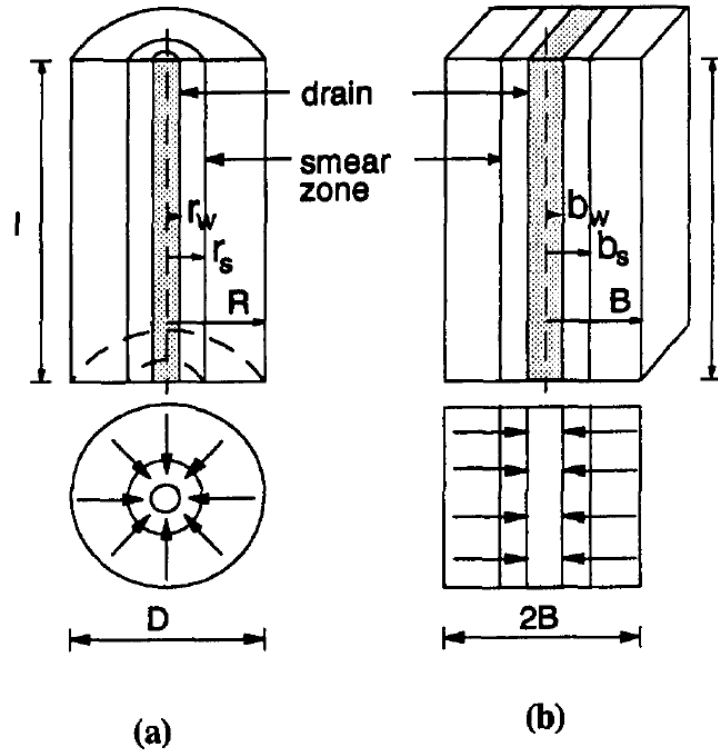| k'_{hp} | [m/s] | horizontal permeability of smear zone in plane strain condition |
n, s	[-]	geometry factors (geometric input see also Fig. 48)
α, β	[-]	geometry factors
R_{ax}	[m]	radius of the axisymmetric unit cell (drain influence zone $D = 2R$, calculated acc. to Equ.(76) or (77))
r_w	[m]	radius of the column in the axisymmetric unit cell
r_s	[m]	radius of the smear zone in the axisymmetric unit cell
b_s	[m]	half width of smear zone in plane strain condition
B	[m]	half width of unit cell in plane strain condition
b_w	[m]	width of column in plane strain condition

First, the horizontal permeability k_h has to be determined in laboratory or field tests. Afterwards, the horizontal plane strain permeability k_{hp} can be computed using Equ. (87). As next step, the horizontal plane strain permeability in the smear zone k'_{hp} can be calculated by Equ. (89). (Indraratna & Redana 2000)

If Indraratna & Redana (2000) and Indraratna & Redana (1997) are compared, a conflict about the conversion approach is recognized. Indraratna & Redana (2000) clearly recommends:

"In such "explicit" smear zone modeling [sic] as introduced here, the width of the unit cell of drain and its surrounding smear zone is kept the same for both axisymmetric and plane strain models, but the axisymmetric permeability is converted to an equivalent plane strain value. In other words, the half-width of the drain (b_w) and the half-width of the smear zone (b_s) in plane strain are taken to be the same as their correspondig axisymmetric radii, which gives $b_w = r_w$ and $b_s = b_s$."

Indraratna & Redana (1997) write about the same approach, but recommend:

"The vertical drain system may be converted into equivalent parallel drain walls by adjusting the spacing of the drain wall and the coefficient of permeability of the soil. […] The width of the drain may be determined by considering the total capacity of the drain in both systems to be the same. For example, in a system of vertical drain arranged at a spacing of S in a square pattern, the width of the drain and the smear zone may be expressed by

$$b_w = \frac{\pi \, r_w{}^2}{2 \, S} \; and \; b_s = \frac{\pi \, r_s{}^2}{2 \, S} \tag{ 93 }$$

For drains arranged in a triangular pattern, the equivalent widths are given by

$$b_w = \frac{1.143 \, \pi \, r_w{}^2}{2 \, S} \; and \; b_s = \frac{1.143 \, \pi \, r_s{}^2}{2 \, S} \tag{94}$$

Where S is the field spacing (center to center) [sic] between any two adjacent drains."
In the following chapter (6.2), the geometry of the drain and smear zone is not changed during conversion to plane strain conditions.

Indraratna & Redana (2000) note, that the precision of the numerical analyses depends on the correct estimation of the soil properties, especially of the horizontal permeability in axisymmetric conditions before conversion to equivalent plane strain conditions. Additionally, it is very difficult to examine the expansion of the smear zone and its particular properties. (Indraratna & Redana 2000) & (Weber et al. 2010) In the same paper Indraratna & Redana (2000) point out:
"In general, the accurate prediction of pore water pressure is more difficult than the prediction of settlements, […]".
If smear effect and well resistance are included in the calculations, the calculations of the pore water pressure are more realistic. As the smear effect has a much higher influence on the pore water pressure distribution, the well resistance may be neglected. (Indraratna & Redana 2000)

6.1.5 EA-Equality of the column in plane strain conditions

By changing the column with a radius r to an equal wall with the width $w = 2r$ the EA-value has to be converted acc. to Equ. (95).

$$E_{ax} \cdot A_{ax} = E_{pl} \cdot A_{pl} \rightarrow E_{pl} = \frac{E_{ax} \cdot A_{ax}}{A_{pl}} \tag{95}$$

E_{ax}	[kN/m²]	Young's modulus in axisymmetric condition
A_{ax}	[kN/m²]]	Column area in axisymmetric condition
E_{pl}	[kN/m²]]	Young's modulus in plane strain condition
A_{pl}	[kN/m²]]	Column area in plane strain condition

6.2 Comparison and verification of the conversion

In this chapter, the conversion from axisymmetric conditions to plane strain conditions is checked for columns with a radius r=0.3 m and anisotropic permeability conditions ($k_x \neq k_y$). In the following analysis Hird et al. (1992)'s (later called Hird's approach) and

Indraratna & Redana (1997, 2000)'s approach (later called Indraratna's approach) are used.

6.2.1 Resulting input values for the plane strain simulation with PLAXIS

In Tab. 19, the input values for the comparison of the conversion to plane strain conditions are summarized. The horizontal permeability of the drainage zone is reduced due to the mentioned formulas in chapter 6.1. No changes in geometry are considered. The vertical permeability is not changed and only the Young's modulus of the column has to be reduced by using Equ. (95). The vertical permeability is kept the same for all calculations.

Tab. 19   Summary of Input values of the conversion study

	Axisymmetric	Plane-strain Hird	Plane-strain Indraratna & Redana	Unit
k_h	1 E-7	4.646 E-8	5.841 E-8	[m/s]
k_v	1 E-8	1 E-8	1 E-8	[m/s]
$k_{h,s}$	5 E-8	Averaged over drainage zone	2.237 E-9	[m/s]
$k_{v,s}$	5 E-9	Averaged over drainage zone	5 E-9	[m/s]
$B = R$	2.0	2.0	2.0	[m]
$b_w = r_w$	0.3	0.3	0.3	[m]
$b_s = r_s$	0.4	Not explicitly modelled	0.4	[m]
E_{col}	2 E4	1.88 E4	1.88 E4	[kN/m²]

6.2.2 Results of the comparison between axisymmetric and plane strain models – p_{water} curves and groundwater head

Similar calculations as described in chapter 5 were carried out in plane strain conditions for column radius r = 0.3 m. In Fig. 49, Fig. 50 and Fig. 51, the pore water pressures p_{water} over time are presented for different depths. Hird's approach (green) does fit very well to the axisymmetric case. In the depth of -30 m Indraratna's approach (red) fits better than Hird's (green).
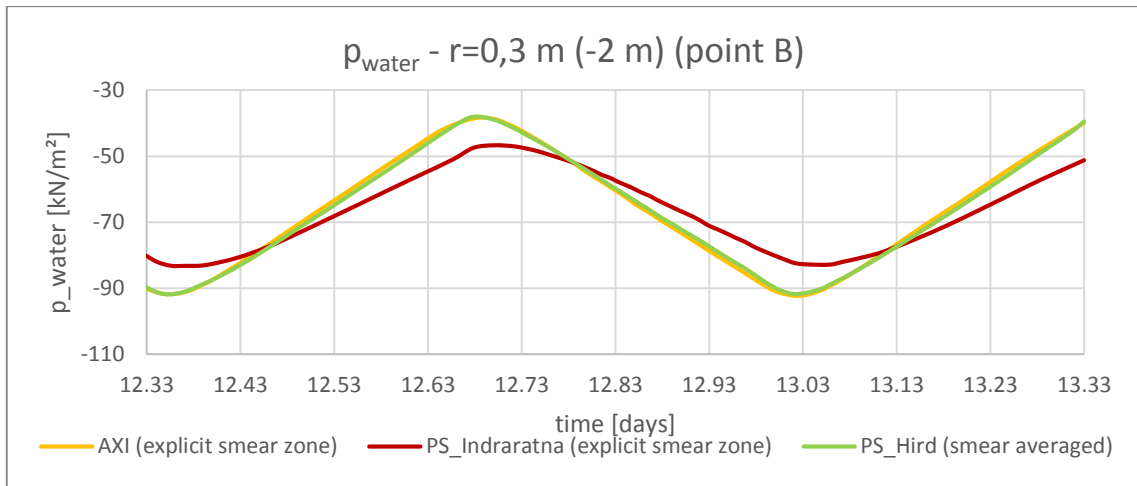
Fig. 49   Comparison of p_water over time in depth of -2 m incl. smear (Point B)
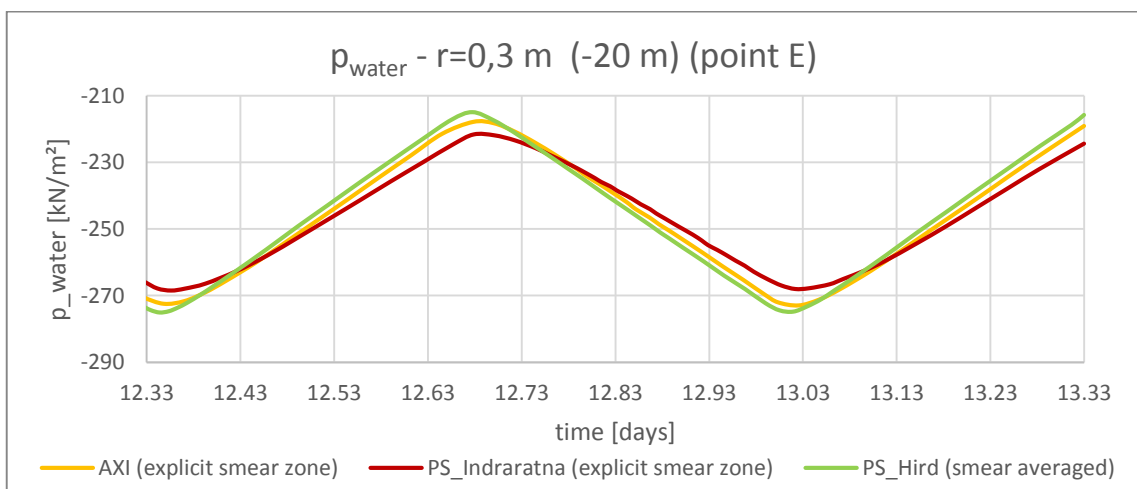
Fig. 50   Comparison of p_water over time in depth of -20 m incl. smear (Point E)
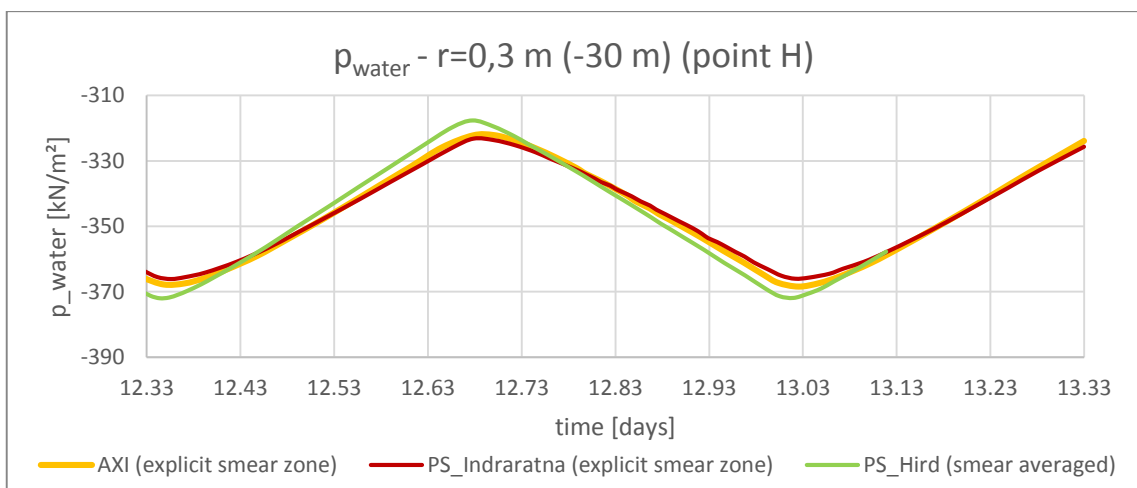
Fig. 51   Comparison of p_water over time in depth of -30 m incl. smear (Point H)

In Fig. 52, Fig. 53 and Fig. 54, the groundwater head over the width of the model is shown for different depths. The axisymmetric curve without smear (grey dotted) is plotted in the figures as a reference for comparison and verification. The axisymmetric case without smear (grey dotted) produces slightly smaller groundwater heads over the entire

model width and over the full columns length than the axisymmetric case with explicit modelled smear zone (yellow dotted).

Hird's approach with the averaged smear effect (green) is fitting quite well to the axisymmetric case including smear (yellow dotted), especially in the upper part of the model. In a depth of -30 m below ground surface Hird's approach with averaged smear effect (green) has a deviation to the axisymmetric case of approximately 50 cm at a distance of 2 m from the column axis. The shape of the groundwater head over the width of the model looks similar to the axisymmetric case including smear (yellow dotted).

Indraratna's approach with explicitly modelled smear zone (red) produces a kink at both sides of the explicitly modelled smear zone. Another disadvantage of Indraratna's approach with smear zone (red) is that the resulting groundwater head over the entire depth is too high. In comparison, Indraratna's approach without considering a smear zone (blue) does not produce any kinks and fits quite well to Hird's approach (green), and also to the axisymmetric curve with explicit modelled smear zone (yellow dotted). Nevertheless, Indraratna's approach without considering a smear zone (blue) underestimates the groundwater head more than Hird's approach with averaged smear effect (green), especially in the deeper levels.

The results of the conversions are similar after an impoundment (and therefore are not shown in this study).
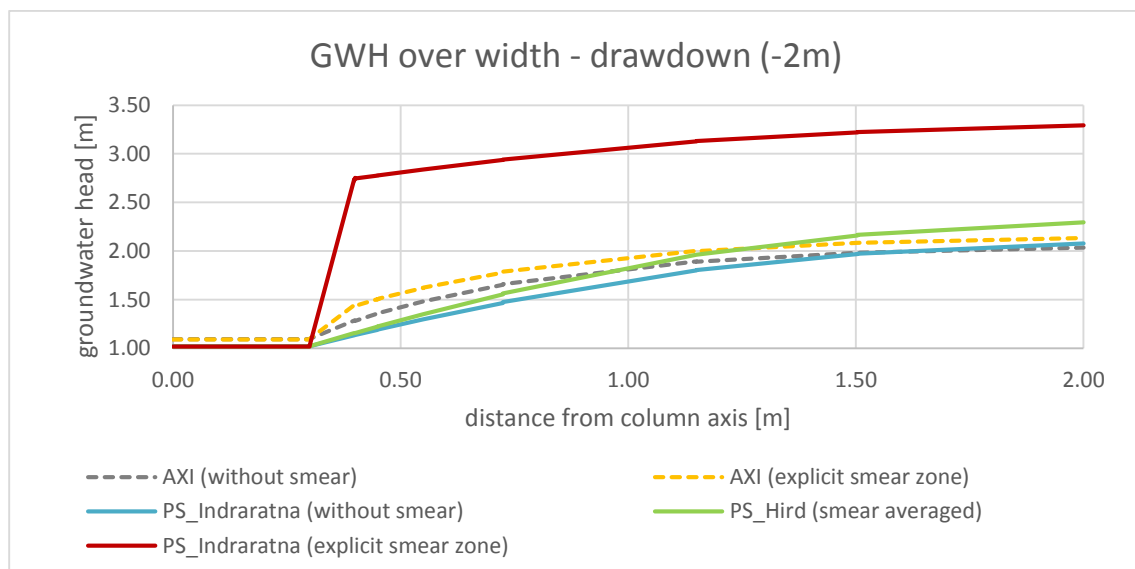

Fig. 52   Comparison of groundwater head in a depth of -2 m
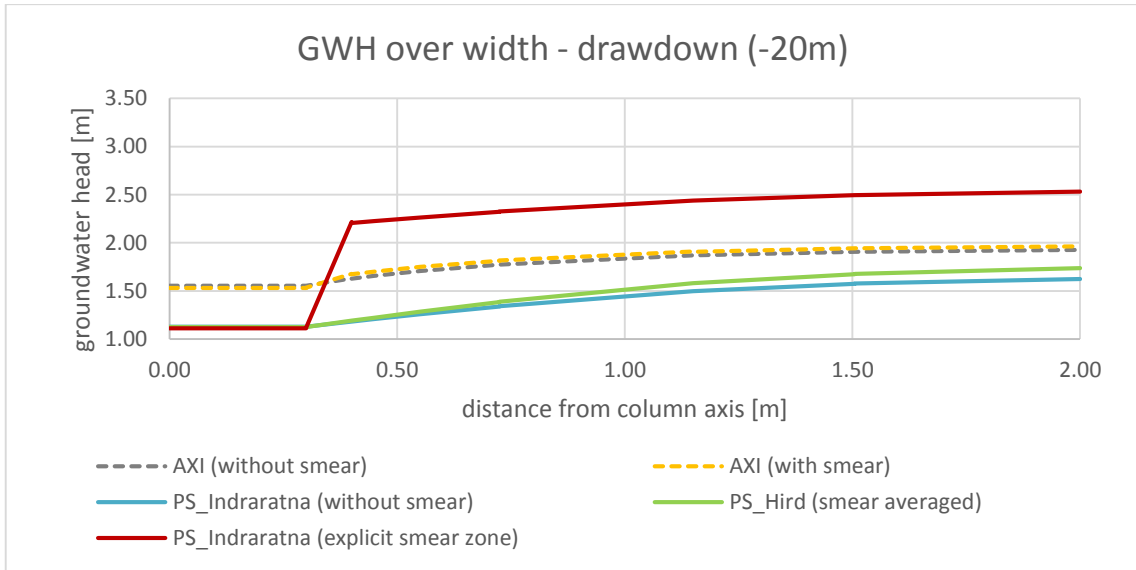
Fig. 53   Comparison of groundwater head in a depth of -20 m
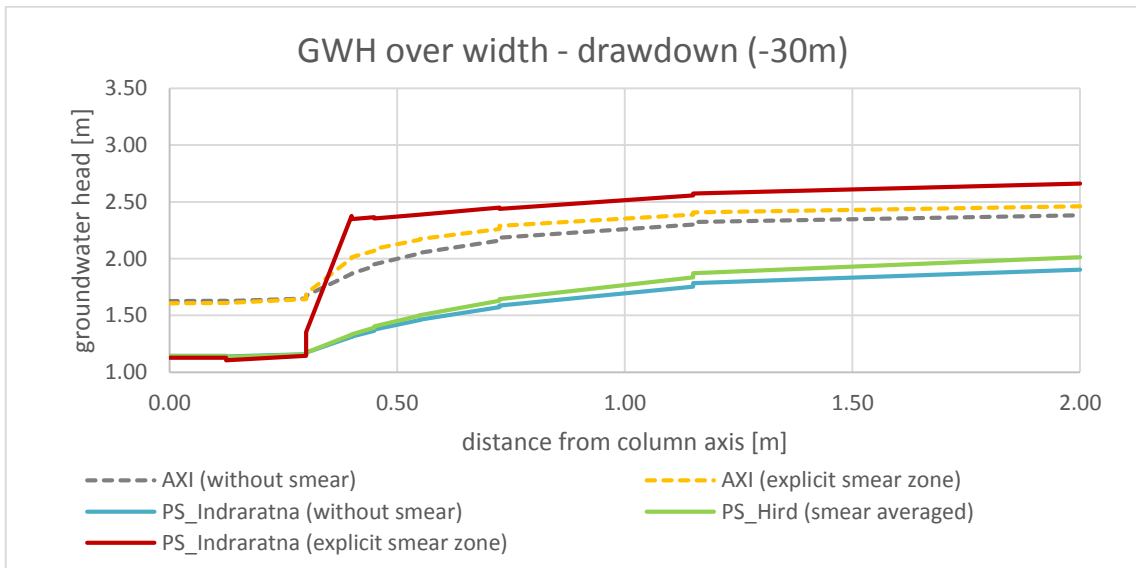
Fig. 54   Comparison of groundwater head in a depth of -30 m

6.2.3 Results of consolidation analysis - axisymmetric vs. plane strain model

In addition to the pore water pressures, the consolidation behaviour of the plain strain model is compared with the results of the axisymmetric model. The results are shown in Fig. 55 and Fig. 56 and they are summarized in Tab. 20. The presented diagrams are evaluated for point E, which is in a depth of -20 m (acc. to Tab. 15). Again, it can be recognized that Hird's approach with averages smear effect (green) shows a good fit with the results of the axisymmetric model (grey and yellow dotted), but Indraratna's approach with smear explicitly modelled (red) produces too high pore water pressures after drawdown. After impoundment, Indraratna's approach (red) produces also too high pressures, the system behaviour is similar as after drawdown.
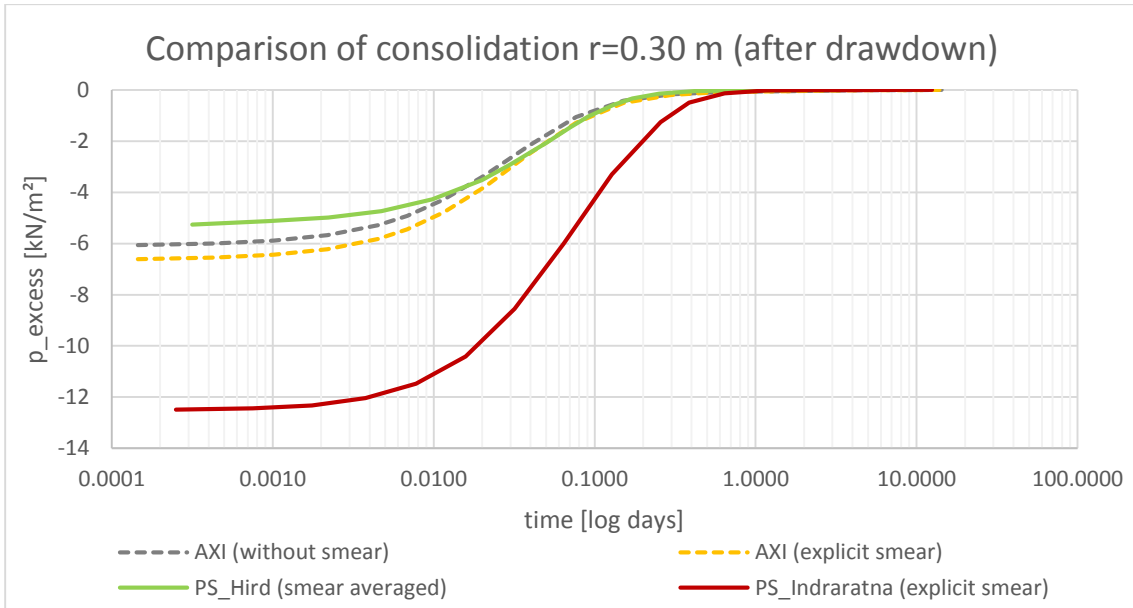
Fig. 55   Comparison of consolidation curves after drawdown
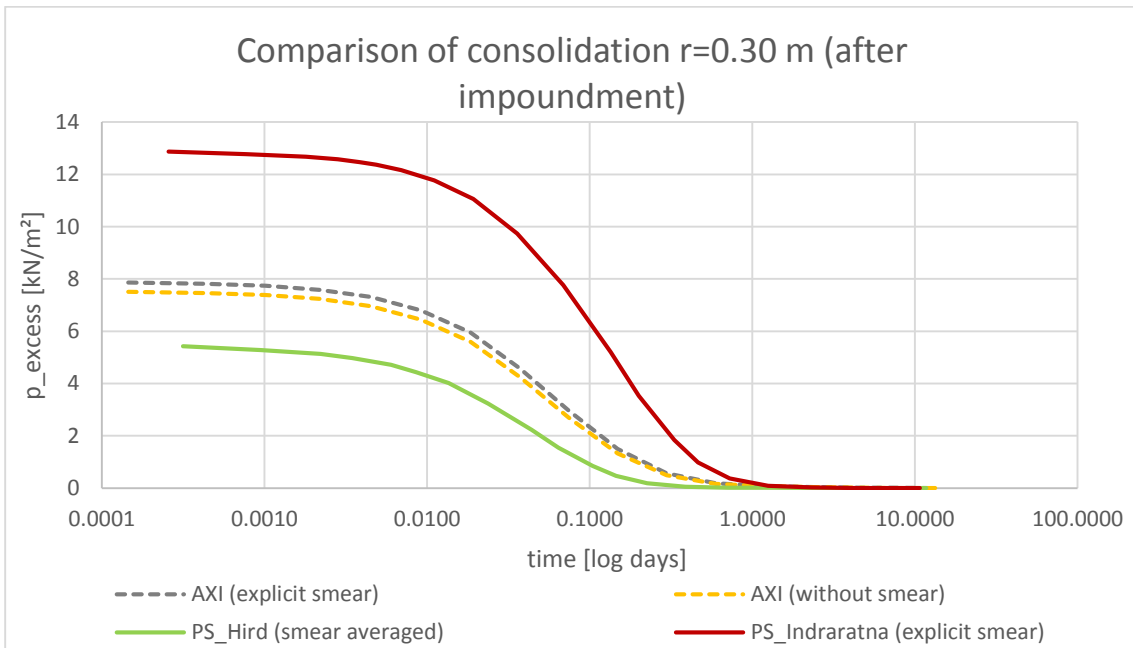
Fig. 56   Comparison of consolidation curves after impoundment

Tab. 20   Summary and comparison of the consolidation study – isotropic permeability case (with smear zone) – axisymmetric vs. plane strain condition

		p_{excess} at time = 0 days	Time til 1 kN/m²
drawdown	AXI, r = 0.30 m (explicit smear)	~ -6.6 kN/m²	~ 14.3 days
	PS, r=0.30 m_Indraratna (explicit smear)	~ -12.5 kN/m²	~ 12.5 days
	PS, r=0.3 m_Hird (smear averaged)	~ -5.3 kN/m²	~ 11.1 days

impoundment	AXI, r = 0.30 m (explicit smear)	~ 7.9 kN/m²	~ 11.9 days
	PS, r = 0.30 m_Indraratna (explicit smear)	~ 12.9 kN/m²	~ 10.7 days
	PS, r = 0.30 m_Hird (smear averaged)	~ 5.4 kN/m²	~ 11.7 days

6.2.4 Results for the hydraulic gradient - axisymmetric vs. plane strain model

Finally, the hydraulic gradient of the plane strain calculations was checked against the results of the axisymmetric model. The results are presented in Fig. 57, Indraranta's approach with an explicitly modelled smear zone (red), produces non-realistic high gradients next to the column (in the smear zone). Hird's approach with the averaged smear effect (green) generates more reasonable gradients, but compared to the axisymmetric case (grey and yellow dotted) the plane strain hydraulic gradients are approximately 50 % smaller than the axisymmetric results with included smear zone.

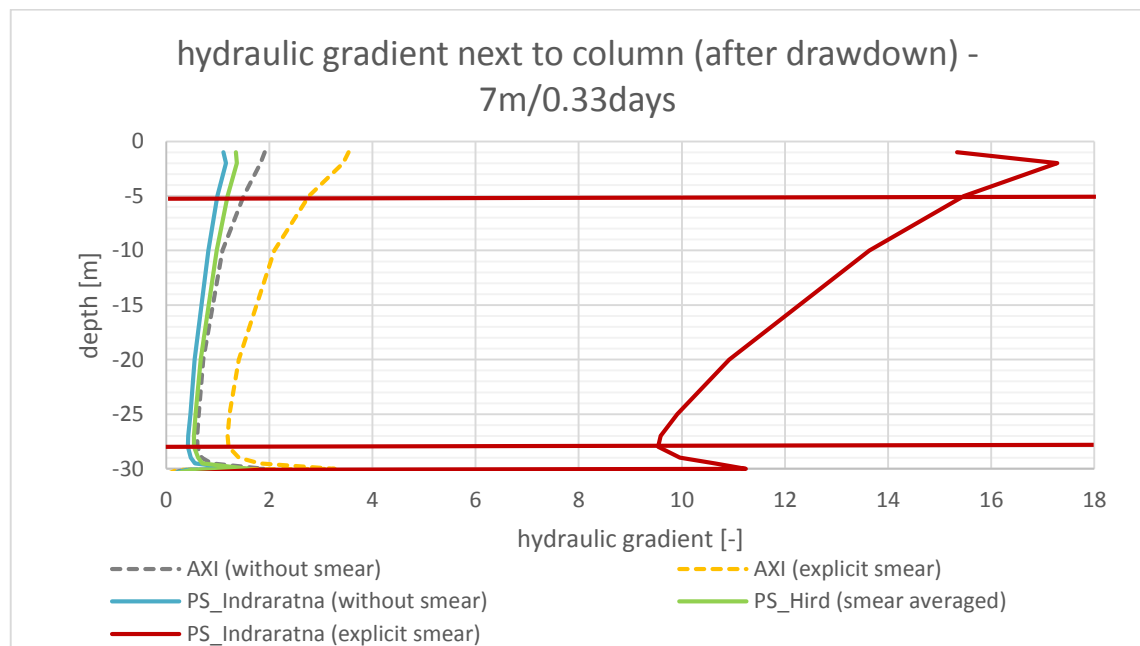Fig. 57   Comparison of the hydraulic gradient next to the column over depth (after drawdown) for r=0.30 m

6.3   Conclusion of equivalent plane strain conversion

In chapter 6.1 a literature review about the conversion of soil permeability and / or geometry of vertical drains from axisymmetric conditions to plane strain conditions is summarized. In chapter 6.2 two approaches (Hird and Indraratna) are chosen and tested

for the specific problem of the presented preliminary study. The results of the simulation after conversion to plane strain conditions, with and without a smear zone, are compared to the axisymmetric case.

The outcome of the comparison is, that Hird et al.(1992)'s approach with the averaged smear effect results in good matches in most cases:

- The p_{water}-time-curve is reproduced quite well over the entire depth of the model. The differences between the results of the axisymmetric model and the plane strain model are increasing with depth, but remain moderate.

- The agreement on the groundwater head over the width of the model is also very good in the upper part of the model (-2 m). In the middle (-20 m) and in the lower (-30 m) part of the model the deviation of Hird's plane strain curve is increasing, but still stays in an acceptable range.

- In the consolidation analysis, the calculated time of Hird's approach fits reasonably well to the axisymmetric case after drawdown (approximately 3 days difference) and after impoundment (nearly no difference) (compare Fig. 55, Fig. 56 and Tab. 20).

- Concerning the hydraulic gradient next to the column, Hird's approach produces values within a reasonable range, but in general the gradients are lower. It is recommended that the hydraulic gradient next to the column should be evaluated in the axisymmetric model. If an evaluation in plane strain conditions is necessary, it is important to know that the values are slightly underestimated using Hird's approach.

If Indraratna & Redana (2000)' approach with the explicitly modelled smear zone is used for the conversion of the relevant parameters for the plane strain model, the match with the results of the axisymmetric model is not that well as for Hird et al. (1997)'s approach:

- The p_{water}-curve of Indraratna's approach does not fit the axisymmetric case well, except for the lower part (approximate depth of 30 m). (compare Fig. 49, Fig. 50, Fig. 51).

- The groundwater head distribution over the model width is not in agreement over the entire column length. The resulting groundwater head is too high in the entire model. At both sides of the explicitly modelled smear zone, kinks occur in the curve (compare Fig. 52, Fig. 53, Fig. 54).

- Using Indraratna's approach, during the simulation of the water level fluctuation too high excess pore water pressures are generated in the subsoil. The deviation of Indraratna's approach to the axisymmetric case (both with explicitly modelled smear zones) after drawdown is slightly higher (approximately 6 kN/m²) than after impoundment (approximately 5 kN/m²). (compare Fig. 55 and Fig. 56). The consolidation time after drawdown is approximately 2 days shorter than in axisymmetric conditions, but after impoundment the time fits better (approximately 1 day difference) (see Tab. 20).

- The hydraulic gradients according to Indraratna's approach are significantly too high.

- The mentioned uncertainties concerning the adjustment of the geometry (see chapter 6.1.4) have not been clarified. However, the preliminary study shows that without changing the geometry, the approach according to Indraratna does not result in comparable pore water pressure distributions.

Due to the above-mentioned reasons, it can be stated that Hird's approach is the better choice for this specific problem. Additionally, the extent of the smear zone is not known exactly before installing the gravel columns and therefore and explicit modelled zone is not representative or rather does not produce better or more realistic results. For the model simulation of the power plant next to a slow moving slope in chapter 7, Hird's approach is used.

7 System behaviour of gravel columns beneath a water storage basin

In this chapter, a project of a slow-moving slope next to a water storage basin is modelled, using 2D plane strain simulations in Plaxis 2D (Brinkgreve 2016). The main assumptions (see chapter 7.1, 7.2, 7.3 and 7.4) and the results (see chapter 7.5, 7.6 and 7.7) of the simulations are summarized.

7.1 Project

The pump storage power plant is located in Austria. The storage basin is situated next to a slope, which is slowly moving towards the basin. The average slope inclination is 30° with a horizontal extension of approximately 290 m. The slope consists of a sliding mass, a transition zone and solid rock. The sliding mass has a mean thickness of 22 m. In Fig. 58 an overview of the project area is shown.
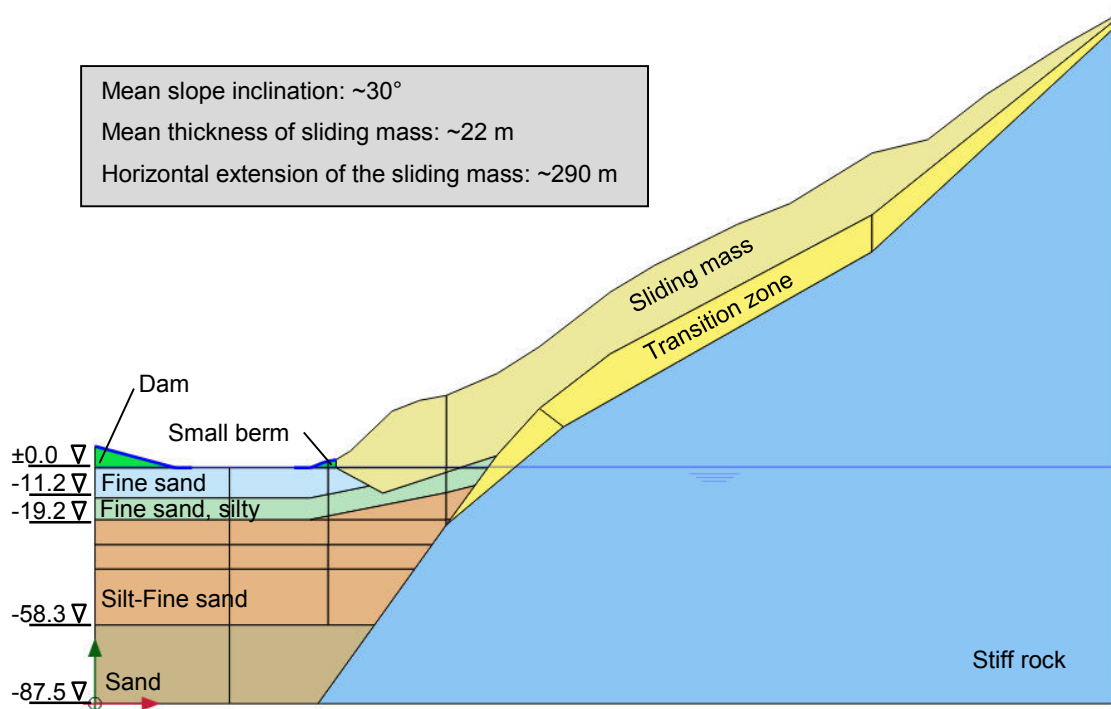

Fig. 58   Overview storage basin and slow-moving slope

The subsoil of the storage basin consists of several different layers of fine grained materials with very low permeabilities. The material parameters, which are used for the 2D simulation with anisotropic permeability conditions, are summarized in "Appendix C – Input parameter for Plane strain simulation (anisotropic)". For isotropic permeability conditions the horizontal permeabilities k_x in the upper three layers (Fine sand, Fine sand silty, Silt-Fine sand) were reduced to the vertical permeability k_y of the

corresponding layer (see "Appendix D - Input parameter for Plane strain simulation (isotropic)"). The present soil consists of fine layers of clayey silt and fine sand. The permeability was determined on soil samples in the laboratory with a flow direction mainly perpendicular to the layers. Due to the layered structure, an anisotropic permeability can be assumed. Nevertheless, anisotropic and the isotropic cases are considered in the following analyses.

Due to the fluctuation of the water level in the storage basin and the slow-moving slope, excess pore water pressures are generated in the fine grained layers. The main purpose of installing gravel columns at the slope toe is the reduction of these excess pore water pressures in the subsoil and the increase of the factor of safety (FOS) of the adjacent slope. The columns are going to be installed in a triangular pattern with a spacing of 2.31 m.

7.2 Model

The model is shown in Fig. 59. The lower boundaries of the slope and the subsoil are closed for water seepage and fully fixed for deformation due to the intact rock.
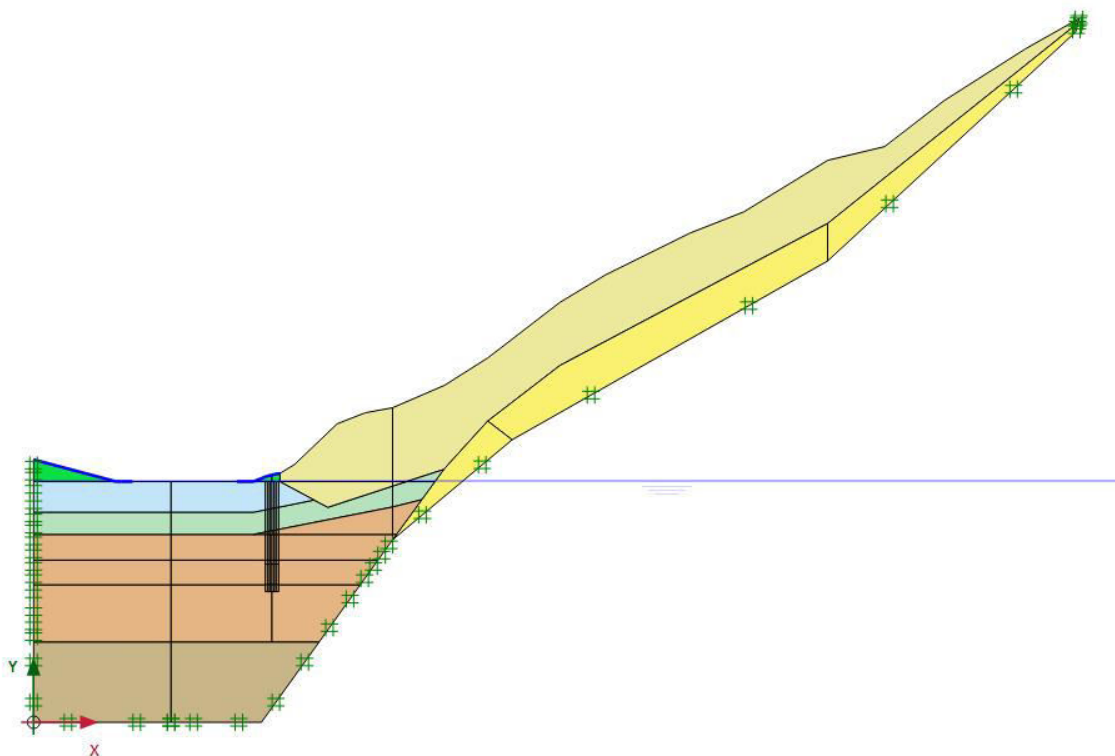

Fig. 59   Overview of Plaxis 2D model (Reference case – without columns)

For the analyses 6-noded triangular elements are used because they this element type is less time consuming than the 15-noded type. In Fig. 60 the zoomed in overview of the

mesh at the slope toe is presented. For the area of the slope toe and the transition zone a very fine mesh is chosen due to the high deformation and hydraulic gradients.
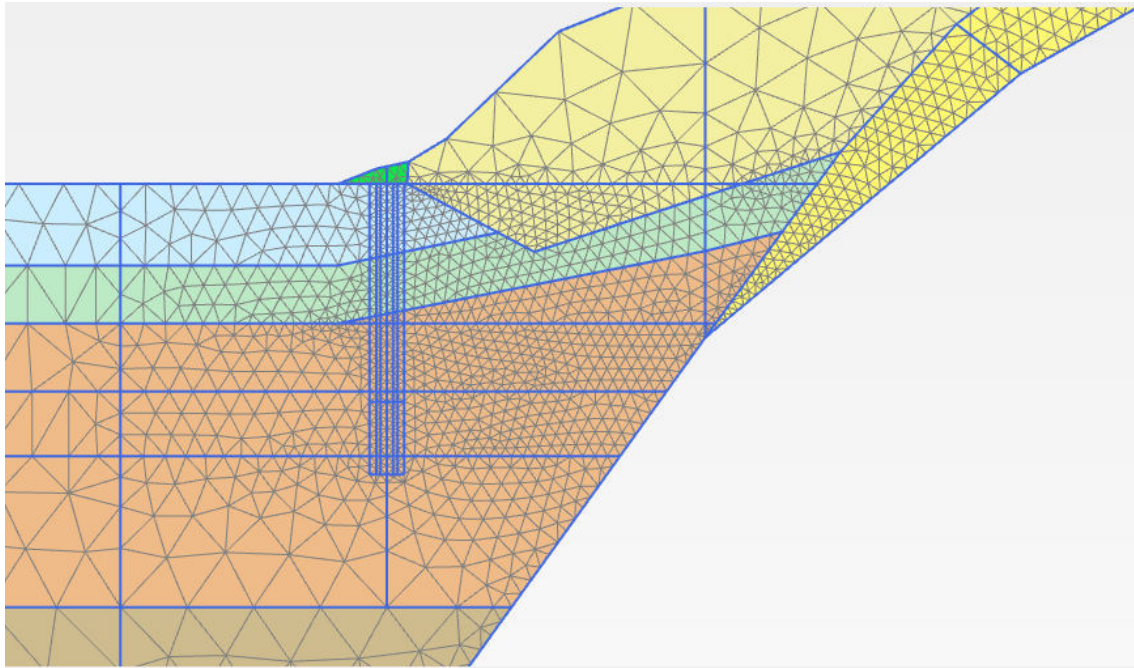

Fig. 60   Overview of generated mesh at the slope toe (Reference case – without columns)

In these 2D plane strain simulations four cases (shown in Fig. 61) are analysed under anisotropic and isotropic permeability conditions:

    (1) Reference case – without columns,
    (2) Two columns with a length of 30 m, radius of 0.3 m,
    (3) Two columns with a length of 40 m, radius of 0.3 m,
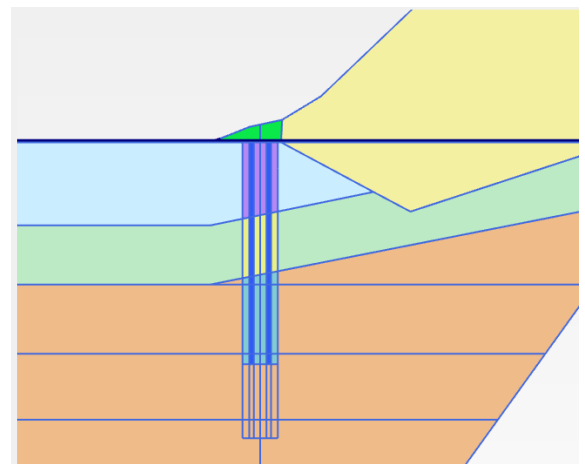   (4) Three columns with a length of 30 m, radius of 0.3 m.

As matching method for the 2D plane strain calculation Hird et al.(1992)'s approach is used, because it showed the best results in the preliminary studies (compare chapter 6.3). The reduced permeabilities of the drain influence zone are summarized in "Appendix C – Input parameter for Plane strain simulation (anisotropic)" for anisotropic and in "Appendix D - Input parameter for Plane strain simulation (isotropic)" for isotropic permeability conditions.

The preliminary study showed that there are only minor differences in the pore water distributions between the two gravel column radii of 0.30 and 0.45 m. Thus, in the following 2D plane strain analyses only the column radius of 0.30 m is used. (The column radius has more influence on the hydraulic gradient next the column, but is not evaluated
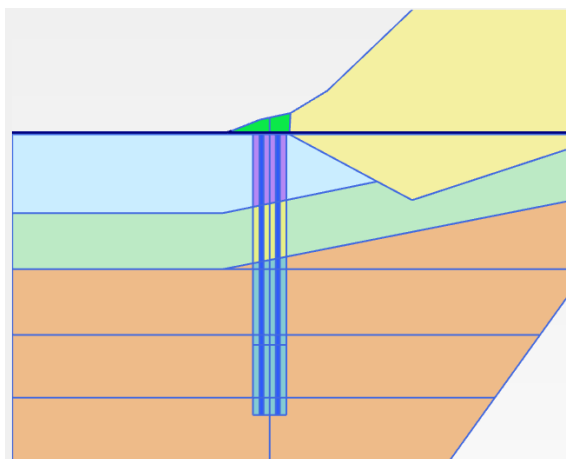
in plane strain conditions, because the gradients are too low because of using Hird et al. (1992)'s approach (compare chapter 6.3).)
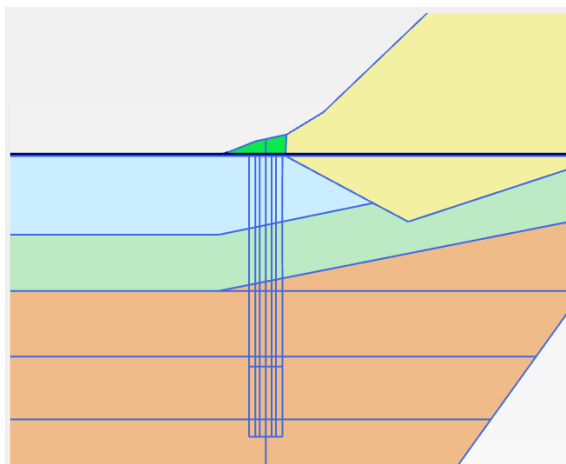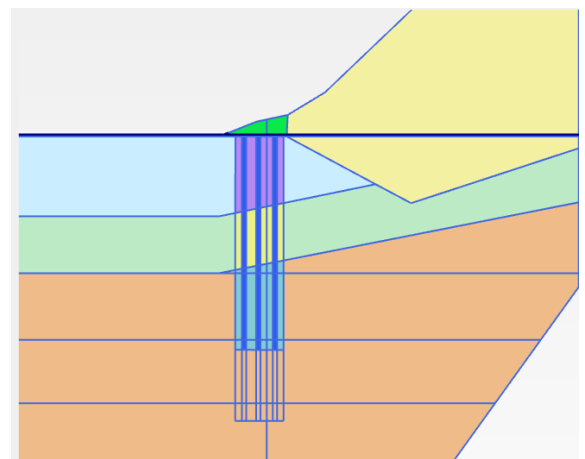

(1) Reference case – without columns

(2) Two columns, length of 30 m, radius of 0.3 m

(3) Two columns, length of 40 m, radius of 0.3 m

(4) Thre columns, length of 30 m, radius of 0.3 m

Fig. 61   Overview of the simulation cases for 2D plane strain calculations

7.3   Analysed nodes

For a comparable evaluation of the pore water pressure development, ten nodes were chosen within the model (shown in Fig. 62). The coordinates of those evaluation nodes are summarized in Tab. 21.
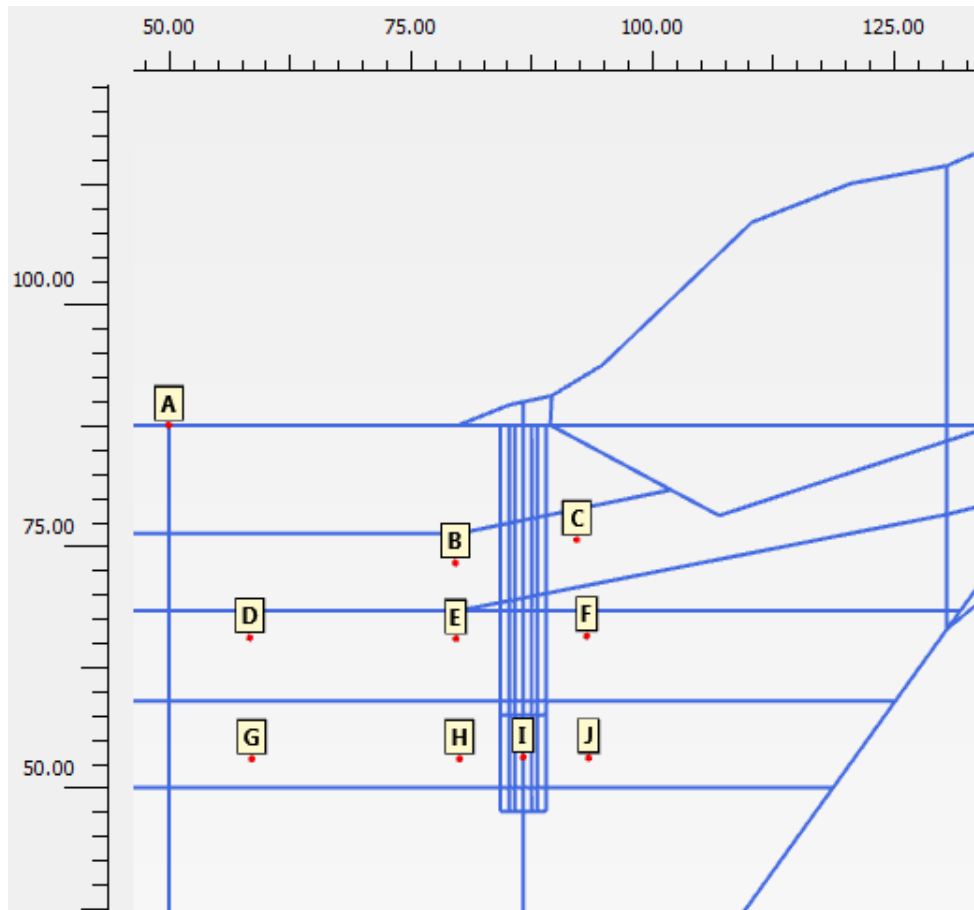
Fig. 62 Overview of evaluation notes for pore water pressure development over time

Tab. 21 Coordinates of the evaluation nodes of the 2D model

Point	X [m]	Y [m]
A	50.00	87.51
B	79.69	73.26
C	92.25	75.65
D	58.39	65.52
E	79.73	65.42
F	93.28	65.68
G	58.60	52.96
H	80.12	52.97
I	86.69	53.13
J	93.49	53.05

7.4 Calculation Sequence

The simulation consists of 18 phases (phases explorer is plotted in Fig. 64).

(A) **Geology:** The first six phases are used to rebuild a realistic starting situation for the project.

(B) **Column Installation:** In section (B) the gravel columns are installed as staged construction. This process includes material changes for the column clusters and the drain influence zone around the columns. During this process, undrained behaviour is ignored.

(C) **Excess pore water pressures (EPP):** In this phase additional pore water pressures are activated in the Silt-Fine Sand layer to reproduce the pore water pressures, which were measured in the subsoil on site as an appropriate initial condition.

(D) **Auf_Ab:** In this calculation phase a water height difference of 7 m within a period of 0.33 days is applied to the FE model. The water level fluctuation was simulated 17 times, which took a time of 11.33 days. This calculation phase is performed to get an appropriate stress situation in the subsoil.

(E) **Fluctuating water level (HM):** In this section, a measured head function over 5.722 days is applied to the FE model (shown in Fig. 63). Furthermore, in phase "HM_drawdown" the head function lasts only 4.01 days to analyse the behaviour and the factor of safety (FOS) after drawdown. In phase "HM_impoundment" the head function lasts 2.372 days to analyse the behaviour and the FOS after impoundment.
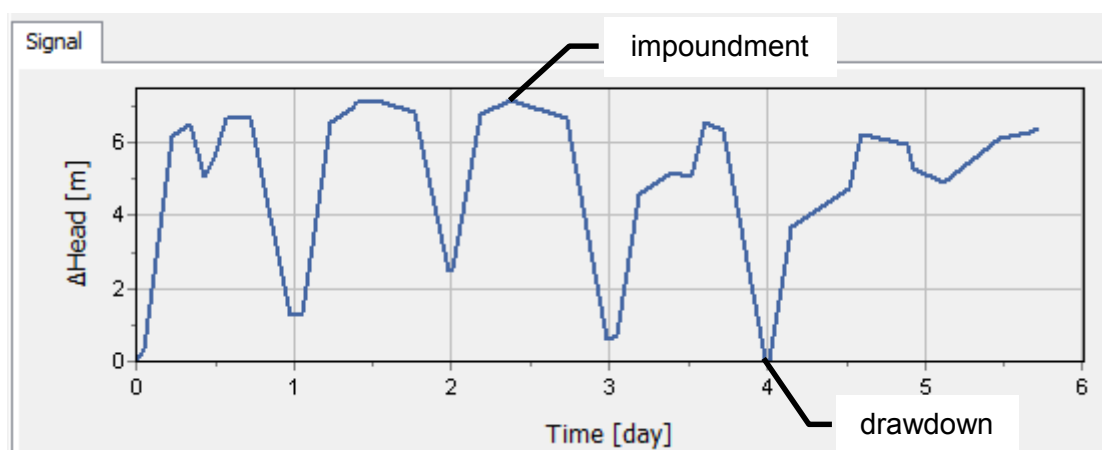

Fig. 63   Head function (ΔHead [m] over time [days]) of calculation phases of section (E)

(F) **Consolidation:** In this section, the consolidation behaviour of the system after installing the columns is analysed without any changes of the water level.
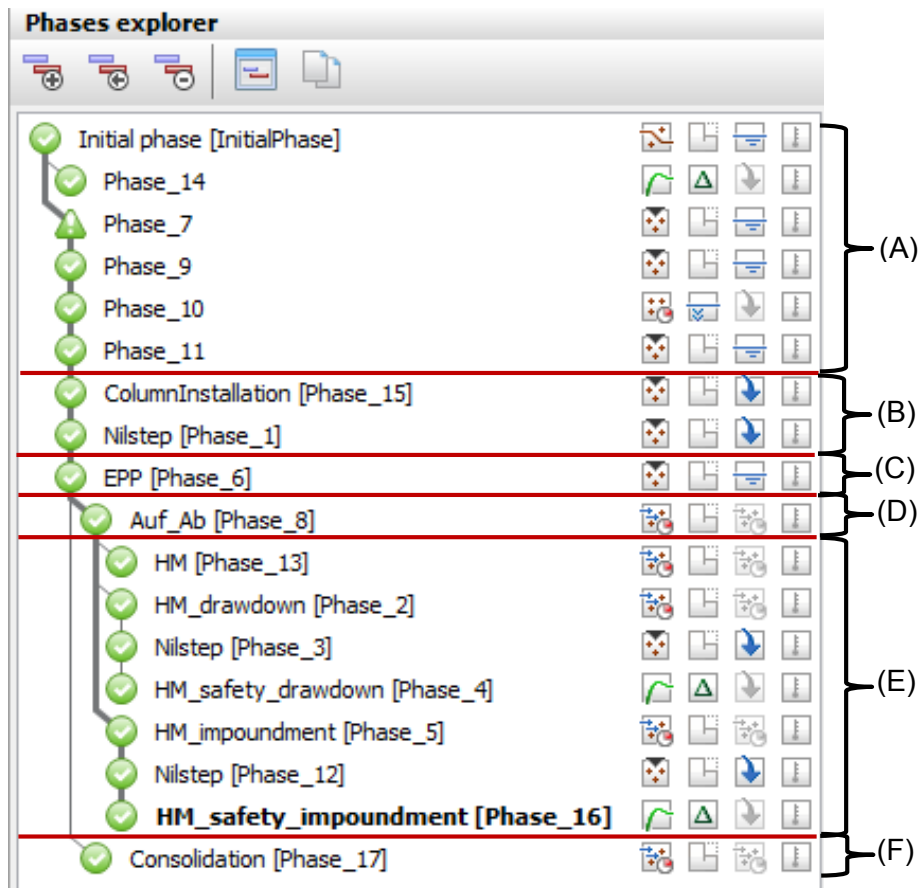
Fig. 64   Overview of the calculation sequence for 2D plane strain caluclations

7.5   Results

In this chapter, the results of the 2D plane strain simulations are presented and discussed.

7.5.1   Groundwater head plots

In Fig. 65, the groundwater head is plotted for anisotropic permeability conditions for the area of the slope toe after a drawdown. In Fig. 66 the groundwater head after impoundment is shown. In Fig. 67 and Fig. 68 the same situations are plotted for isotropic permeability conditions.

The 4 cases, as shown in Fig. 61, are:

(1) Reference case – without columns (upper left corner),

(2) Two columns with a length of 30 m, radius of 0.3 m (upper right corner),

(3) Two columns with a length of 40 m, radius of 0.3 m (lower left corner),

(4) Three columns with a length of 30 m, radius of 0.3 m (lower right corner).

With the used material parameters (see chapter 7.1), the water level fluctuation mainly influences the area beneath the water storage basin. The upper right area below the slope is also influenced significantly by the water level in the slope. The equipotential lines in that area are nearly vertical (=nearly hydrostatical). This effect can be seen in Fig. 65 (1) (anisotropic permeability conditions) and Fig. 67 (1) (isotropic permeability conditions) without installed columns to an approximate depth between 12.0 and 20.0 m. The installed columns show equipotential lines, which are similar to a hydrostatic distribution, also in higher depths, corresponding approximately to the column length of 30 m (see Fig. 65 (2) & (4)) or 40 m (see Fig. 65 (3)) for anisotropic permeability conditions. With installed columns, this "hydrostatic" effect is also apparent under isotropic permeability conditions. However, only for the drawdown but not for the impoundment situation.

After the impoundment, the water level in the storage basin is almost equal to the water level in the slope (see Fig. 66 & Fig. 68). Therefore, the effect of the high water level in the slope on the (excess) pore water distribution in the subsoil is smaller than after the drawdown. Theas means, the groundwater head in the high permeable gravel columns is similar to the groundwater head in the slope. Therefore, the influence of the columns on the groundwater head beneath the slope toe is high after an impoundment.

The influence of the column installation can be seen for both permeability situations, but for anisotropic permeability conditions the influence of the columns on the groundwater head distribution is higher, which means the columns are "working" better when the horizontal permeability k_x is higher.

For anisotropic permeability conditions, two columns with a length of 30 m (see Fig. 66 (2)) and three columns with a length of 30 m (see Fig. 66 (4)) show the same effect for the slope-sided (=right of columns) area. On the basin-sided area (=left of columns) three columns lead to a slightly higher effect of the gravel columns in the area of -30 to -40 m below ground surface, especially near the columns (also under anisotropic permeability conditions). A similar behaviour can be seen in Fig. 68 (2) and (4) for isotropic permeability conditions.

For anisotropic permeability conditions, two columns with a length of 30 m (see Fig. 66 (2)) and two columns with a length of 40 m (see Fig. 66 (3)) show the same effect for the slope-sided (=right of columns) area until an approximate depth of 30 m below ground level. If columns with increased length are used, the groundwater head is reduced significantly also in a depth of -30 to -40 m below ground level (under anisotropic

permeability conditions). On the basin-sided area (=left of columns), the longer columns also lead to a higher influence of the gravel columns in the area of -30 to -40 m below ground. For isotropic permeability conditions (see Fig. 68 (2) and (3)), the influence on the slope-side is increased to a depth of -40 m when using longer columns. If columns with increased length are used, on the basin-side the effect of the longer columns is negligible under isotropic permeability conditions.
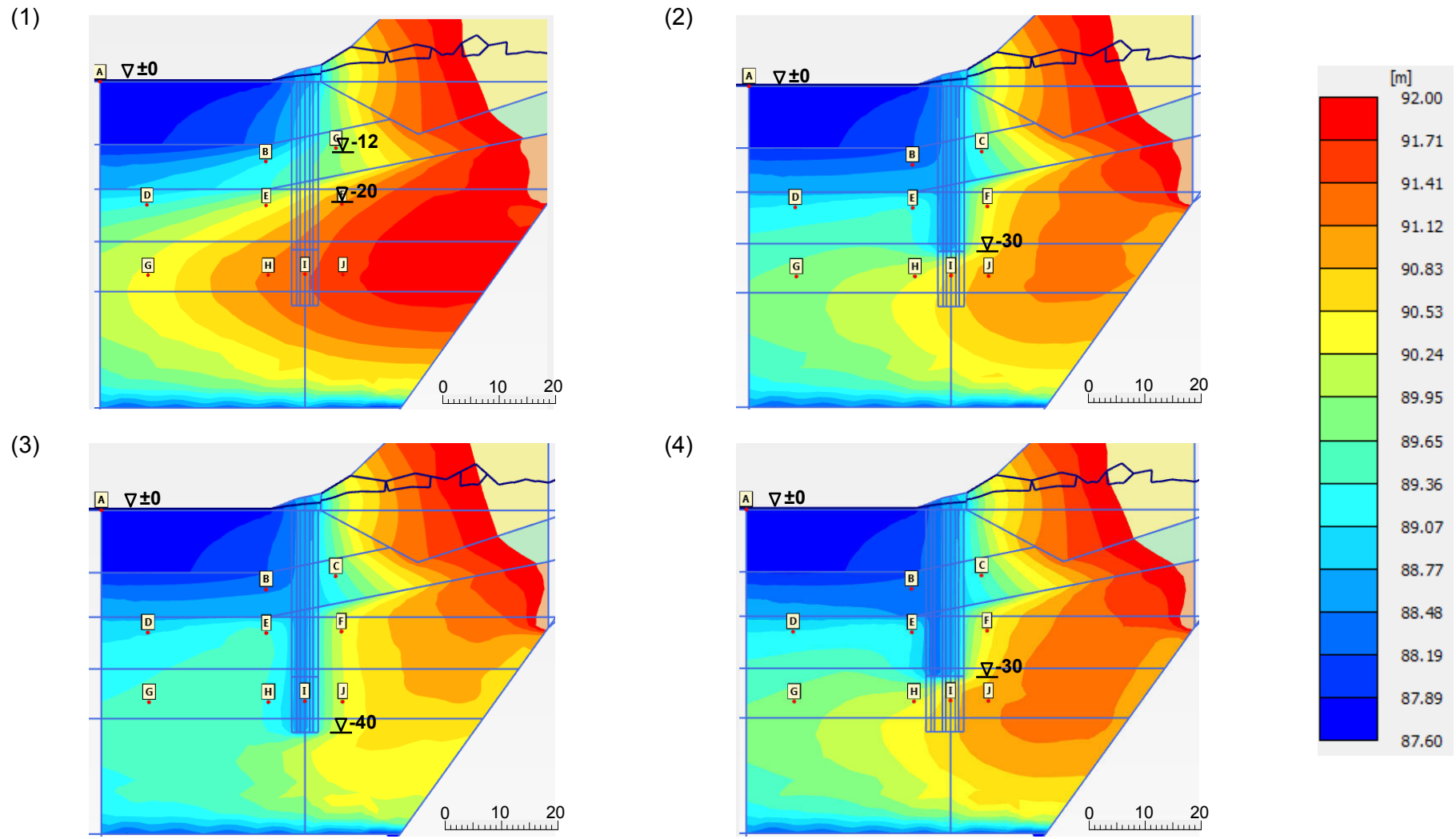
Fig. 65   Groundwater head [m] after drawdown for anisotropic permeability conditions
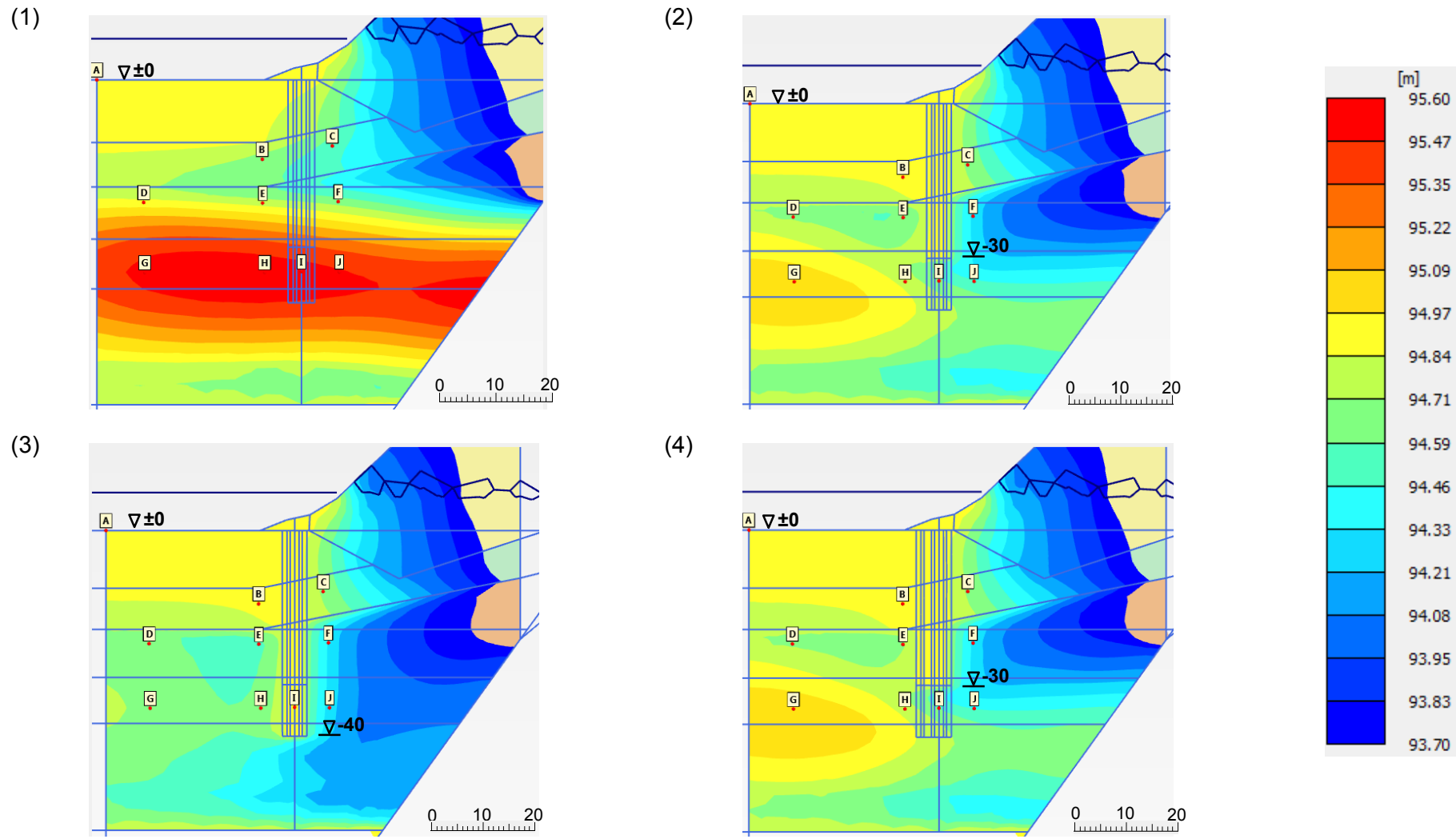
(1)

(2)

(3)

(4)

Fig. 66   Groundwater head [m] after impoundment for anisotropic permeability conditions
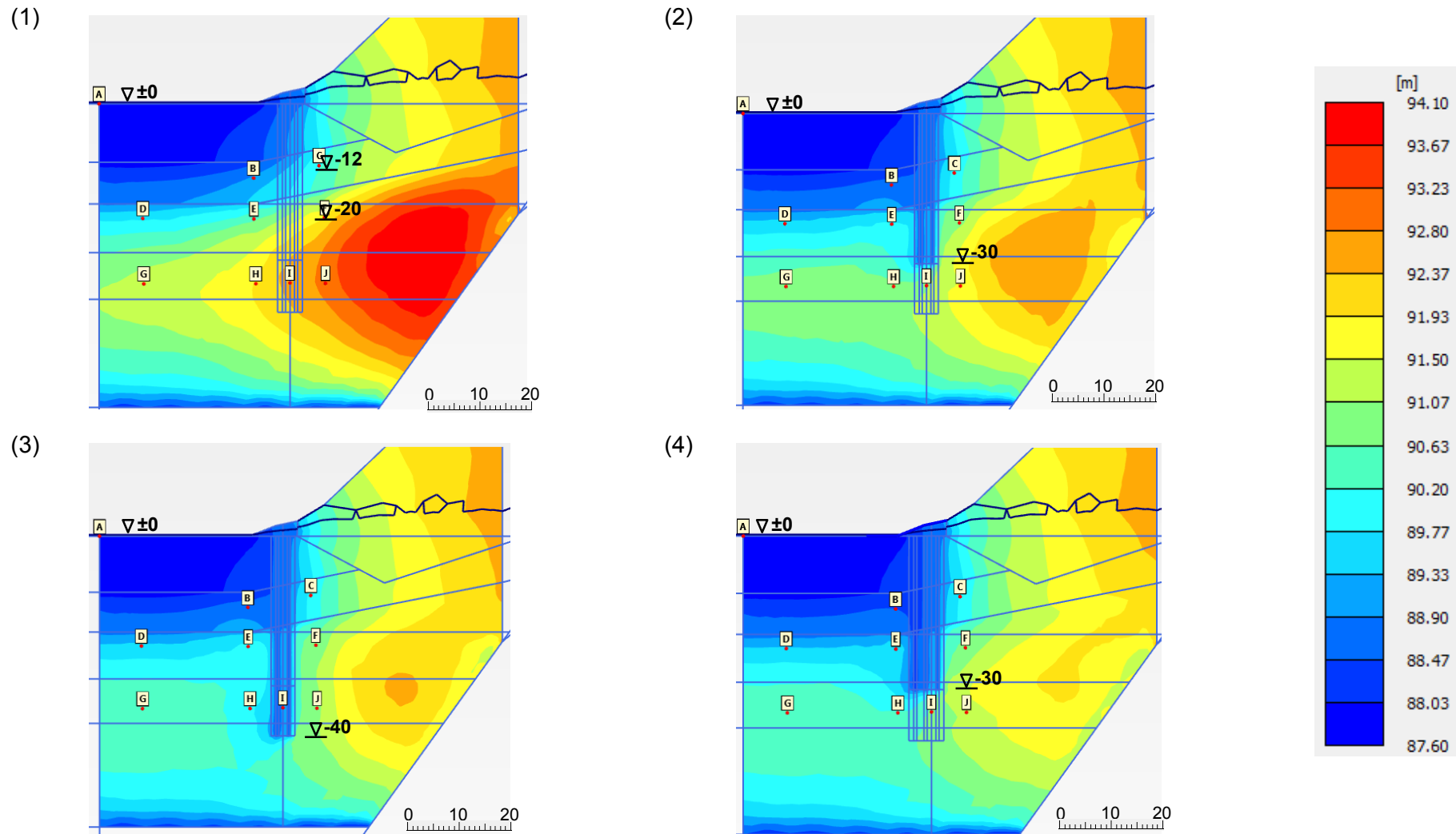
Fig. 67   Groundwater head [m] after drawdown for isotropic permeability conditions
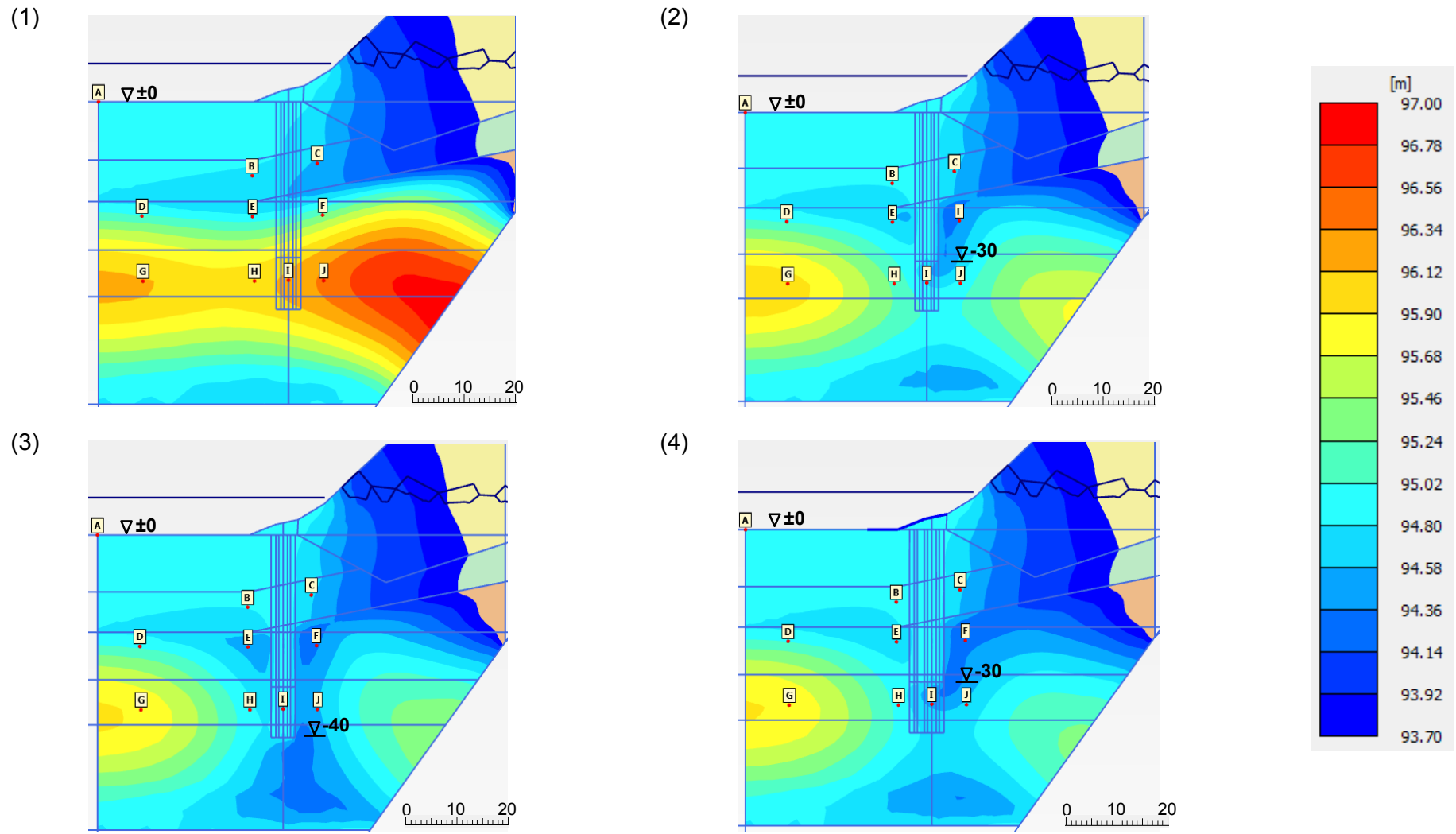
(1)

(2)

(3)

(4)

Fig. 68   Groundwater head [m] after impoundment for isotropic permeability conditions

7.5.2 Excess pore water pressure over time

The excess pore water pressure over time was calculated in each of the evaluation points (see Fig. 62 and Tab. 21) for all four simulation cases to analyse the effect of the columns in anisotropic and isotropic permeability conditions. The results for point D, E, F and J (acc.to Fig. 62 and Tab. 21) are presented and described in this chapter (see diagrams in Fig. 73 to Fig. 76). The diagram for all analysed nodes (acc. to 7.3) are plotted in "Appendix E – 2D plane strain simulation - Excess pore water pressure over time".

The in-situ measurements showed a "mean" excess pore water pressure level of ~40 kPa in a depth of 30 m. This general excess pore water pressure could not be reproduced with the used finite element model. Therefore, the pore water pressure in the Silt-Fine Sand layer is set to a certain value to reproduce the excess pore water pressures, which were measured in the subsoil on site as an initial condition. Subsequently, several impoundments and drawdowns were modelled to get an appropriate stress state in the subsoil.

The columns are more effective under anisotropic than under isotropic permeability conditions (compare between Fig. 69 and Fig. 70, Fig. 71 and Fig. 72, Fig. 73 and Fig. 74, Fig. 75 and Fig. 76). In the mentioned figures, all simulation cases are shown in different colours: blue (the system behaviour without installed columns), red (2 columns a 30m), light green (2 columns a 40 m) and purple (3 columns a 30 m).

Under isotropic permeability conditions, the pressures are generally higher than under anisotropic permeability conditions. The simulation shows, that with installed columns the fluctuating water level over time is also apparent in the pore water pressures. The system behaviour is similar to the one without gravel columns, but the starting value is shifted to a lower value for all evaluated points for both permeability conditions. This "shift" occurs because the excess pore water pressures dissipates faster during the Auf_Ab-phase (see calculation sequence (E) in chapter 7.4) due to the influence of the gravel columns. For anisotropic permeability conditions, this shift is larger, than for isotropic permeability conditions, because under anisotropic conditions the excess pore water pressures dissipate more quickly. This fact led to the consolidation analyses, which are presented in chapter 7.5.3. Additionally, the interpretation of the groundwater head plots (shown in chapter 7.5.1) has to be done with caution, because due to the different consolidation behaviour of the excess pore water pressures during the Auf_Ab-phase the pressure distribution in the subsoil differs already at the beginning of the HM-calculation phase. Therefore, to analyse the effect of the columns the shape of the

equipotential lines is comparable, but absolute values of groundwater head should not be compared.

Under both permeability conditions, the biggest shift is produced when installing two 40 m long columns. In anisotropic conditions, there is nearly no difference between installing two or three 30 m long columns, but in isotropic conditions in points G, H, I and J the shift is larger using three 30 m long columns.

The water level fluctuation in the basin are visible in the pore water pressure results of the system with columns in a similar way as this is the case for a system without columns (see Fig. 69 to Fig. 76). The fluctuating excess pore water pressures result also from the high water level in the slope. The left side of the columns (=basin-sided) (shown by Point E in Fig. 69 & Fig. 70) is less influenced by this higher water level in the slope than the right side of the columns. Therefore, the fluctuation of the excess pore water pressure is slightly suppressed due the columns at the basin side (see coloured curved brackets in the following figures). The right side of the columns (=slope-sided) (shown by Point F in Fig. 71 & Fig. 72) is significantly influenced by the mountain water level (which is almost constant in height). The influence of this water level on the pore water pressures in the subsoil is not affected by the installed columns. Therefore, there occurs no suppression in the fluctuation of the excess pore water pressures (see coloured curved brackets in the following figures). The approximate values of the curved brackets in the following figures are given in kN/m².
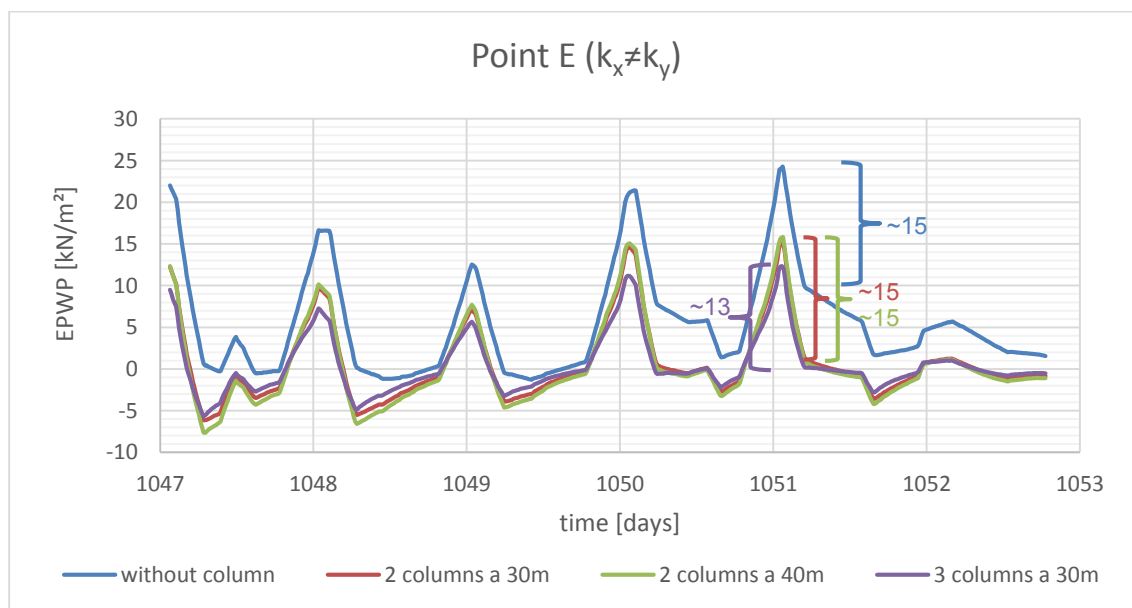

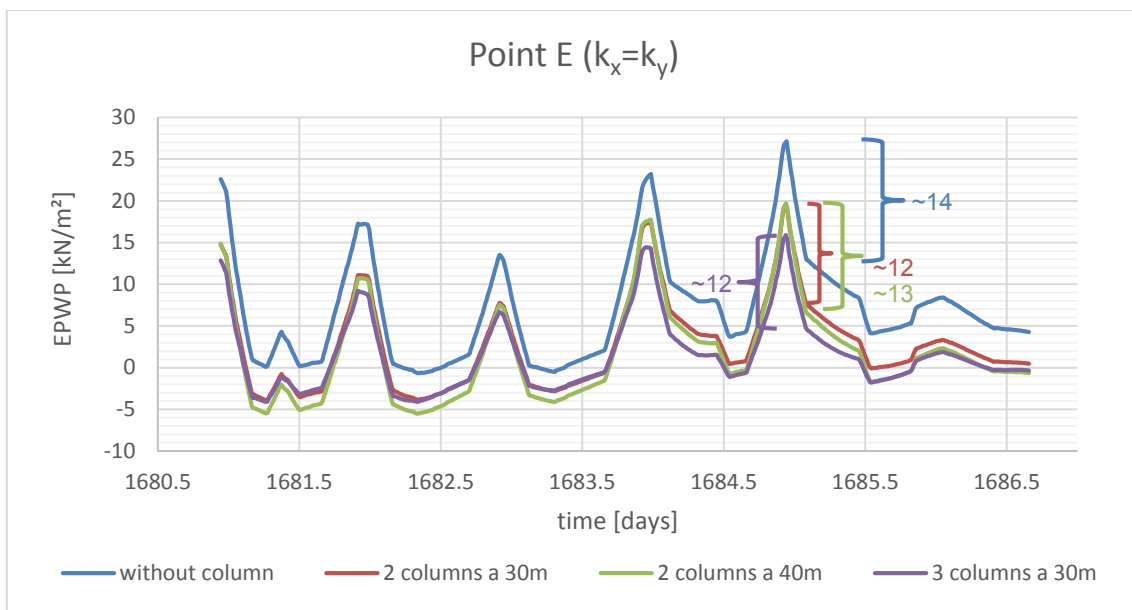Fig. 69 Excess pore water pressure over time ($k_x{\neq}k_y$) – Point E

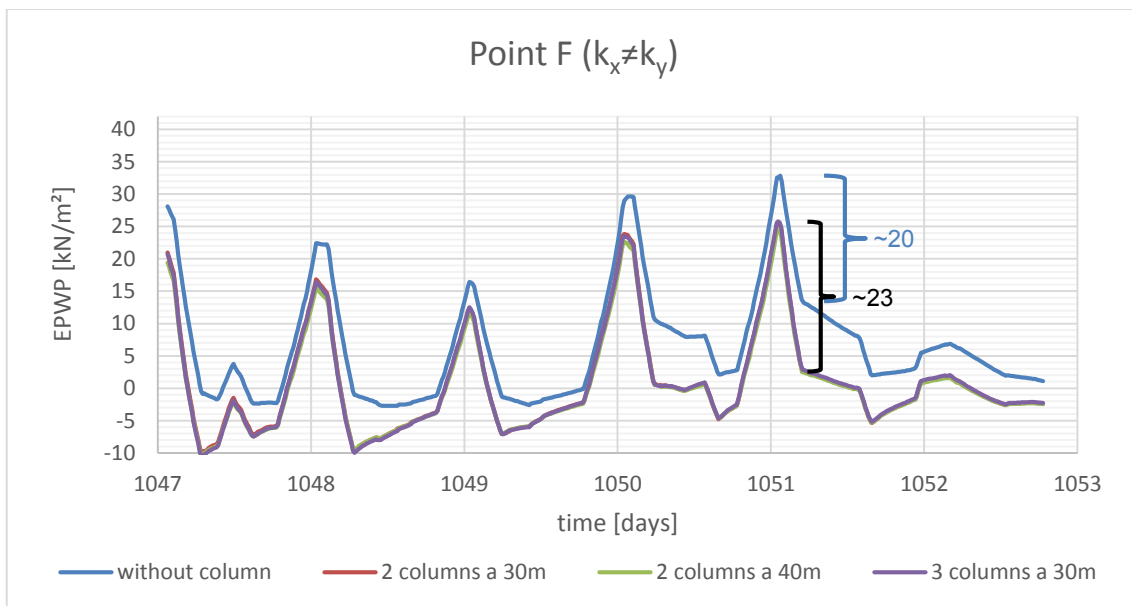Fig. 70 Excess pore water pressure over time ($k_x=k_y$) – Point E

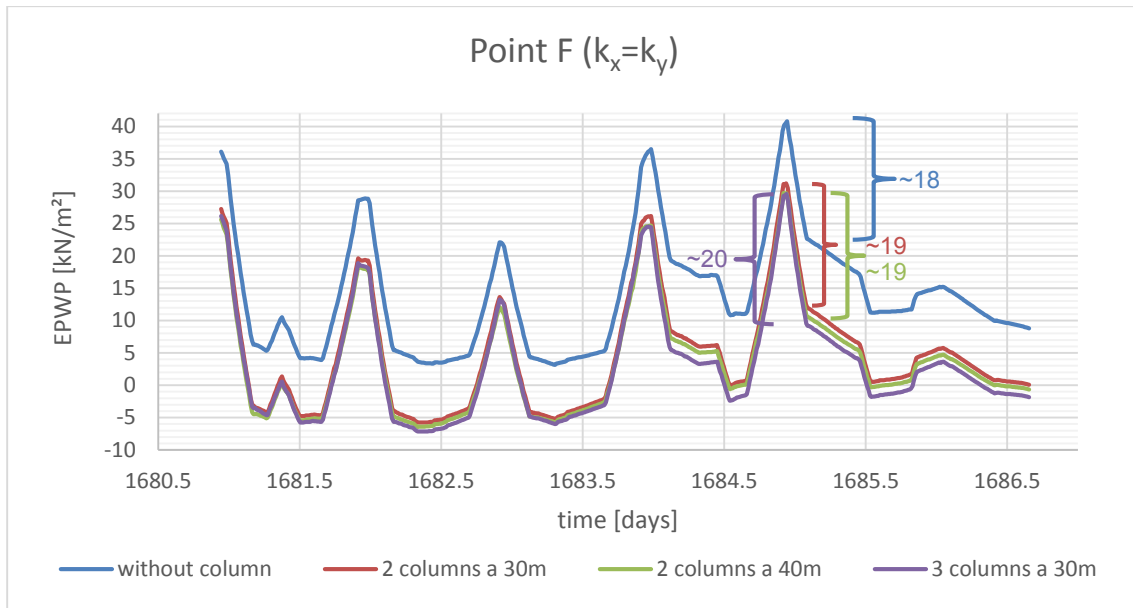Fig. 71 Excess pore water pressure over time ($k_x{\neq}k_y$) – Point F

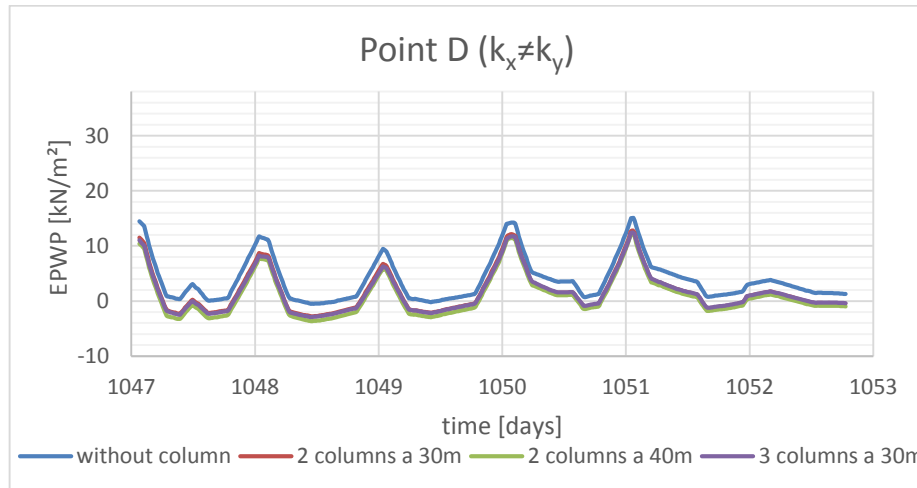Fig. 72   Excess pore water pressure over time ($k_x=k_y$) – Point F

Fig. 73   Excess pore water pressure over time ($k_x{\neq}k_y$) – Point D
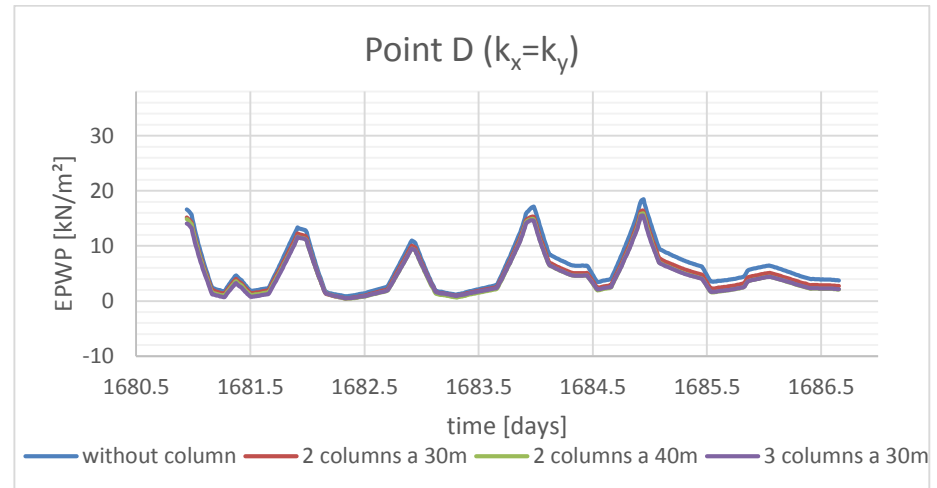

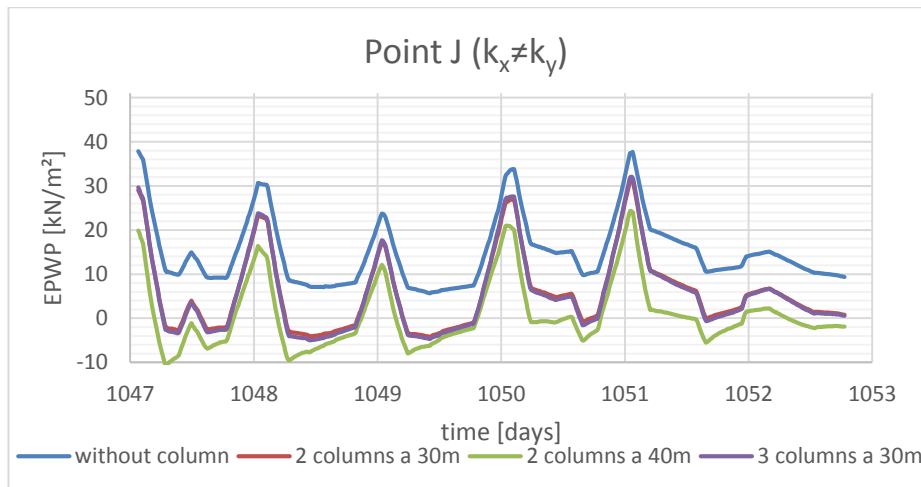Fig. 74   Excess pore water pressure over time ($k_x{=}k_y$) – Point D

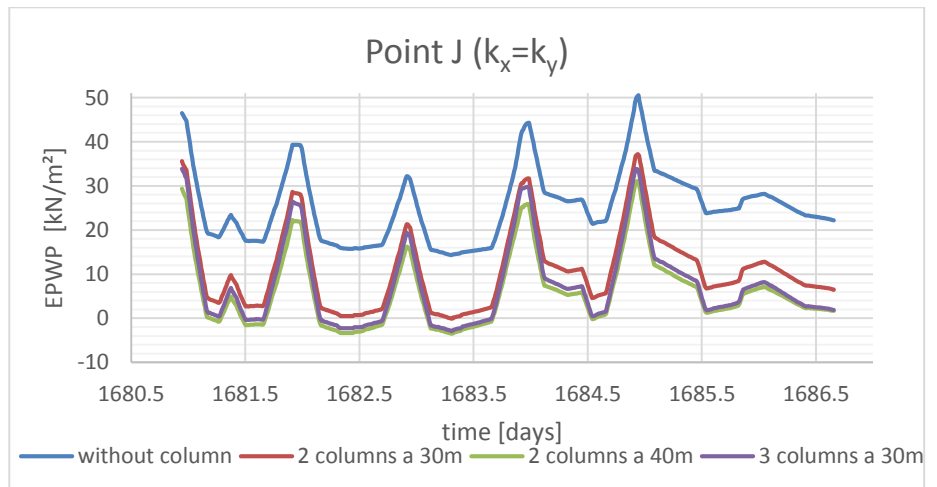Fig. 75   Excess pore water pressure over time ($k_x{\neq}k_y$) – Point J

Fig. 76   Excess pore water pressure over time ($k_x{=}k_y$) – Point J

7.5.3 Consolidation after EPP-calculation phase

In addition to the groundwater head and excess pore water pressure analysis after the fluctuating water level, the consolidation behaviour of the system with installed columns, but without fluctuating water level was studied. The consolidation curves are presented for the characteristic points D, E and F in an approximate depth of 22 m below ground surface (compare Fig. 62 and Tab. 21 and see red marked points in Fig. 77). The points' distance to the column centre (middle of the two rows) are approximately:

- Point D: ~28 m

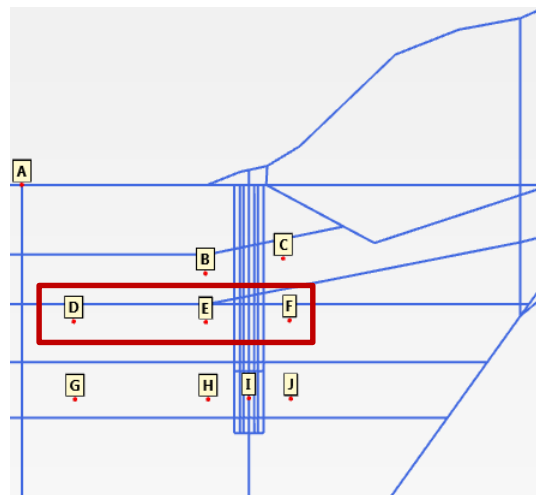- Point E: ~7 m

- Point F; ~13 m

Fig. 77   Points for consolidation evaluation

The results of the consolidation analysis are presented in Fig. 78 to Fig. 83 and summarized in Tab. 22.

As aforementioned, the pore water pressure in the Silt-Fine Sand layer is set to a certain value to reproduce the excess pore water pressures, which were measured in the subsoil on site. This initial excess pore water pressures are approximately the same which are reached in the subsoil after a drawdown without columns (see Fig. 78 to Fig. 83 at time t=0). This excess pore water pressure, which linearly decreases from 30 m to 20 m and from 30 m to 50 m beneath the ground surface, was used as a starting value for the subsequent consolidation analyses.

In Tab. 23 an overview of the consolidation time to reach p_{excess} smaller than 1 kN/m² in the entire model is given. The consolidation time for the entire system without installed

columns, under isotropic permeability conditions, takes approximately 46 days longer than under anisotropic permeability conditions (see Tab. 23). Additionally, the consolidation time for the entire system does not change at all for isotropic permeability conditions for all simulation cases, because points which are far away from the columns are not affected by the columns (see Tab. 23). For anisotropic permeability conditions only the 40 m long columns reduce the overall consolidation time by approximately 52 days.

It is easy to recognize, that the influence on the consolidation time next to the columns is higher (e.g. see point E & F) than for points with a higher distance to the columns (e.g. see point D) (for both permeability conditions) (see Fig. 78 to Fig. 83). Furthermore, the influence of the horizontal permeability k_x on the consolidation behaviour is apparent (see Tab. 22 and compare Fig. 79 to Fig. 82 and Fig. 80 to Fig. 83). The higher horizontal permeability k_x improves the performance of the gravel columns significantly (see Tab. 22).

Under anisotropic permeability conditions (compare Fig. 78 to Fig. 81), the influence of the columns is still recognizable at point D, which is far away from the columns. This is not the case for isotropic permeability conditions. For the points E and F an influence on p_{excess} can be seen even for isotropic permeability conditions, but for anisotropic conditions the influence is higher (compare Fig. 79 and Fig. 80 to Fig. 82 and Fig. 83).

Tab. 22   Overview of consolidation time in the characteristic points D, E and F

| | | Days until p_{excess} < 1 kN/m² | |
		$k_x \neq k_y$	$k_x = k_y$
Point D	without column	~63.3 days	~62.1 days
	2 columns a 30m	~41.0 days	~63.9 days
	2 columns a 40m	~28.8 days	~63.9 days
	3 columns a 30m	~41.0 days	~63.9 days
Point E	without column	~63.3 days	~62.1 days
	2 columns a 30m	~17.6 days	~42.8 days
	2 columns a 40m	~13.2 days	~28.8 days
	3 columns a 30m	~17.6 days	~28.8 days
Point F	without column	~63.3 days	~93.6 days

	2 columns a 30m	~41.0 days	~63.9 days
	2 columns a 40m	~13.2 days	~42.8 days
	3 columns a 30m	~17.6 days	~42.8 days

Tab. 23   Overview of consolidation time for entire system

| | | Days until $p_{excess} < 1$ kN/m² | |
		$k_x \neq k_y$	$k_x = k_y$
Entire system	without column	~94.9 days	~141.0 days
	2 columns a 30m	~93.6 days	~142.8 days
	2 columns a 40m	~42.9 days	~142.8 days
	3 columns a 30m	~93.6 days	~142.8 days
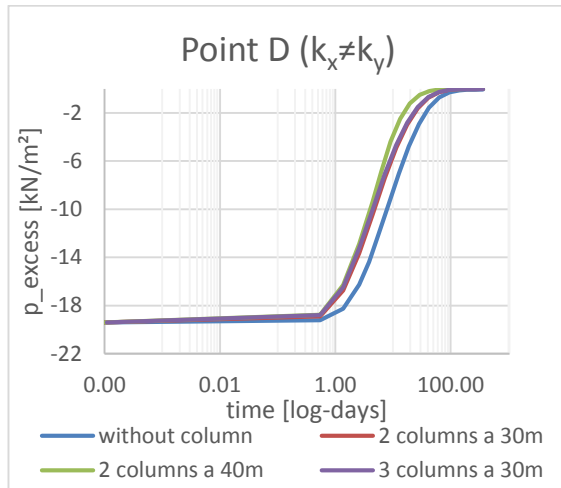
Fig. 78   Consolidation after EPP ($k_x{\neq}k_y$) Point D
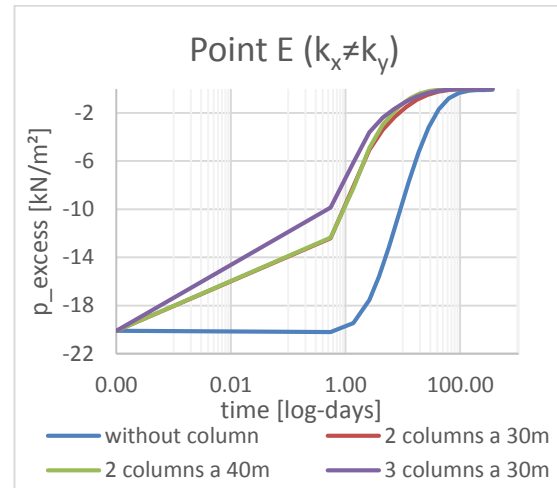
Fig. 79   Consolidation after EPP ($k_x{\neq}k_y$) Point E
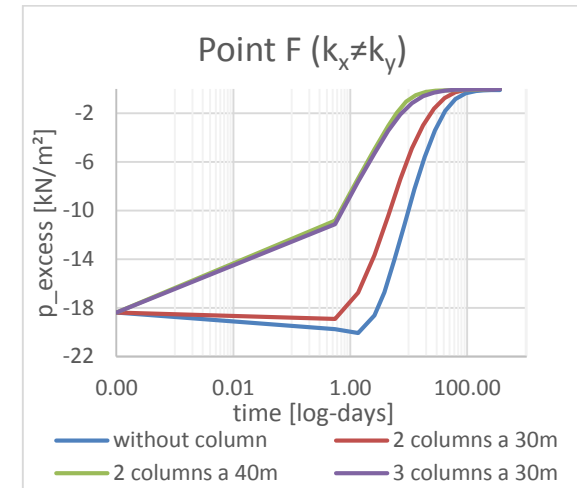
Fig. 80   Consolidation after EPP ($k_x{\neq}k_y$) Point F
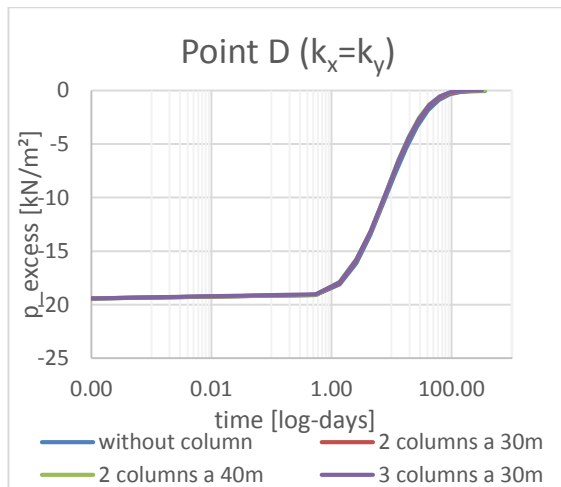
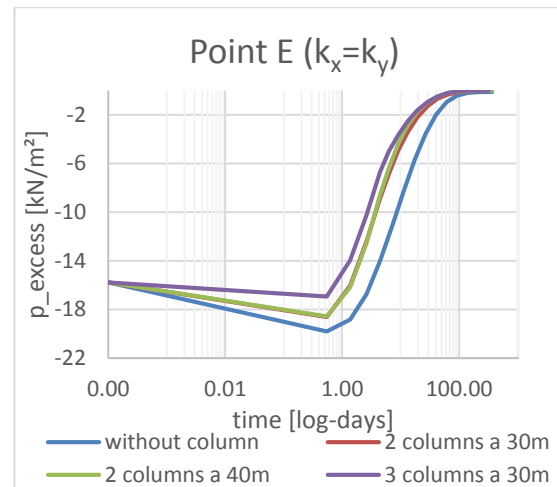Fig. 81   Consolidation after EPP ($k_x{=}k_y$) Point D

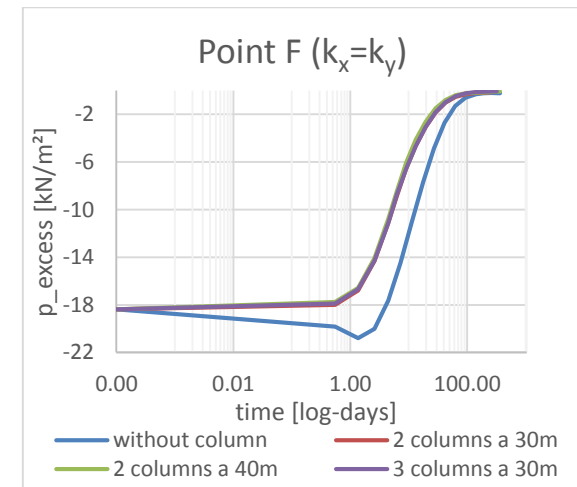Fig. 82   Consolidation after EPP ($k_x{=}k_y$) Point E

Fig. 83   Consolidation after EPP ($k_x{=}k_y$) Point F

7.6 Safety analysis of the adjacent slope

A comprehensive safety analysis of the slope was carried out for the different cases. The FOS was calculated after drawdown, as well as after impoundment.

All safety simulations are done with activated Plaxis function "ignore undrained" (=drained conditions). The results of those simulations are summarized in chapter 7.6.1 and 7.6.2 for different permeability conditions.

All factors of safety without activated Plaxis function "ignore undrained" (=undrained conditions) show a similar failure mechanism, but are approximately 5 to 6 % lower than under "drained" conditions.

7.6.1 Safety analyses for anisotropic permeability conditions

For anisotropic permeability conditions, the average initial safety factor for the slow-moving slope is approximately 1.15. After simulating the fluctuating water level, the safety factor without columns after drawdown is between 1.1 and 1.13, after impoundment between 1.12 and 1.15. With installed columns, the factor of safety does not change significantly.

7.6.2 Safety analyses for isotropic permeability conditions

For isotropic permeability conditions the average initial safety factor for the adjacent slope is approximately 1.15. After simulating the fluctuating water level, the safety factor without columns after drawdown is between 1.1 and 1.13, after impoundment between 1.13 and 1.15. With installed columns, the factor of safety does not change significantly.

7.7 Conclusion of the plane strain simulations

In chapter 7, 2D plane strain calculations were carried out to analyse the comprehensive behaviour of gravel columns beneath a water storage basin. The influence of the gravel columns on the excess pore water pressures beneath the basin and on the factor of safety (FOS) of the adjacent slope were examined.

As matching procedure to convert the behaviour of the gravel columns from axisymmetric to 2D plane strain conditions Hird et al.(1992)'s approach (see chapter 6.1.1) was used, because this procedure resulted in a good match between the axisymmetric and the plane strain results (see verification section in chapter 6.3).

Three possible configurations for the column installation (two columns a 30 m, two columns a 40 m, three columns a 30 m) were analysed and the influence of the different options was always compared to the reference case without columns.

In the following paragraphs, the main outcome of the 2D plane strain simulations are summarized:

- In the groundwater plots in chapter 7.5.1 the influence of the gravel columns is presented. An influence on the groundwater head over the studied area is recognizable under both permeability conditions, but under anisotropic permeability conditions the influence on the groundwater head distribution is higher. This proves the importance of the horizontal permeability for the effectiveness of gravel columns acting as vertical drains in fine grained soils. The water level fluctuation in the water storage basin mainly influences the area beneath this basin. The mountain water level in the slope also influences the upper right area below the slope. In that area, the equipotential lines in that area are nearly vertical (=nearly hydrostatical).
  After the impoundment the water level in the storage basin is almost equal to the mountain water level in the slope (see Fig. 66 & Fig. 68). As a result, the influence of the high water level in the slope on the (excess) pore water distribution in the subsoil is smaller than after the drawdown.

- Under anisotropic permeability conditions, Two columns with a length of 30 m (see Fig. 66 (2)) and two columns with a length of 40 (see Fig. 66 (3)) show the same influence on the groundwater head distribution for the slope-sided (=right of columns) area to the depth of 30 m below ground level. At deeper areas (approximately -30 to -40 m below ground level) the groundwater head is reduced significantly when using 40 m long columns. Also, on the basin-sided area (=left of columns), the longer columns reduce the groundwater head in deeper areas (approximately -30 to -40 m below ground level).

- For isotropic permeability conditions (see Fig. 68 (2) and (3)), the influence of the longer columns (down to -40 m below ground level) on the slope-side is increased to this depth of -40 m below. Nevertheless, the longer columns only show a negligible influence on the basin-side.

- The excess pore water pressures are higher under isotropic than under anisotropic permeability conditions. This outcome is due to the different

consolidation behaviour of the soil during the Auf_Ab-phase. The water level fluctuation is visible in the excess pore water pressure for all simulation cases.

- In the right side of the columns (=slope-sided) is more influenced by the mountain water level. The height of the mountain water level is not influenced by the columns and therefore the slope-sided excess pore water pressures are not suppressed. (see chapter 7.5.2)

- On the left side of the columns (=basin-sided) the mountain water level has minor influence, but the water level fluctuation has major influence on the excess pore water pressures. Due to the columns the fluctuation of the excess pore water pressures is slightly suppressed on the basin-side. (see chapter 7.5.2)

- The consolidation time for the entire system without installed columns, in isotropic permeability conditions, is approximately 45 days longer than in anisotropic permeability conditions (see Tab. 23). The columns only influence the consolidation time of points which are near the column (for both permeability conditions) (see Fig. 78 to Fig. 83).
  Again, the horizontal permeability k_x is very important for the system behaviour.

- The factor of safety (FOS) of the adjacent slope is not influenced by the gravel columns. For anisotropic permeability conditions, the FOS after drawdown is between 1.1 and 1.13, after impoundment between 1.12 and 1.15. For isotropic permeability condition, the values are approximately the same (after drawdown between 1.1 and 1.13 and after impoundment between 1.13 and 1.15).
  (All FOS were calculated with activated "ignore undrained"-Plaxis function. Without activated "ignore undrained"-Plaxis function, the FOS are approximately 5 to 6 % smaller.)

The most important outcomes of the 2D plane strain simulation are:

- As already seen in the preliminary study (see chapter 5), the horizontal permeability k_x is very important for the system behaviour.

- An influence of the gravel columns on the pore water pressures is recognizable under both permeability conditions. The influence is limited to the area near the columns. The water level differences are still apparent in the pore water pressures in the subsoil. The magnitude of the fluctuation is approximately the same as without installed columns (nearly no suppression of the pore water pressure fluctuation). The necessary consolidation time near the columns decreases by approximately 50 days, assuming an appropriate initial excess pore

water pressure in the Silt-fine Sand layer (compare Tab. 22 point E and F) at the beginning of the consolidation phase.

- In Fig. 84 the failure mechanism of the entire system is shown for two installed columns with 30 m length under anisotropic permeability conditions. The shape of the failure mechanism is similar for all examined cases under both permeability conditions. Although the failure mechanism "crosses" the gravel columns, the factor of safety (FOS) of the adjacent slope does not change with installed columns (compare chapter 7.6). However, it has to be mentioned that the friction angle of the sand columns $\varphi = 30°$ was assumed at the lower limit to be on the safe side.

Incremental deviatoric strain $\Delta\gamma_s$
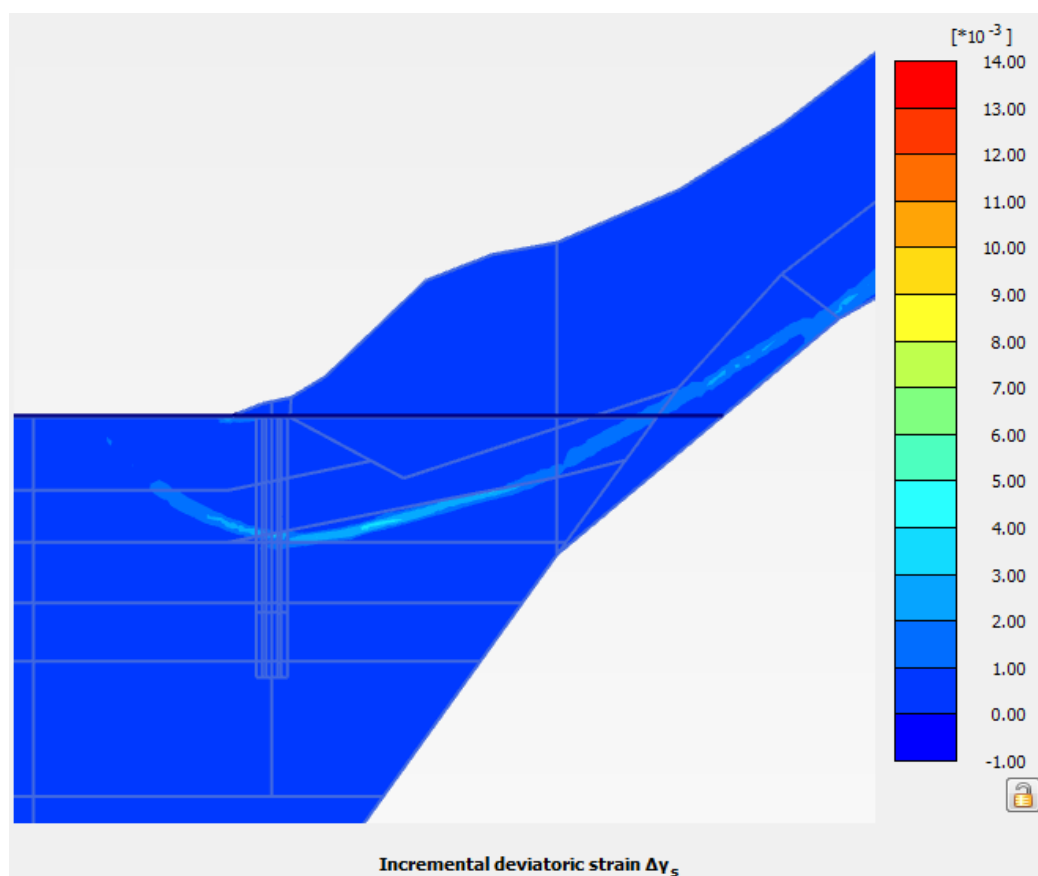
Fig. 84   Failure mechanism with installed columns (2x 30 m) under anisotropic permeability conditions ($k_x \neq k_y$)

8 Conclusion

The main goal of this thesis was to analyse the influence of gravel columns, installed in a fine-grained subsoil, beneath a storage basin on the pore water pressures. Furthermore, it was examined how this change in the pore water pressures influences the factor of safety of the adjacent slope next to the storage basin.

At first, the contact erosion problem between the present subsoil in the basin and the new installed columns is investigated. Therefore, a comprehensive literature review about contact erosion problem at the boundary between a cohesive (=fine grained present subsoil) and a non-cohesive (=coarse grained gravel material) soil, with a flow perpendicular to the layers was performed (see chapter 2). The verification against contact erosion is done using geometrical and hydraulic filter criteria. Two criteria of each type, which fulfil the boundary conditions, are chosen:

- **Geometrical filter criteria:** Cistin & Ziems (BAW 2013b), Sherard (Sherard & Dunnigan 1989)

- **Hydraulic filter criteria:** Muckenthaler (Henzinger (2009) cf. Muckenthaler (1989)), Rehfeld (1967)

These criteria were applied to the present subsoil to find the suitable column material (upper and the lower limit of the suitable grain size distribution).

The outcome of this suitability study are the following two grain size distributions, shown in Fig. 85 and Fig. 86.
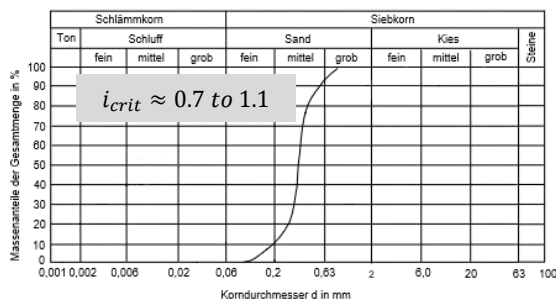
Fig. 85   Lower limit – uniform middle sand
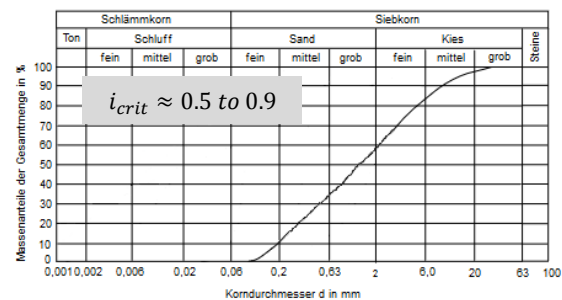
Fig. 86   Upper limit – sand gravel

As next step, a numerical study using Plaxis 2D (Brinkgreve 2016) was done. Due to Redana (1999), Indraranta & Redana (2000) and Weber et al. (2010) the most important factors for modelling gravel columns are (see chapter 4):

- Permeability of the present subsoil,

- Smear zone around the columns,

- Well resistance, and

- Drain influence zone.

Most of these factors were considered in the numerical study, only the well resistance was neglected because Indraratna & Redana (2000) emphasize that it has a minor effect on the pore pressure in comparison to the smear effect. Redana (1999) also states that well resistance is less important on the system behaviour than smear effect and drain spacing.

In chapter 5, a preliminary axisymmetric study was done and the main conclusions are:

- On the one hand, the smear zone has a minor influence on the pore water pressures, even a thicker smear zone has only small influences on the generated pore pressures. But on the other hand, the smear zone has a major influence on the hydraulic gradient next to the column. Assuming a smear zone of 10 cm the hydraulic gradient next to the column increases by approximately 50 %. According to the criteria presented in chapter 3.2, the hydraulic gradients are too high for the chosen material of the gravel columns. Even the lower limit grain size distribution cannot sustain this gradient. Therefore, the two geometric criteria have to be fulfilled for a stable material behaviour in case of the present project. However, it has to be mentioned, that the geometric conditions in the preliminary axisymmetric study does not match the real conditions exactly (drainage zone D_{axi}=2.0 m vs. D_{real}=2.43 m).

- The hydraulic gradient depends on the fluctuation velocity. The higher the fluctuation velocity, the higher the hydraulic gradient becomes.
  An increased column radius (r=0.45 cm) reduces the hydraulic gradient by approximately 15%.

- The horizontal permeability k_x has a high influence on the pore water pressures and the hydraulic gradients. If the horizontal permeability is set to the value of $1 \cdot 10^{-8} \, m/s$ the influence of the columns is reduced significantly (compare Fig. 34, Fig. 35 and Fig. 40, Fig. 41). The hydraulic gradient is 2-3 times higher, if isotropic permeability conditions are assumed in the subsoil.

- The two examined radii (0.3 m and 0.45 m) show only minor differences in the resulting pore water distributions. Hence, for the 2D plane strain analyses the

column radius of 0.3 0m is used. (The radius has more influence on the hydraulic gradient next to the column, but the gradient is only evaluated for the axisymmetric condition.)

A literature review about matching procedures between axisymmetric and plane strain conditions is done in chapter 6. Afterwards two approaches (Hird and Indraratna) are chosen and tested for the specific problem of the presented preliminary study:

- Hird et al.(1992)'s approach with averaged smear effect, and

- Indraratna & Redana (2000)' approach with explicitly modelled smear effect.

The outcome of this comparison is, that Hird et al.(1992)'s approach with the averaged smear effect results in good matches between the axisymmetric and the plane strain calculation in most of the analysed cases. Therefore, Hird's approach is chosen for the following 2D calculations. Additionally, the extent of the smear zone is not known exactly and therefore an explicitly modelled zone is not representative or rather does not produce better or more realistic results. For the hydraulic gradient next to the column, Hird's approach produces values within a reasonable range, but in generally underestimates the hydraulic gradient by approximately 50 % in the plane strain calculations (compared to the axisymmetric case). Therefore, it is recommended to evaluate the hydraulic gradient from the axisymmetric model.

Finally, the system behaviour of the gravel columns beneath a storage basin, interacting with a slow-moving slope, is analysed in a 2D plane strain calculation, using Plaxis 2D (Brinkgreve 2016).

Three possible outlines for the column installation (two columns a 30 m, two columns a 40 m, three columns a 30 m) were analysed during this simulation and the influence of the different options was always compared to the reference case without any columns.

The most important outcomes of the 2D plane strain simulation are:

- An influence of the gravel columns on the pore water pressures is recognizable under both permeability conditions, but is small. The influence is limited to the area next to the columns. The water level fluctuation is still apparent in the pore water pressures in the subsoil. A small suppression of the excess pore water fluctuation occurs at the basin-side in the area next to the columns. Also, the consolidation time (next to the columns) decreases by approximately 50 days.

- As already seen in the preliminary study (see chapter 5), the horizontal permeability k_x is very important for the system behaviour. For isotropic permeability conditions, the influence of the gravel columns on the pore water pressure is reduced, in comparison to the anisotropic conditions.

- The gravel columns do not influence the factor of safety (FOS) of the adjacent slope.

9 References

BAW. (2013a). MAK. *Merkblatt Anwendung von Kornfiltern an Bundeswasserstraßen*. Karlsruhe: Bundesantalt für Wasserbau.

BAW. (2013b). MMB. *Merkblatt Materialtransport im Boden*. Karlsruhe: BAW Bundesanstalt für Wasserbau.

Biswas, S. (2005). *Study of cohesive soil-granular filter interacton incorporateing critical hydraulic gradient and clogging.* Wollongong: University of Wollongong.

Brinkgreve, R. (2016). *PLAXIS 2D 2016 - Manual.* Delft: Plaxis BV.

Busch, K.-F., Luckner, L., & Thiemer, K. (1993). *Geohydraulik. Lehrburh der Hydrogeologie Band 3.* Berlin und Stuttgart: Gebrüder Bornträger.

Chai, J.-C., Miura, N., & Sakajo, S. (1995). Behavior of vertical drain improved subsoil under embankment loading. *Soils and Foundations, Vol. 35, No. 4*, pp. 49-61.

Dar, A. (2006). *Filter design critera for cohesive soils with and without non-cohesive content.* Srinagar, Jammu & Kashmir (India): Department of Civil Engineering, National Institute of Technology Sinagar.

Davidenkoff, R. (1964). *Deiche und Erddämme, Sickerströmung - Standsicherheit.* Düsseldorf: Werner-Verlag.

Davidenkoff, R. (1967). *Dimensionierung von Brunnenfiltern.* Karlsruhe: Bundesanstalt für Wasserbau.

Fuchs, S. (2010, (15)). Deterministische kf-Wert-Schätzung nach petrographischer Bohrgutansprache. *Grundwasser - Zeitschrift der Fachsektion hydrogeologie*, pp. 177-189.

Heibaum, M. (2001). Geotechnical Filters - the important link in scour protection. *2nd International Confercne on Schour and Erosion*, (pp. 13-28). Singapore.

Henzinger, C. (2009). *Innere Erosion bei Dämmen.* Wien: TU Wien, Institut für Ingenieurhydrologie.

Hird, C., Pyrah, I., & Russell, D. (1992). Finite element modelling of vertical drains beneath ambankments on soft ground. *Géotechnique 42, No. 3*, pp. 499-511.

Indraratna, B., & Redana, I. (1997, May). Plane-Strain Modeling of Smear Effects Associated with Vertical Drains. *Journal of Geotechnical and Geoenvironmental Engineering, Vol. 123(5)*, pp. 474-478.

Indraratna, B., & Redana, I. (2000). Numerical modeling of vertical drains with smear and well resistance installed in soft clay. *Canadian Geotechniacl Journal, Vol. 37*, pp. 132-145.

Locke, M. (2001). *Analytical and laboratory modelling of granular filters for embankment dams.* Wollongong: University of Wollongong.

Redana, I. (1999). *Effectivenes of vertical drains in soft clay with special reference to smear effect.* Wollongong: Department of Civil, Mining and Environmental Engineering, Univerysity of Wollongong.

Rehfeld, E. (1967). *Die Erosionsbeständigkeit bindiger Lockergesteine - die wichtigste Grundlage zur Dimensionierung von Dichtungsschichten aus natürlichem Erdstoff.* Dresden: Technische Universität Dresden.

Schmitz, S. (2007). *Zur hydraulischen Kontakterosion bei bindigen Basiserdstoffen.* München: Universität der Bundeswehr München.

Sherard, J., & Dunnigan, L. (1989). *Critical filters for impervious soils.* Journal of Geotechnical Engineering ASCE 115(7).

Sherard, J., Dunnigan, L., & Talbot, J. (1984a). *Basic Properties of Sand and Gravel Filters.* Journal of Geotechnical Engineering Div. ASCE 110(6).

Sherard, J., Dunnigan, L., & Talbot, J. (1984b). *Filters for Silts and Clays.* Journal of Geotechnical Engineering ASCE 110(6).

Terzaghi, K., & Peck, R. (1961). *Die Bodenmechanik in der Baupraxis.* Berling/Göttingen/Heidelberg: Springer Verlag.

Weber, T. (2008). *Modellierung der Baugrundverbesserung mit Schottersäulen.* Zürich: vdf Hochschulverlag AG der ETH Zürich.

Weber, T., Plötze, M., Laue, J., Peschke, G., & Springman, S. (2010). Sear zone identification and soil properties around stone columns constructed in-flight centrifuge model tests. *Geotechnique 60, 3*, pp. 197-206.

Witt, K., & Brauns, J. (1988). *Sicherheitsuntersuchungen auf probabilistischer Grundlage für Staudämme. Erosions- und Filtrationsverhalten von Erdstoffen, Teill II.* Deutsche Gesellschaft für Erd- und Grundbau im Auftrag des Bundesministeriums für Forschung und Technologie.

Zou, Y. (2000). *Der vom Spannungszustand und Bodengefüge abhängige Erosionsdurchbruch bindiger Böden.* Wasserwirtschaft Nr. 11.

Zweck, H. (1958). *Versuchsergebnisse über die Zusammensetzung von Filtern.* Vortrag Baugrundtagung, Hamburg.

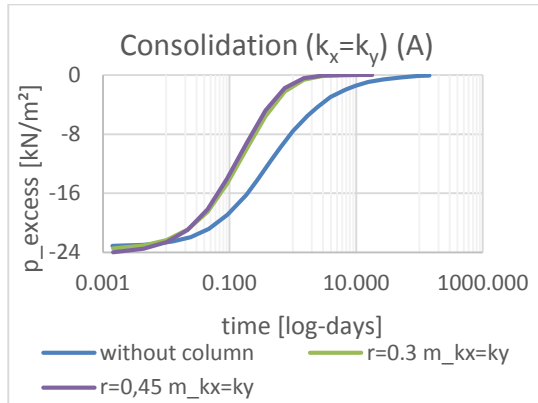# 10 Appendix A – Consolidation for anisotropic permeability
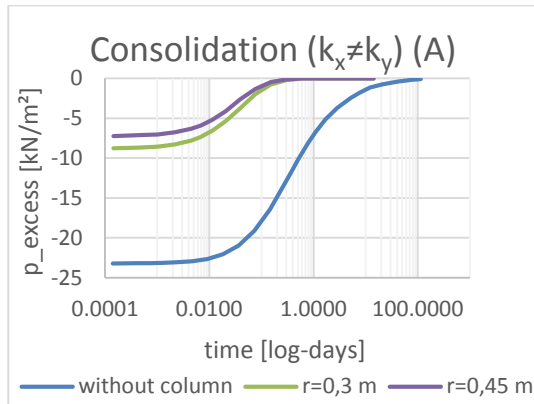
Fig. 87 Consolidation after drawdown ($k_x \neq k_y$) – Point A
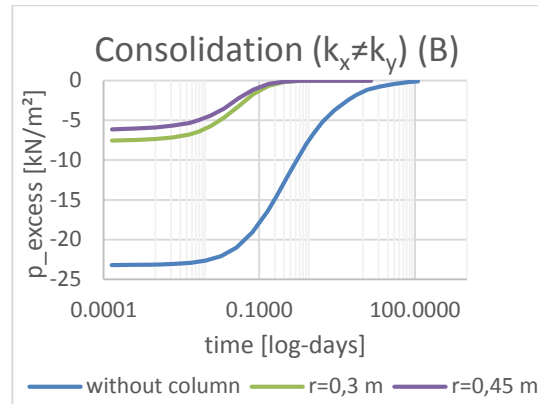
Fig. 88 Consolidation after drawdown ($k_x \neq k_y$) – Point B
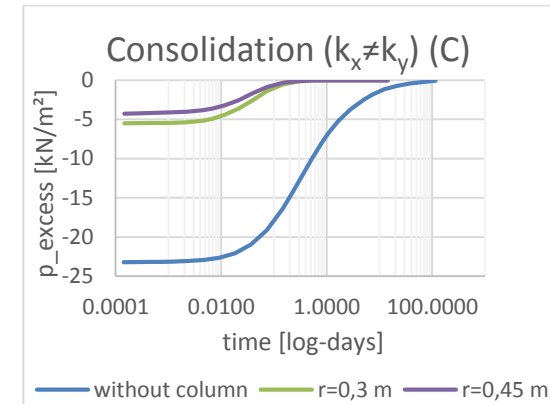
Fig. 89 Consolidation after drawdown ($k_x \neq k_y$) – Point C
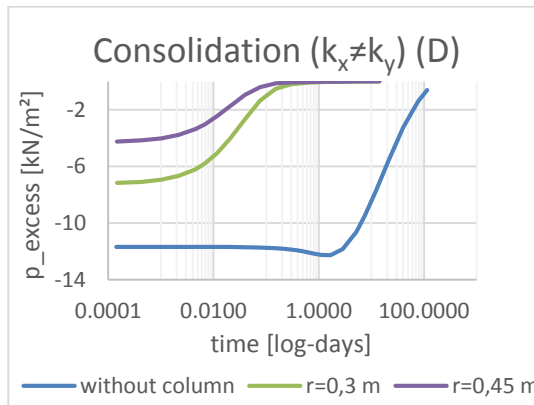
Fig. 90 Consolidation after drawdown ($k_x \neq k_y$) – Point D
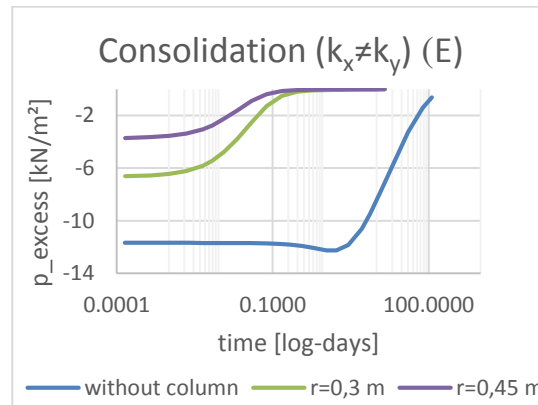
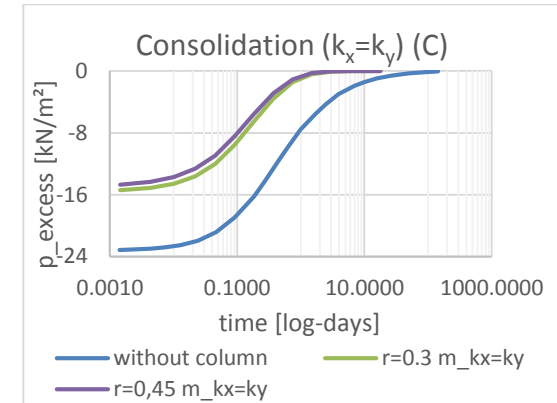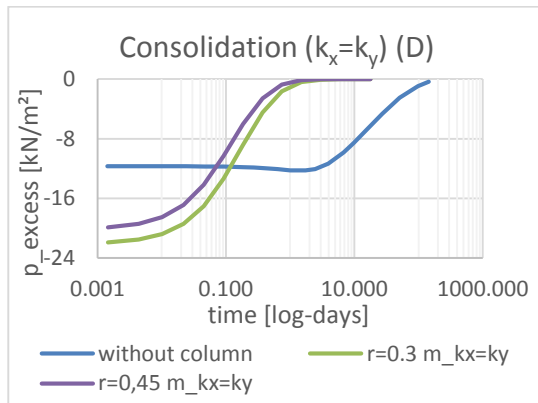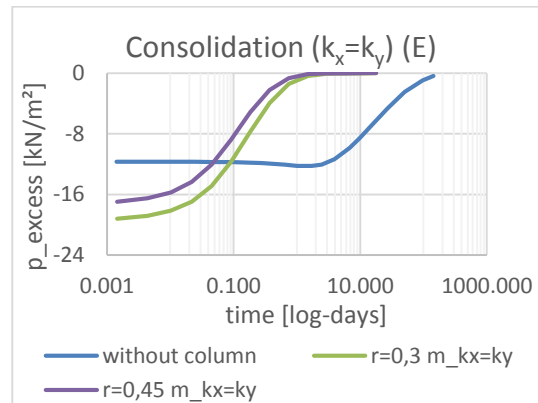Fig. 91 Consolidation after drawdown ($k_x \neq k_y$) – Point E
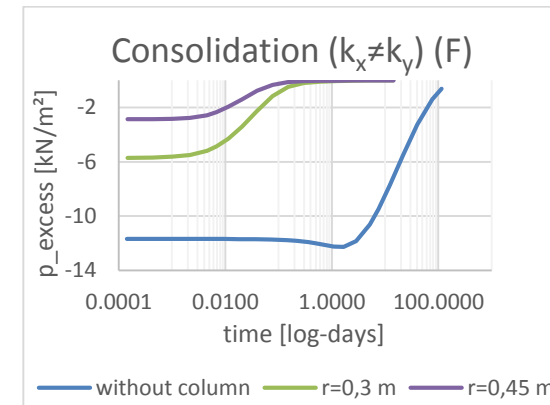
Fig. 92 Consolidation after drawdown ($k_x \neq k_y$) – Point F
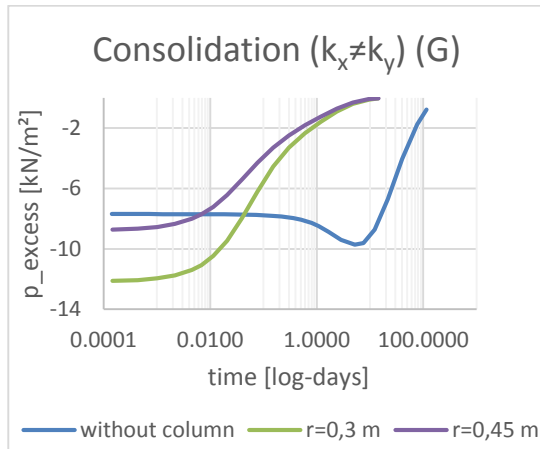
AFTER DRAWDOWN

Fig. 93   Consolidation after drawdown ($k_x \neq k_y$) – Point G
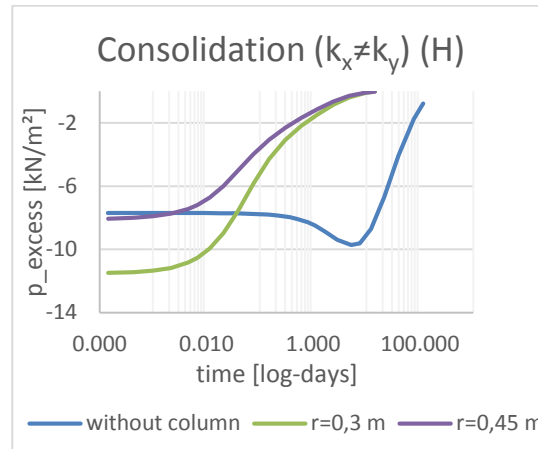
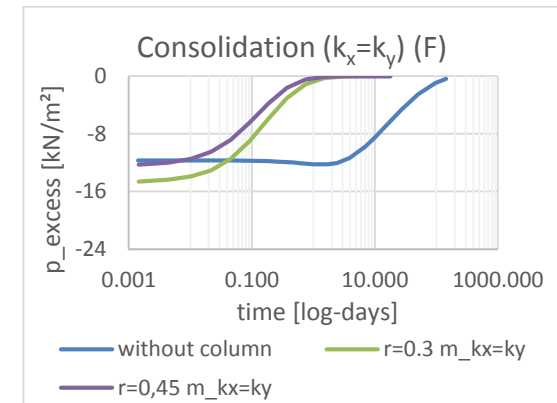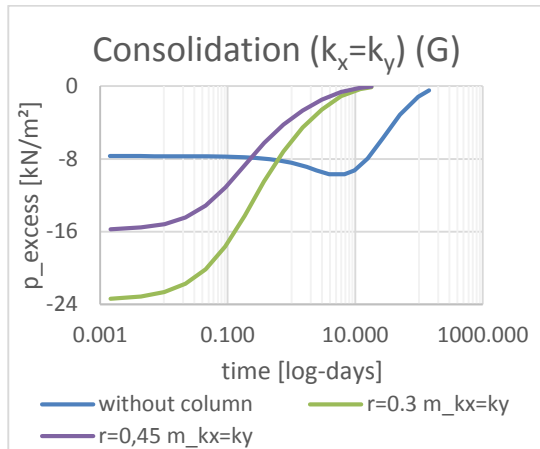Fig. 94   Consolidation after drawdown ($k_x \neq k_y$) – Point H
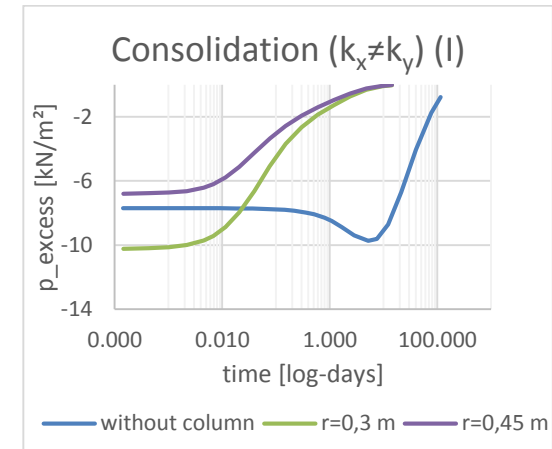
Fig. 95   Consolidation after drawdown ($k_x \neq k_y$) – Point I
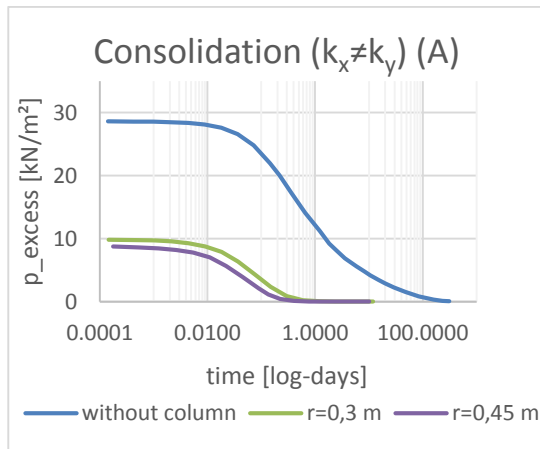
AFTER IMPOUNDMENT

Fig. 96   Consolidation after impoundment ($k_x \neq k_y$) – Point A
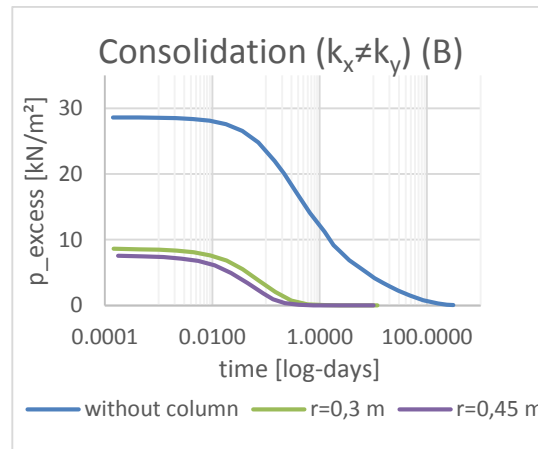
Fig. 97   Consolidation after impoundment ($k_x \neq k_y$) – Point B

Fig. 98   Consolidation after impoundment ($k_x \neq k_y$) – Point C

Computational Geotechnics Group

AFTER IMPOUNDMENT

Consolidation ($k_x \neq k_y$) (D)

Fig. 99 Consolidation after impoundment ($k_x \neq k_y$) – Point D

Consolidation ($k_x \neq k_y$) (E)

Fig. 100 Consolidation after impoundment ($k_x \neq k_y$) – Point E

Consolidation ($k_x \neq k_y$) (F)
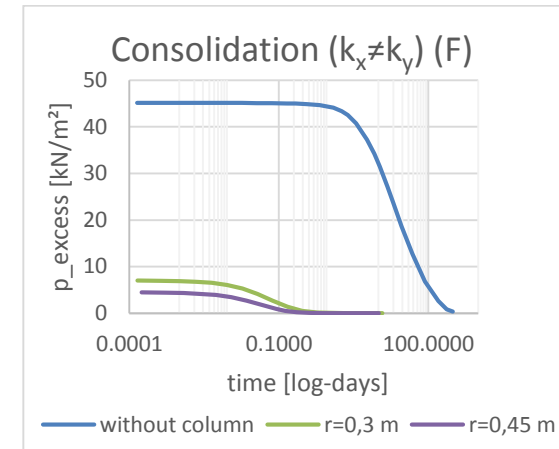
Fig. 101 Consolidation after impoundment ($k_x \neq k_y$) – Point F

AFTER IMPOUNDMENT

Consolidation ($k_x \neq k_y$) (G)
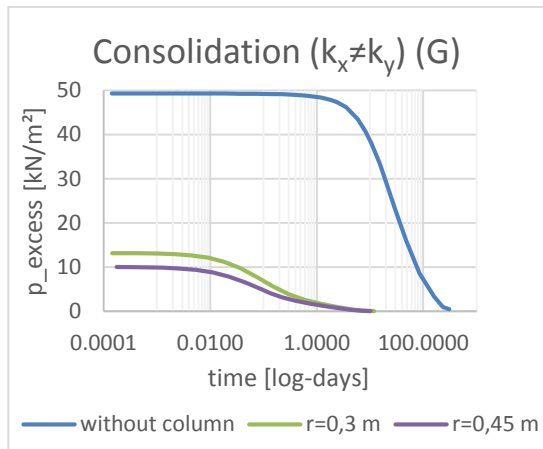
Fig. 102 Consolidation after impoundment ($k_x \neq k_y$) – Point G

Consolidation ($k_x \neq k_y$) (H)
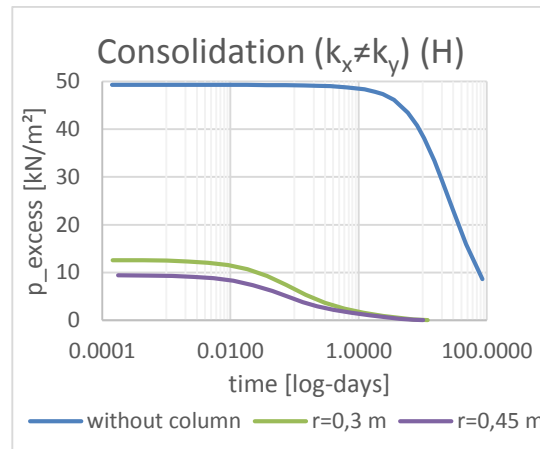
Fig. 103 Consolidation after impoundment ($k_x \neq k_y$) – Point H

Consolidation ($k_x \neq k_y$) (I)
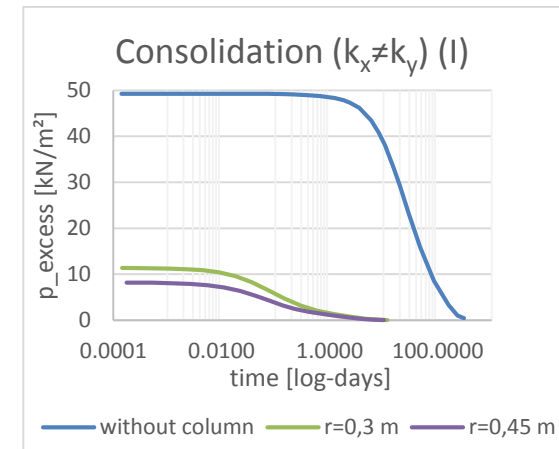
Fig. 104 Consolidation after impoundment ($k_x \neq k_y$) – Point I

11 Appendix B - Consolidation for isotropic permeability

Fig. 105 Consolidation after drawdown
($k_x=k_y$) – Point A
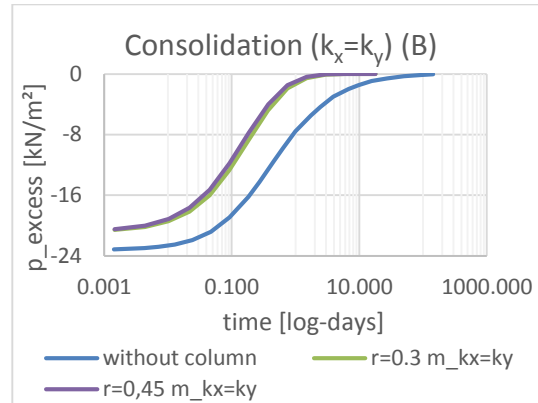
Fig. 106 Consolidation after drawdown
($k_x=k_y$) – Point B

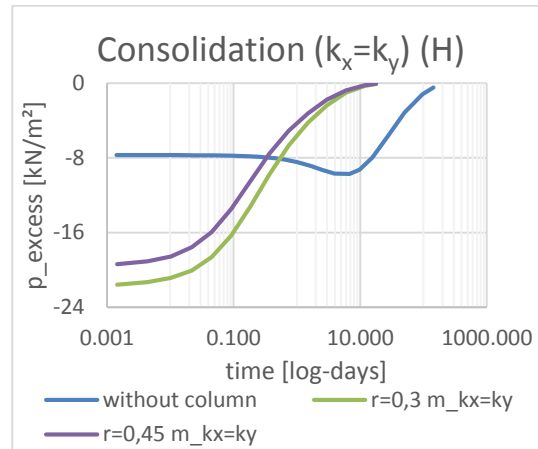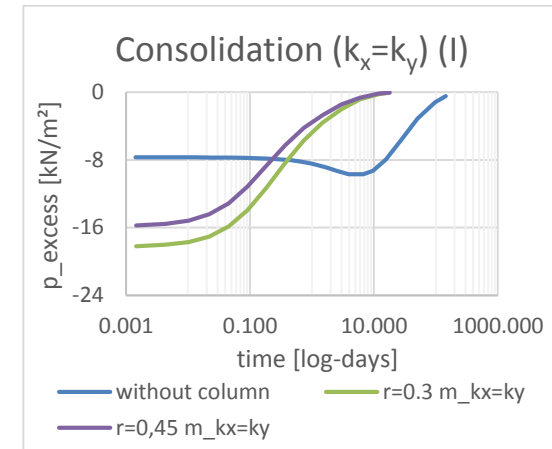Fig. 107 Consolidation after drawdown
($k_x=k_y$) – Point C

Fig. 108 Consolidation after drawdown
($k_x=k_y$) – Point D

Fig. 109 Consolidation after drawdown
($k_x=k_y$) – Point E

Fig. 110 Consolidation after drawdown
($k_x=k_y$) – Point F

AFTER DRAWDOWN

Fig. 111   Consolidation after drawdown ($k_x=k_y$) – Point G

Fig. 112   Consolidation after drawdown ($k_x=k_y$) – Point H

Fig. 113   Consolidation after drawdown ($k_x=k_y$) – Point I
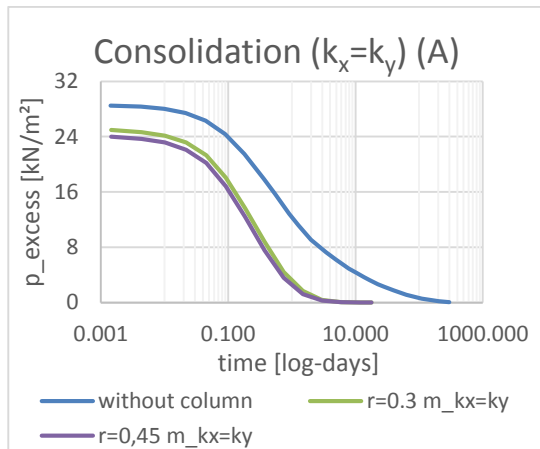
AFTER IMPOUNDMENT

Fig. 114   Consolidation after impoundment ($k_x=k_y$) – Point A
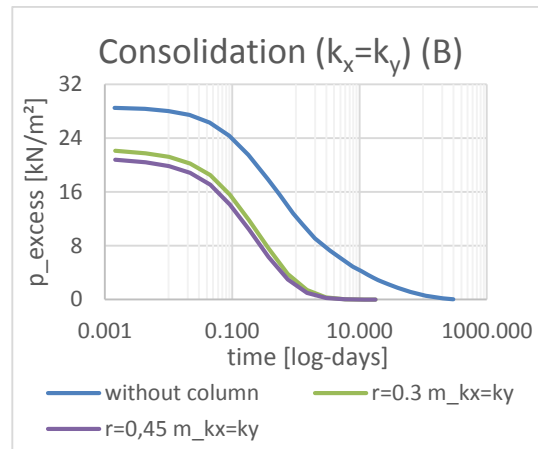
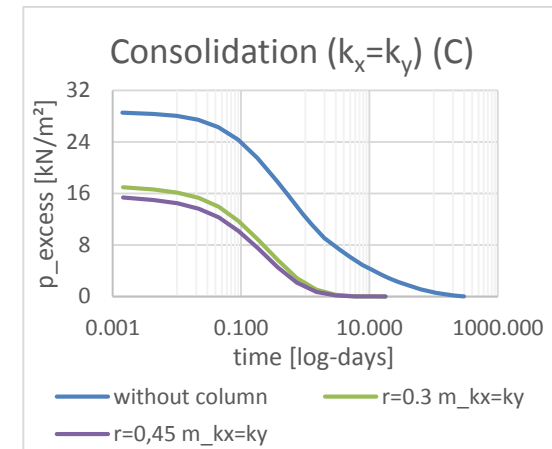Fig. 115   Consolidation after impoundment ($k_x=k_y$) – Point B

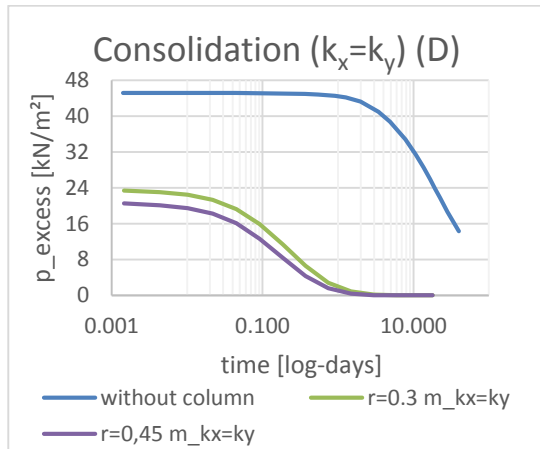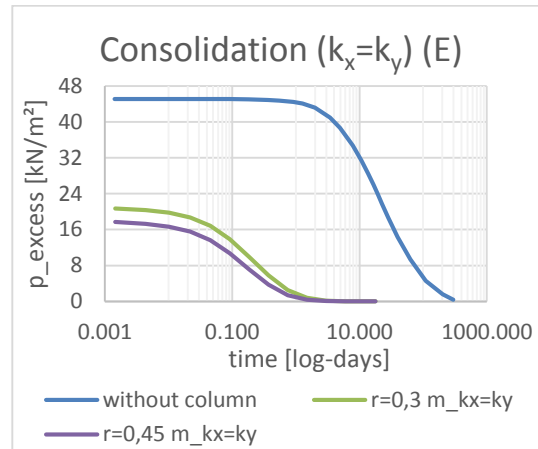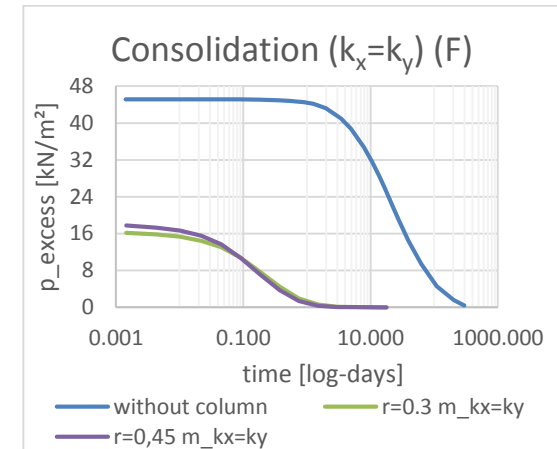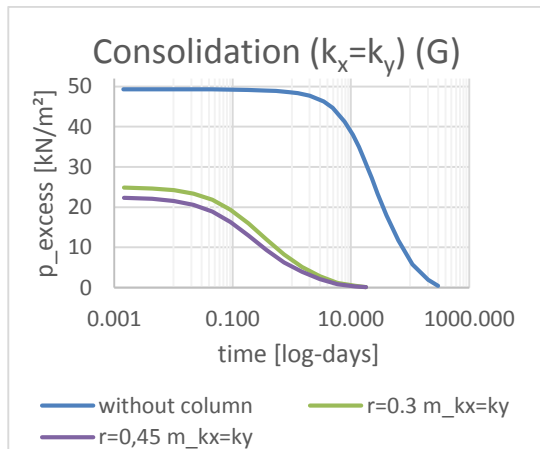Fig. 116   Consolidation after impoundment ($k_x=k_y$) – Point C

AFTER IMPOUNDMENT
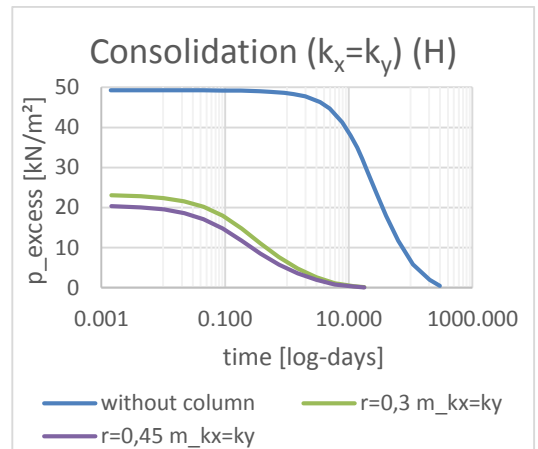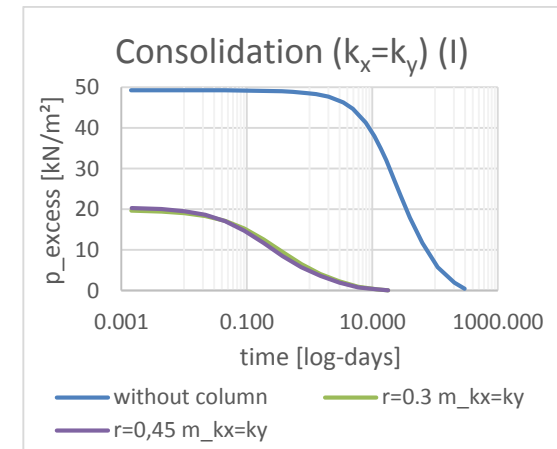
Consolidation ($k_x=k_y$) (D)

Fig. 117   Consolidation after impoundment ($k_x=k_y$) – Point D

Consolidation ($k_x=k_y$) (E)

Fig. 118   Consolidation after impoundment ($k_x=k_y$) – Point E

Consolidation ($k_x=k_y$) (F)

Fig. 119   Consolidation after impoundment ($k_x=k_y$) – Point F

AFTER IMPOUNDMENT

Consolidation ($k_x=k_y$) (G)

Fig. 120   Consolidation after impoundment ($k_x=k_y$) – Point G

Consolidation ($k_x=k_y$) (H)

Fig. 121   Consolidation after impoundment ($k_x=k_y$) – Point H

Consolidation ($k_x=k_y$) (I)

Fig. 122   Consolidation after impoundment ($k_x=k_y$) – Point I

Computational Geotechnics Group

12 Appendix C – Input parameter for Plane strain simulation (anisotropic)

The reference pressure of $p_{ref} = 100\ kN/m^2$ in Plaxis is used for all material sets.

Tab. 24 Input parameters for Dam material (for all permeability conditions)

Dam – Linear elastic		
Drainage Type	drained	[-]
γ_{unsat}	19.00	[kN/m³]
γ_{sat}	21.00	[kN/m³]
E_{Oed}	200.0 E3	[kN/m²]
ν'	0.3	[-]
$k_x = k_y$	1 E-2	[m/s]

Tab. 25 Input parameters for Fine sand material (soil layer in storage basin), ($k_x{\neq}k_y$)

Fine sand – HS small		
Drainage Type	Undrained (A)	[-]
γ_{unsat}	19.00	[kN/m³]
γ_{sat}	20.00	[kN/m³]
E_{50}^{ref}	35.0E3	[kN/m²]
E_{Oed}^{ref}	35.0 E3	[kN/m²]
E_{ur}^{ref}	105.0 E3	[kN/m²]
m	0.5	[-]
c'_{ref}	2.0	[kN/m²]
φ'	35.0	[°]
ψ	0.0	[°]
$\gamma_{0.7}$	0.1 E-3	[-]
G_0^{ref}	175.0 E3	[kN/m²]
$k_x = k_y$	5 E-6	[m/s]

Tab. 26   Input parameters for Fine sand, silty material (soil layer in storage basin), ($k_x \neq k_y$)

Fine sand, silty – HS small		
Drainage Type	Undrained (A)	[-]
γ_{unsat}	19.00	[kN/m³]
γ_{sat}	20.00	[kN/m³]
E_{50}^{ref}	18.0 E3	[kN/m²]
E_{Oed}^{ref}	15.0 E3	[kN/m²]
E_{ur}^{ref}	37.5 E3	[kN/m²]
m	0.7	[-]
c'_{ref}	2.0	[kN/m²]
φ'	32.5	[°]
ψ	0.0	[°]
$\gamma_{0.7}$	0.1 E-3	[-]
G_0^{ref}	62.5 E3	[kN/m²]
k_x	1 E-6	[m/s]
k_y	1 E-7	[m/s]

Tab. 27   Input parameters for Silt-Fine sand material (soil layer in storage basin), ($k_x \neq k_y$)

Silt-Fine sand – HS small		
Drainage Type	Undrained (A)	[-]
γ_{unsat}	19.00	[kN/m³]
γ_{sat}	20.00	[kN/m³]
E_{50}^{ref}	15.0 E3	[kN/m²]
E_{Oed}^{ref}	12.0 E3	[kN/m²]
E_{ur}^{ref}	30.0 E3	[kN/m²]
m	0.7	[-]
c'_{ref}	3.0	[kN/m²]

φ'	27.5	[°]
ψ	0.0	[°]
$\gamma_{0.7}$	0.2 E-3	[-]
G_0^{ref}	50.0 E3	[kN/m²]
k_x	5 E-8	[m/s]
k_y	5 E-9	[m/s]

Tab. 28 Input parameters for Sand material (soil layer in storage basin), (for all permeability conditions)

Sand – HS small		
Drainage Type	Undrained (A)	[-]
γ_{unsat}	21.00	[kN/m³]
γ_{sat}	22.00	[kN/m³]
E_{50}^{ref}	50.0 E3	[kN/m²]
E_{Oed}^{ref}	50.0 E3	[kN/m²]
E_{ur}^{ref}	150.0 E3	[kN/m²]
m	0.5	[-]
c'_{ref}	1.0	[kN/m²]
φ'	37.5	[°]
ψ	0.0	[°]
$\gamma_{0.7}$	0.2 E-3	[-]
G_0^{ref}	375.0 E3	[kN/m²]
k_x	1 E-4	[m/s]
k_y	1 E-4	[m/s]

Tab. 29   Input parameters for Sliding mass (saturated) material (slope material), (for all permeability conditions)

Sliding mass saturated – Mohr Coulomb		
Drainage Type	drained	[-]
γ_{unsat}	20.00	[kN/m³]
γ_{sat}	22.00	[kN/m³]
E_{Oed}	200.0 E3	[kN/m²]
v'	0.3	[-]
c'_{ref}	10.0	[kN/m²]
φ'	40.0	[°]
ψ	0.0	[°]
$k_x = k_y$	1 E-3	[m/s]

Tab. 30   Input parameters for Sliding mass (saturated) material (slope material), (for all permeability conditions)

Transition zone – Mohr Coulomb		
Drainage Type	drained	[-]
γ_{unsat}	22.00	[kN/m³]
γ_{sat}	22.00	[kN/m³]
E_{Oed}	200.0 E3	[kN/m²]
v'	0.3	[-]
c'_{ref}	1.0	[kN/m²]
φ'	34.0	[°]
ψ	0.0	[°]
$k_x = k_y$	1 E-3	[m/s]

Tab. 31   Input parameters for Column sand material, (for all permeability conditions)

Column sand – Mohr Coulomb		
Drainage Type	drained	[-]
γ_{unsat}	17.00	[kN/m³]
γ_{sat}	20.00	[kN/m³]
E'	18.85 E3	[kN/m²]
v'	0.3	[-]
c'_{ref}	1.0	[kN/m²]
φ'	30.0	[°]
ψ	0.0	[°]
$k_x = k_y$	5 E-4	[m/s]

Only the horizontal permeability k_x is adapted for the drain influence zone around the columns after column installation. Those adapted permeabilities are summarized in Tab. 32, Tab. 33 and Tab. 34. The rest of the parameters of the fine grained soil layer beneath the storage basin is not changed (look up in Tab. 25, Tab. 26, Tab. 27).

Tab. 32   Adaption of horizontal permeability of Fine sand material drain influence zone (soil layer in storage basin), ($k_x \neq k_y$)

Fine sand - drain influence zone – HS small		
$reduced\ k_x$	2.326 E-6	[m/s]

Tab. 33   Adaption of horizontal permeability of Fine sand,silty material drain influence zone (soil layer in storage basin), ($k_x \neq k_y$)

Fine sand, silty - drain influence zone – HS small		
$reduced\ k_x$	4.641 E-7	[m/s]

Tab. 34   Adaption of horizontal permeability of Silt-Fine sand material drain influence zone (soil layer in storage basin), ($k_x \neq k_y$)

Silt-Fine sand - drain influence zone – HS small		
$reduced\ k_x$	2.326 E-8	[m/s]

13 Appendix D - Input parameter for Plane strain simulation (isotropic)

The reference pressure of $p_{ref} = 100 \, kN/m^2$ in Plaxis is used for all material sets.

Only the horizontal permeability k_x is changed in the upper three layers, the other necessary parameters for all materials are summarized in "Appendix C – Input parameter for Plane strain simulation (anisotropic)". The rest of the materials is the same for both permeability conditions.

Tab. 35   Input parameters for Fine sand material (soil layer in storage basin), (k_x=k_y)

Fine sand – HS small		
$k_x = k_y$	5 E-6	[m/s]

Tab. 36   Input parameters for Fine sand, silty material (soil layer in storage basin), (k_x=k_y)

Fine sand, silty – HS small		
$k_x = k_y$	1 E-7	[m/s]

Tab. 37   Input parameters for Silt-Fine sand material (soil layer in storage basin), (k_x=k_y)

Silt-Fine sand – HS small		
$k_x = k_y$	5 E-9	[m/s]

Only the horizontal permeability k_x is adapted for the drain influence zone around the columns after column installation. Those adapted permeabilities are summarized in Tab. 38, Tab. 39 and Tab. 40. The rest of the parameters of the fine grained soil layer beneath the storage basin is not changed (look up in Tab. 25, Tab. 26, Tab. 27).

Tab. 38   Adaption of horizontal permeability of Fine sand material drain influence zone (soil layer in storage basin), (k_x=k_y)

Fine sand - drain influence zone – HS small		
$reduced \; k_x$	2.326 E-6	[m/s]

Tab. 39   Adaption of horizontal permeability of Fine sand,silty material drain influence zone (soil layer in storage basin), ($k_x=k_y$)

Fine sand, silty - drain influence zone – HS small		
reduced k_x	4.641 E-8	[m/s]

Tab. 40   Adaption of horizontal permeability of Silt-Fine sand material drain influence zone (soil layer in storage basin), ($k_x=k_y$)

Silt-Fine sand - drain influence zone – HS small		
reduced k_x	2.326 E-9	[m/s]

14   Appendix E – 2D plane strain simulation - Excess pore water pressure over time
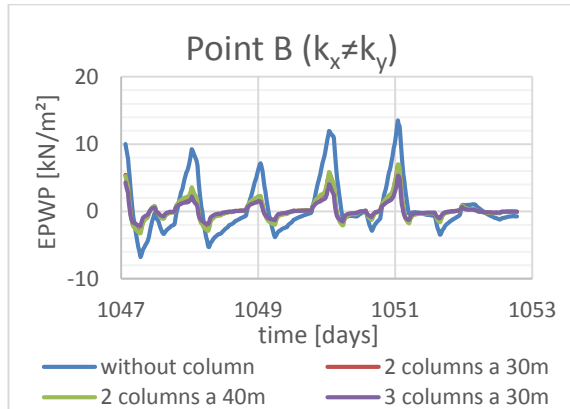
Fig. 123   Excess pore water pressure over time ($k_x \neq k_y$) – Point B
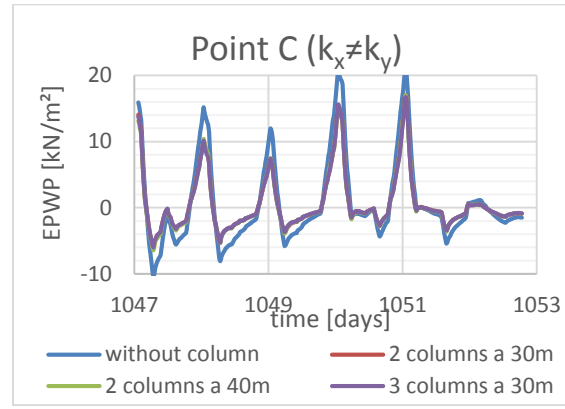
Fig. 124   Excess pore water pressure over time ($k_x \neq k_y$) – Point C
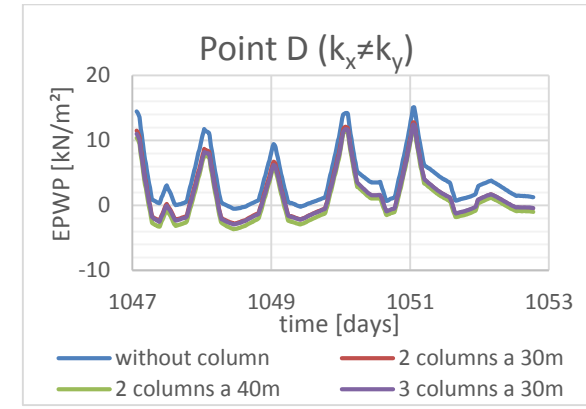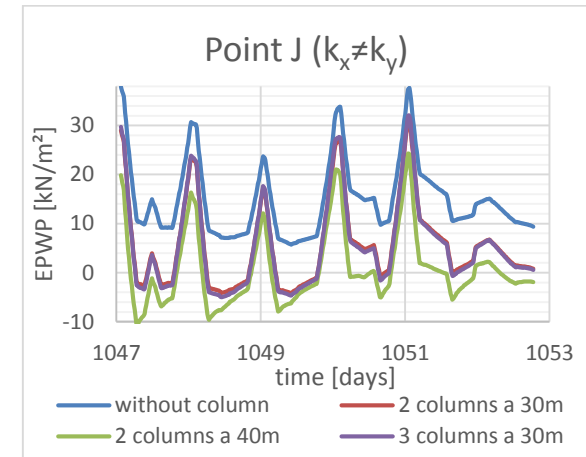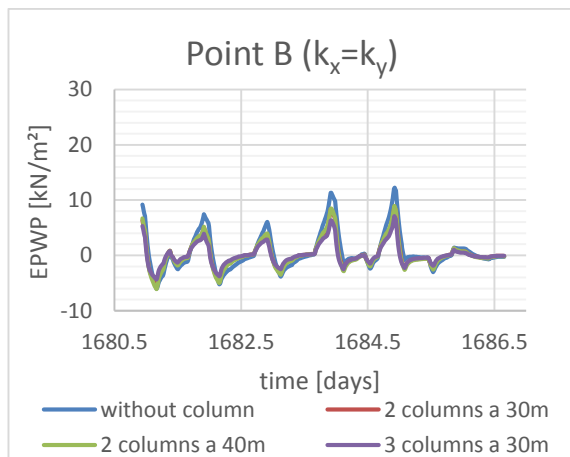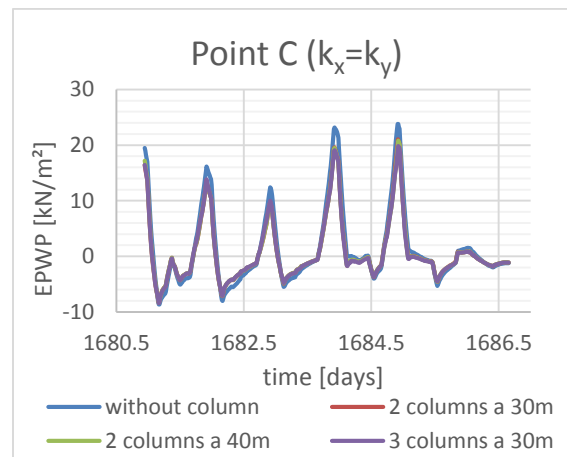

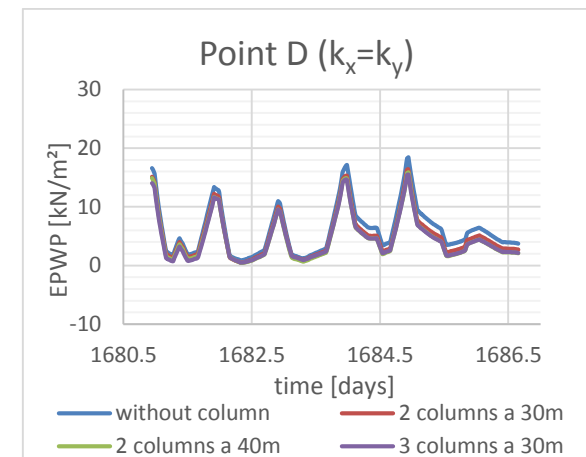Fig. 125   Excess pore water pressure over time ($k_x \neq k_y$) – Point D
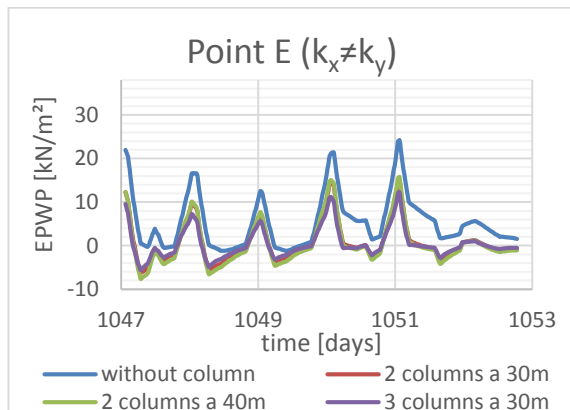
Fig. 126   Excess pore water pressure over time ($k_x \neq k_y$) – Point E
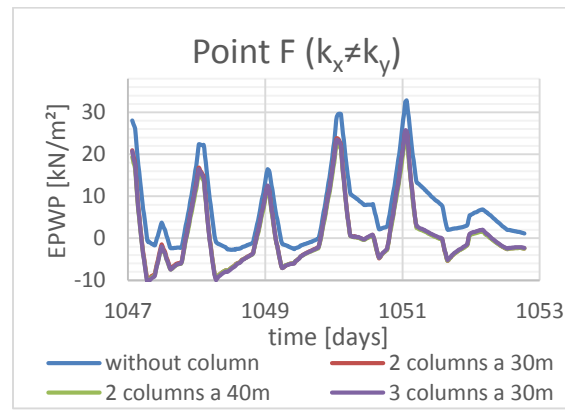
Fig. 127   Excess pore water pressure over time ($k_x \neq k_y$) – Point F
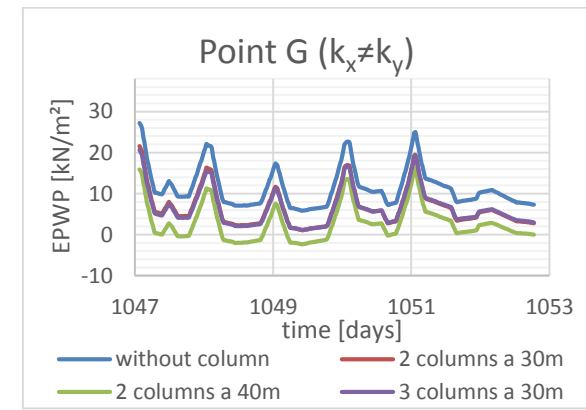
Fig. 128   Excess pore water pressure over time ($k_x \neq k_y$) – Point G
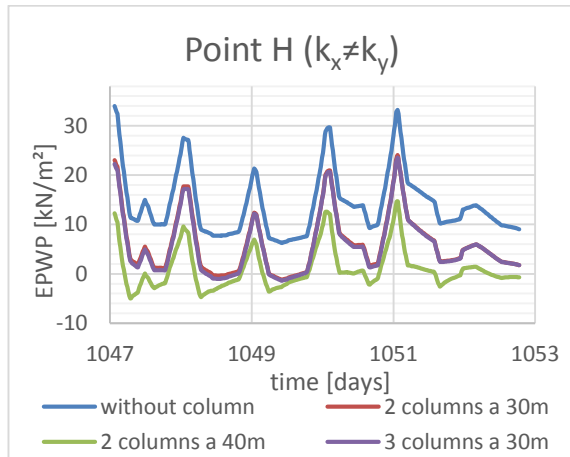
Fig. 129 Excess pore water pressure over time ($k_x{\neq}k_y$) – Point H
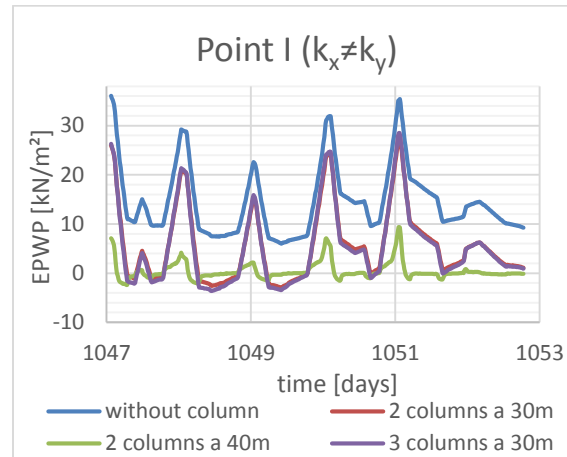
Fig. 130 Excess pore water pressure over time ($k_x{\neq}k_y$) – Point I

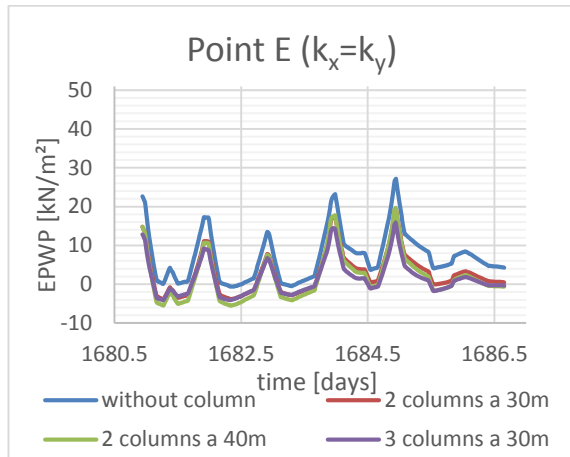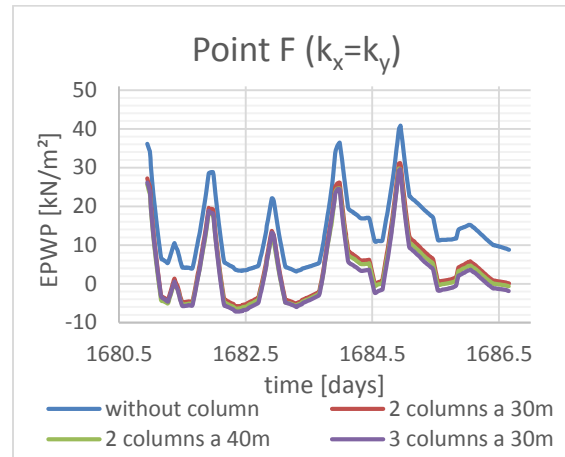Fig. 131 Excess pore water pressure over time ($k_x{\neq}k_y$) – Point J

Fig. 132 Excess pore water pressure over time ($k_x{=}k_y$) – Point B

Fig. 133 Excess pore water pressure over time ($k_x{=}k_y$) – Point C

Fig. 134 Excess pore water pressure over time ($k_x{=}k_y$) – Point D

Fig. 135 Excess pore water pressure over time ($k_x=k_y$) – Point E

Fig. 136 Excess pore water pressure over time ($k_x=k_y$) – Point F
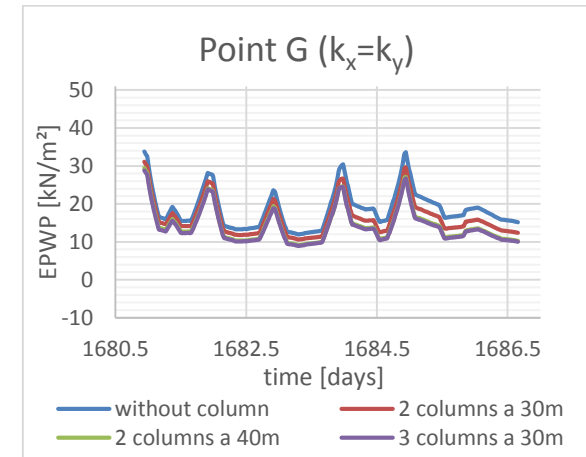

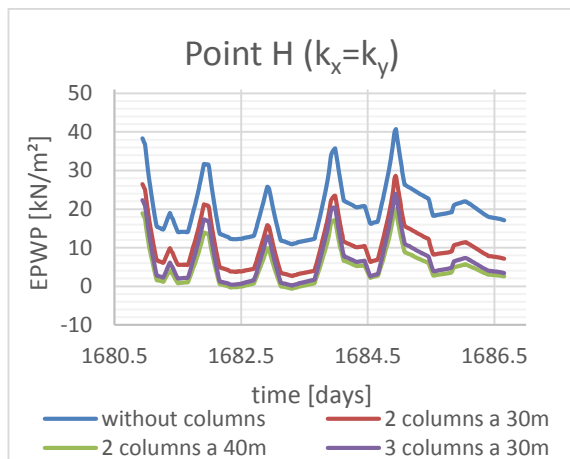Fig. 137 Excess pore water pressure over time ($k_x=k_y$) – Point G

Fig. 138 Excess pore water pressure over time (kx=ky) – Point H
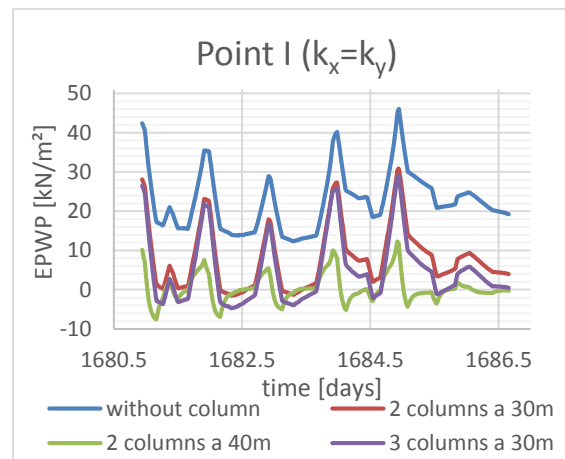

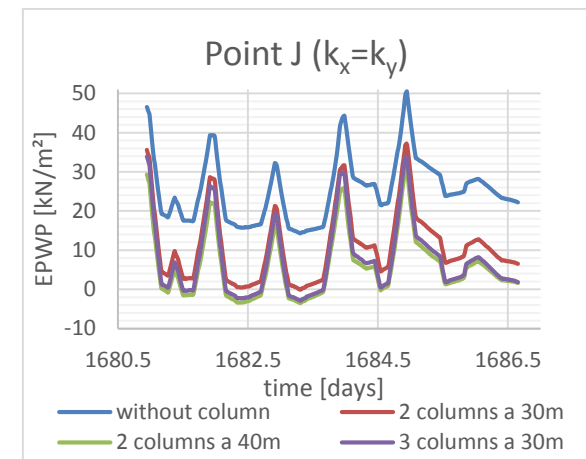Fig. 139 Excess pore water pressure over time (kx=ky) – Point I

Fig. 140 Excess pore water pressure over time (kx=ky) – Point I

Computational Geotechnics Group